On the hindered settling of suspensions of mud and mud-sand mixtures

On the Hindered Settling of Suspensions of Mud and Mud-Sand Mixtures

Proefschrift

ter verkrijging van de graad van doctor
aan de Technische Universiteit Delft,
op gezag van de Rector Magnificus prof. dr. ir. J.T. Fokkema,
voorzitter van het College voor Promoties,
in het openbaar te verdedigen

op woensdag 11 oktober 2006 om 12.30 uur

door

Petra Janske Tessel DANKERS

Doctorandus in de Fysische Geografie
geboren te Texel.

Dit proefschrift is goedgekeurd door de promotor:
Prof. dr. ir. M.J.F. Stive

Toegevoegd promotor:
Dr. ir. J.C. Winterwerp

Samenstelling promotiecommissie:

Rector Magnificus	voorzitter
Prof. dr. ir. M.J.F. Stive	Technische Universiteit Delft, promotor
Dr. ir. J.C. Winterwerp	Technische Universiteit Delft, toegevoegd promotor
Prof. dr. A.J. Mehta	Univeristy of Gainsville, Florida, Verenigde Staten
Prof. dr. ir. J. Berlamont	Katholieke Universiteit Leuven, België
Prof. dr. S.B. Kroonenberg	Technische Universiteit Delft
Dr. G.C. Sills	Oxford University, Groot-Brittannië
ir. W.G.M. van Kesteren	WL|Delft Hydraulics

Cover: The mud flats on the island of Texel.

Abstract

Suspensions of mud-sand mixtures occur in many environments, often at low concentrations, but sometimes at large concentrations. Large concentrations can occur in natural environments such as the turbidity maximum of estuaries, in sheet flow layers, during storms and in some rivers, such as the Yellow River. Furthermore, anthropogenic influences, such as dredging, can increase the sediment concentration. When the sediment concentration becomes larger than 5 - 10 kg/m^3, particles start to interfere with each other and their settling velocity reduces. This is called hindered settling. As a result, particles have a longer residence time in the water, spread over a larger distance, and turbidity is increased. Various primary and secondary effects of increased turbidity are reduced light penetration, reduced primary production, predation difficulties for sight feeders, and a shift in algae bloom period. Especially suspensions with a large mud-sand ratio have these effects as the ability of mud to block light is much larger than that of sand.

Studies on the settling and consolidation of mud, or cohesive sediment, are well documented. However, most studies deal either with low sediment concentrations, below the hindered settling regime, or with very high sediment concentrations, i.e. the consolidation regime. Knowledge on how suspensions in the hindered settling regime behave, how fast they settle and how their settling velocity and behaviour can be predicted, is scarce.

In this research, experiments are performed with suspensions of mud and of mud-sand mixtures in the hindered settling regime. The data obtained from these experiments are used to get more insight in the settling velocity of mud suspensions and mud-sand mixtures, but also in the interaction between the mud and sand fractions in these suspensions. Furthermore, the data are used for the validation of a hindered settling model.

A first series of experiments was performed with the clay mineral kaolinite in small (40 cm) settling columns. The settling of the upper interface in the experiments is recorded visually and gives more insight in how quickly mud suspensions with different initial concentrations settle. The settling of the mud suspensions in these experiments is analysed with Kynch's theory. This theory predicts two different types of settling: settling with two interfaces and settling with one interface. The occurrence of interfaces in the experiments compares favourably with the predictions of Kynch's theory. The experiments are further used to obtain some parameters that, at a later stage, are used in model simulations. These parameters are the gelling concentration, the parameter that accounts for non-linearity in the return flow effect, and the settling velocity of a single mud floc in still water.

Next, experiments with natural mud and sand are performed. All suspensions in these experiments are composed of a low volumetric concentration of sand and a high volumetric concentration of mud. The experiments are performed in large settling columns with a height of 2 metres. The occurrence of interfaces is derived from vertical concentration profiles, which are measured with an X-ray system. The mud settling velocities can also be derived from the vertical concentration profiles, whereas the sand settling velocities are determined from recorded video images (PTV/PIV measurements). These PTV/PIV measurements also give insight into the behaviour within the mud-sand mixtures and the

interaction between the different fractions. It is observed that the sand generates highly irregular flow motions, even when the volumetric concentration is very low. Furthermore, the video images show that sand grains can settle further than expected in a consolidating soil, as they can travel through dewatering channels of the consolidating mud.

Both sets of experiments are further analysed with a 1DV model. This model uses an advection-diffusion equation to describe hindered settling. The 1DV model results show a fair agreement with the measured kaolinite suspension settling velocities and the measured natural mud suspension settling velocities. Furthermore, the predicted vertical concentration profiles agree reasonably well with the measured concentration profiles for mud and mud-sand mixtures. The predicted sand settling velocities, however, do not properly match with the measured sand settling velocities. This indicates that the settling of sand through highly concentrated mud suspensions is not yet fully understood.

The combination of mathematical theories, experimental work and modelling proved to be successful. This research has increased the understanding of the behaviour and settling of highly concentrated mud suspensions and mud-sand mixtures. As a result, questions that relate to increased turbidity levels and environmental impact might be answered better.

Samenvatting

In veel zeeën en rivieren bestaat het gesuspendeerde materiaal uit een mengsel van zand en slib. Vaak zijn de concentraties van deze mengsels laag, maar in sommige gevallen, bijvoorbeeld in het turbiditeitsmaximum van estuaria, in sheet flow lagen, tijdens stormen op zee, en in sommige rivieren (bijvoorbeeld de Gele Rivier in China) is de concentratie vele malen hoger. Naast natuurlijke oorzaken kunnen er ook antropogene oorzaken zijn voor hoge slib-zand concentraties, bijvoorbeeld baggerwerkzaamheden.

Als de concentratie groter wordt dan 5 - 10 kg/m^3 gaan de zandkorrels of slibvlokken elkaar in de weg zitten en wordt hun valsnelheid gereduceerd. Dit wordt hindered settling genoemd. Ten gevolge van hindered settling blijven de sediment deeltjes langer in het water hangen en kunnen ze zich over een grotere afstand verspreiden. Hierdoor neemt de turbiditeit toe. Een toename van de turbiditeit heeft verschillende primaire en secundaire gevolgen, zoals een afname van de lichtdoordringing, een afname van de primaire produktie, predatie moeilijkheden voor zichtjagers en een verschuiving van de periode van algenbloei. Deze effecten treden vooral op bij suspensies met een hoge slib-zand ratio, omdat de invloed van slib op de lichtdoordringing groter is dan de invloed van zand.

Het uitzakken (lage concentraties) en consolideren (zeer hoge concentraties) van slibsuspensies is het onderwerp geweest van menig onderzoek. Er is echter weinig bekend over suspensies met een concentratie tussen deze twee types in, de zogenaamde hindered settling fase. Het onderzoek, gepresenteerd in dit proefschrift, houdt zich bezig met de hindered settling fase. Er zijn experimenten uitgevoerd met hooggeconcentreerde slib suspensies en slib-zand suspensies. De resultaten hiervan zijn gebruikt om meer inzicht te krijgen in het sedimentatie gedrag van slib en zand en in de interactie tussen deze verschillende fracties. Verder zijn de resultaten van de experimenten ook gebruikt voor de validatie van een hindered settling model.

Een eerste experimentele set is uitgevoerd met het kleimineraal kaoliniet in lage (40 cm) valkolommen. De grensvlakken, veroorzaakt door het uitzakken van de slib suspensies, konden met het oog gevolgd worden, en geven inzicht in de valsnelheid van het slib. Vervolgens is het gedrag van de slib suspensies geanalyseerd aan de hand van de theorie van Kynch. Deze theory beschrijft twee verschillende typen van sedimentatie; het sedimenteren met 1 grensvlak en het sedimenteren met 2 grensvlakken. De resultaten van de experimenten kwamen goed overeen met de voorspellingen aan de hand van de theory van Kynch. In een later stadium zijn de resultaten van de experimenten ook gebruikt voor het bepalen van model parameters, zoals de gelling concentratie, de return flow parameter en de valsnelheid van slibvlokken in stilstaand water.

Een tweede experimentele set is uitgevoerd met slib-zand mengsels (lage volumetrische concentratie zand en hoge volumetrische concentratie slib) in lange valkolommen (2 meter). Het uitzakken van de grensvlakken is bepaald aan de hand van concentratieprofielen. Deze concentratieprofielen zijn gemeten met een X-ray profiler. De valsnelheid van de slibsuspensie volgde uit de concentratieprofielen, terwijl de valsnelheid van de zandkorrels bepaald werd aan de hand van video opnames (PTV/PIV metingen). Deze PTV/PIV metingen geven, naast de valsnelheid van het zand, ook inzicht in het gedrag van en de

interactie tussen de verschillende sedimentfracties. Hierdoor is bekend geworden dat de zandkorrels, ondanks de lage concentratie, een sterke chaotische stroming veroorzaken. Ook is bekend geworden dat de zandkorrels gebruik maken van ontwateringskanaaltjes in het consoliderende slib en hierdoor veel verder kunnen uitzakken dan vantevoren was gedacht.

Uiteindelijk zijn beide datasets verder geanalyseerd met een 1DV model. Dit model gebruikt een advectie-diffusie vergelijking voor het beschrijven van hindered settling. De model resultaten komen goed overeen met de gemeten valsnelheden van kaoliniet en natuurlijk slib. De door het model voorspelde vertikale concentratieprofielen komen redelijk goed overeen met de gemeten vertikale slib en slib-zand concentratieprofielen. De voorspelde valsnelheden van zand komen, daarentegen, niet goed overeen met de gemeten snelheden. Dit geeft aan dat het sedimenteren van zand door een hooggeconcentreerde slibsuspensie nog niet goed wordt begrepen.

De in dit onderzoek gepresenteerde combinatie van mathematische theoriën, experimenteel onderzoek en model onderzoek, blijkt een goede combinatie te zijn. Door middel van dit onderzoek is er meer inzicht gekomen in het gedrag en sedimenteren van hooggeconcentreerde slib suspensies en slib-zand suspensies. Hierdoor kunnen vragen, gerelateerd aan hoge turbiditeitsniveaus en de impact hiervan op het ecosysteem, in de toekomst wellicht beter beantwoord worden.

Contents

1

Introduction

1.1 Background

In early times, mud was considered beneficial. The flooding of the rivers Euphrates and
Tigris in Mesopotamia resulted in large areas with mud deposits. These fertile deposits
were, at the start of civilisation, a good base for agriculture, but the material was also
used for building purposes and for the introduction of written language. Later, when
trading started to take place and harbours were built, mud became also a nuisance, as
the thick deposits decreased the navigable depth in rivers and harbours. Early methods
of dredging were already found along the Nile, Euphrates, Tigris and Indus rivers, carried
out with spades and baskets by Roman infantry, prisoners of war and slaves (Herbich,
2000).

Nowadays, in the modern world, mud is still an important building material and re-
gions with mud deposits, especially along rivers with regular natural flooding, are still
fertile. Furthermore, it has become clear that mud is an important factor in the ecosys-
tem, especially as it contains large amounts of nutrients and organic material, serving as
a source of food for organisms. On the other hand, ships keep on growing larger. This
results in more and more ports that struggle with rapid siltation. Due to the large input
of pollutants into rivers since the 1960's, a lot of the deposited mud in harbours can be
considered toxic waste. As a result, the fate of mud is an important issue for decision-
makers who deal with infrastructure projects possibly influencing mud concentrations in
the water and the mud transport paths. Ignorance of processes on the behaviour of mud
suspensions can lead to solutions and decisions that negatively influence the ecosystem
and the economy. It is therefore important to increase knowledge on the behaviour of
mud.

Mud is a sediment mixture of water, organic material and inorganic components such
as clay minerals, quartz and silicates. The particles in the sediment mixture have a grain
size smaller than 63 μm. Cohesive sediment, or mud, occurs in many environments.
Often, mud is present together with sand. In most natural environments the suspended
concentrations of these sediments are rather low, not exceeding a few 100 mg/l. In specific
cases the concentration can, however, be higher. Suspended concentrations of mud or mud-
sand mixtures can reach a few g/l and even more in the so-called turbidity maximum of
estuaries, close to the bed, in the swash zone, in dredge plumes, at dredge disposal sites

and in some rivers, such as the Yellow River. In these cases we are dealing with highly concentrated suspensions of mud and sand. The behaviour and settling velocity of the particles in these highly concentrated suspensions is influenced by the mutual interference of settling particles, resulting in a reduced settling velocity, which is referred to as hindered settling. These highly concentrated mud-sand mixtures have largely been neglected in earlier research. This is understandable, as highly concentrated suspensions do not occur often. However, when they are present, their impact on the ecosystem can be much larger than the impact of low concentrations, and their role in the sediment budget of estuaries can be of significance.

With respect to the influence on ecology, a division has to be made between sediment mixtures with mainly sand and some cohesive sediment and sediment mixtures with mainly cohesive sediment. Consequences for the ecosystem are small if the suspended load consists mainly of sand. Sand settles fast and the main influence on the ecosystem is the burial of organisms. If most of the suspended sediment consists of mud, the impact is much larger. Cohesive sediment settles slowly, thereby increasing the turbidity, and the sediment can be transported over a larger area, increasing the area of impact. Furthermore, mud flocs have a larger influence on light transmission than sand grains. A high turbidity of mud flocs therefore results in decreased light penetration, which, in turn, affects primary production. Primary production provides food for marine organisms at the base of the food chain. Other consequences of decreased light penetration and increased suspended loads are predation difficulties for sight-feeders (Essink, 1999), shifted algae bloom periods (Groenewold & Dankers, 2002), shifts in species composition of phytoplankton communities (Jankowski & Zielke, 1996), a decrease in the ratio of organic/inorganic material, affecting zoöplankton that has to feed on more sediment to catch enough food (Douben, 1989), suboptimal functioning of gills by clogging (Essink, 1999) and release of chemical substances that may be absorbed in the food chain (IADC/CEDA, 2000). Of course, the impact largely depends on factors such as background turbidity, type and abundance of species, characteristics of the sediment and the type of system.

The exact effect of highly concentrated suspensions on the ecosystem is difficult to determine. The residence time of sediment in the water column, and thus the settling velocity of the sediment particles, is an important factor. At present, reliable indications of residence time of highly concentrated mud suspensions cannot be given. Existing theories that predict settling velocities in highly concentrated suspensions have not been tested with controlled measurements, because data on the settling of highly concentrated mud suspensions are scarce and data of highly concentrated mud sand mixtures hardly exist.

The research presented in this thesis deals with the settling of highly concentrated suspensions of mud and of mud-sand mixtures with the aim to gather and analyse data on these suspensions to come to a better understanding of the processes in highly concentrated settling suspensions.

1.2 Objective of the study

The main objective of this research is to gain a better understanding of the behaviour of highly concentrated suspensions of mud and mud-sand mixtures. The main questions to be addressed are:

- How do highly concentrated suspensions settle?

- What are the settling velocities of these suspensions?

- What are the settling velocities of the two fractions in mud-sand mixtures?

- How do the two fractions interact?

- How can the settling of highly concentrated mud suspensions and mud-sand mixtures be predicted?

These questions are addressed by carrying out a combination of experimental research and modelling. From the experiments, settling velocities can be determined and the settling behaviour of suspensions can be evaluated. The data from the experiments will in part serve as an input for models.

1.3 Research methodology

Performing settling experiments with highly concentrated suspensions is a challenging goal. Such experiments are not straightforward and the measuring of sand settling velocities in mud suspensions has never been realised before. As a result, there is no standard method to perform these experiments. New techniques are designed, and their applicability has to be proven.

Two types of settling experiments are performed. The clay mineral kaolinite is used in small settling columns in a first series of experiments. The goal of these experiments is to obtain data on suspension settling velocities and concentration time series by visual observations and concentration measurements. With these data, the settling behaviour can be analysed and compared to existing theories.

The second set of experiments consists of three types of tests; natural mud in small columns, natural mud in large columns, and mud-sand mixtures in large columns. The goal of the first two types is to obtain specific parameters. The goal of the third type is to measure both the settling velocity of the suspension and the settling velocity of the sand grains and to evaluate the interaction between the two fractions during settling.

As a last step, part of the data from the kaolinite experiments and the natural mud experiments will be used to calibrate a hindered settling model. The mud-sand experiments are used for validation of the hindered settling model.

1.4   Outline of thesis

This thesis starts with an introduction to the basics of cohesive sediment in Chapter 2, where also hindered settling is explained and existing hindered settling theories and models are presented. These theories are applied to data in Chapter 3, where the set-up and analysis of the hindered settling experiments with kaolinite are given. In Chapter 4, the set-up and analysis of the hindered settling experiments with mud-sand mixtures are presented. Finally, the data sets from Chapters 3 and 4 are further analysed in Chapter 5 with a hindered settling model that can deal with both mud suspensions and mud-sand mixtures. The research conclusions are presented in Chapter 6.

2

Literature review

2.1 The behaviour of mud

2.1.1 General description

Mud is a sediment mixture with primary particles smaller than 63 μm. It consists of organic and inorganic components, water and sometimes gas. The inorganic fraction can contain quartz, feldspar, clay minerals, calcite, dolomite, hydroxides, silicates, carbonates, sulfides and small fractions of other minerals, depending on its geographic origin. The organic material in mud consists of living and dead material as bacteria and remnants or products of phytoplankton, benthic algae, faecal pellets, peat and macromolecules produced by bacteria (EPS and proteins). The amount of organic material in mud strongly depends on the source and season. In intertidal areas it may amount to 10 - 20% of the dry weight of sediment and due to the large amounts of adsorbed water even as much as 70 - 90% of the wet weight (Groenewold & Dankers, 2002). In general particles with a grain size diameter (D) $\leq 63\mu m$ are called silt, while primary particles with $D \leq 2\mu m$ are called clay. However, it is important to realise that these fraction names refer to size, and do not distinguish the composition of the particles (Winterwerp & Van Kesteren, 2004). Within the clay fraction there is a sub-fraction referred to as colloids. The size of these particles is in the order of 0.1 μm or less and they do not settle in water. This is the fraction that plays an important role in turbidity levels (Winterwerp & Van Kesteren, 2004).

Two important properties of clay are plasticity and cohesion (Partheniades, 1980). Plasticity is the ability of a clay mass to undergo deformation before breaking. Cohesion is the ability of a material to stick or adhere together.

Chemically clay consists of silicates of aluminium and/or iron and magnesium. These minerals form two fundamental building blocks of the clay. The silicon-oxygen sheet is one of these building blocks. It is formed by a SiO_4 tetrahedron. The other building block is the Al- and Mg-O-O-H sheet, which forms an octahedron. Smectites, illites and kaolinites are the most common clay minerals. Smectite is formed in surface and subsurface environments by hydrolysis of volcanic material. Smectites that are buried deep chang through the adsorption of potassium to illite. Kaolinite originates from weathering and hydrothermal alteration of granite (Winterwerp & Van Kesteren, 2004). The clay

minerals have predominantly crystalline arrangements; i.e. the atoms are arranged in specific geometric patterns. Clayey materials can be considered to consist of a number of these clay minerals stacked to form a sheet or layered structure (Partheniades, 1980).

There are several forces that act between clay minerals. Some of them will be discussed here. The Van der Waals force is of an electro-chemical nature and acts on an atomic and molecular scale. It is generated by the mutual influence of the motion of electrons within the atoms and is always attractive. The attractive potential of Van der Waals force between two atoms is inversely proportional to the 7th power of the distance. In order to become effective, particles must come very close to each other (Partheniades, 1980).

Negatively charged clay minerals in water will attract ions of opposite charge, called "counter ions", to compensate their own electric charge. Thus, a clay particle will be surrounded by a diffused layer of counter-ions. This layer is called the diffusive double layer. It neutralises the negative charge of the minerals, so that particles can approach closer and the Van der Waals force may be able to bind them together.

The net interaction between two particles is found from a balance of the repulsive and the attractive energy (figure 2.1). According to Van Olphen (1977) it can be shown that there is almost no net repulsion at high electrolyte concentrations, as the double layer is strongly compressed, which results in a maximum particle coagulation rate.
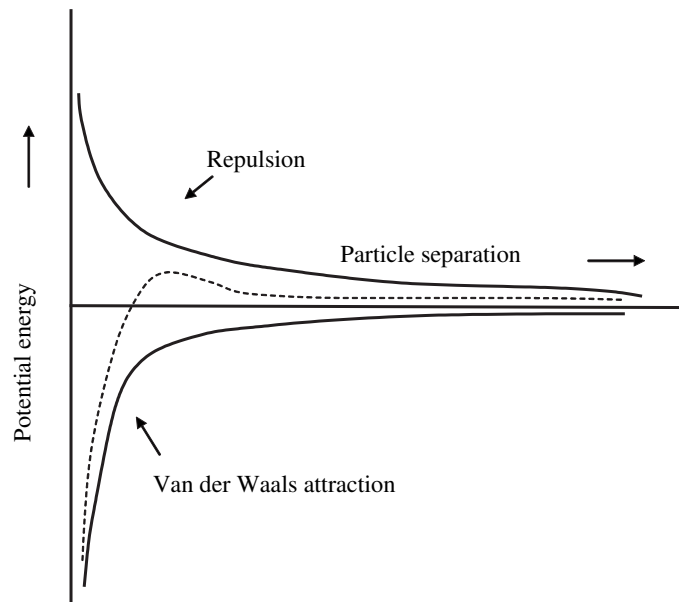

Figure 2.1. The interaction between Van der Waals force and repulsive forces. After Partheniades (1980).

2.1.2 Flocculation

Clay minerals form primary particles, which aggregate with silt particles and organic material to form flocs. Flocs contain a large amount of water. As a result, low mass concentrations of clay, silt and organic material can result in a high volumetric concentration of mud flocs. These mud flocs can break-up again. The process of aggregation and break-up is called flocculation.

Aggregation of particles occurs when two particles collide and stick together. The rate of aggregation depends on the frequency of collisions, the efficiency of the collisions in sticking together and the number of particles. Particle collisions occur due to Brownian motion of particles, turbulence within the suspending liquid (due to wave breaking or turbulence in the boundary layer) and differential settling of the suspended particles (Van Leussen, 1994; Winterwerp, 1999). The collision frequency then depends on these mechanisms and on the concentration.

The different mechanisms for flocculation result in different structures of the aggregates. In literature, the term perikinetic flocculation is used for flocculation caused by Brownian motion. It is found that the aggregates formed in this manner have a ragged and weak structure. Aggregates formed by orthokinetic flocculation, i.e. flocculation controlled by turbulence, tend to be spherical and relatively strong. Flocs formed by differential settling have a low density and are very weak (Van Leussen, 1994).

The sticking efficiency upon collision is determined by the particle charge, the ion concentration in the water and by biopolymers and organic coating on the particles. An increasing salinity, which means an increase of ion concentration, is therefore often an important flocculant. The increasing electrolyte concentration due to salt results in a compression of the diffusive double layer. This thinner layer then decreases the repulsive forces between particles, leading to a more intensive flocculation. However, Van Leussen (1994) concluded from literature research on salt flocculation that often salt does not enhance flocculation, but decreases floc sizes. In many cases the interference between salt and fresh water bodies increases shear and decreases the floc size.

Organic coatings on suspended particles can have a major influence on the particle surface charge. It is believed that organic material can alter the charge of even strongly negatively charged particles. Biopolymers can significantly alter the collision efficiency of particles. Here, the binding mechanism is not the reduction of the surface potential of the particles but polymers that adsorb on the surfaces of the particles. When the particles meet each other, bridges will be formed between the polymers on the particles and thus an aggregate will be formed.

It can be stated that physical processes mainly determine the collision frequency and that chemical and biological processes mainly determine the stickiness. Not all collisions will result in aggregation and the sticking efficiency is not large.

Dyer (1989) proposed a conceptual model of floc size on the basis that flocculation is mostly determined by concentration and by shear stress due to turbulence. Figure 2.2 shows an increase in floc size with shear stress till a certain point. Consider for example a concentration of 10 mg/l. The floc diameter increases rapidly with shear stress <1 Pa and decreases rapidly with shear stress >1 Pa. If we consider a constant shear stress of about
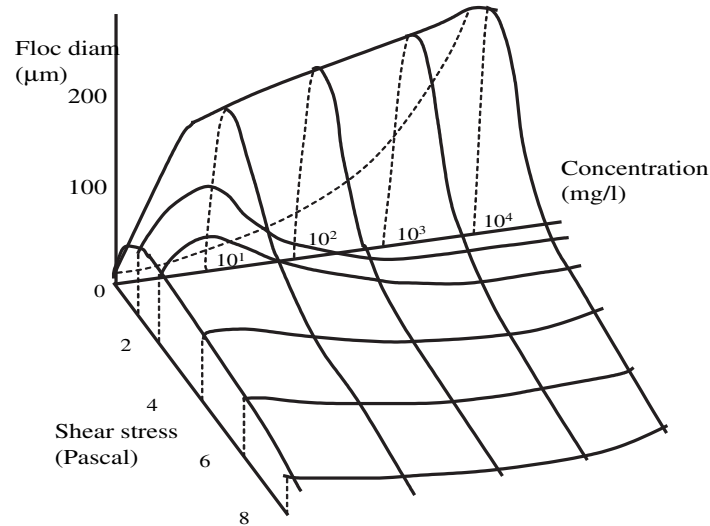
Figure 2.2. Conceptual flocculation diagram. After Dyer (1989).

2 Pa the floc diameter increases till a concentration of 5 mg/l and decreases again for concentrations > 5 mg/l. This initial increase in floc size with concentration and shear stress is due to the higher occurrence of collisions. The decrease in floc size is due to floc break-up resulting from the increased fluid shear and the impact of collisions (Dyer, 1989). Note that in this model the effects of salinity and biopolymers for example, are not taken into account.

Winterwerp (1998) also studied the effect of shear stress and concentration on floc-culation. All secondary hydrodynamic effects, such as the influence of the particles on the turbulence structure itself, are omitted. He compared the maximum settling velocity computed with a simple flocculation model using low-concentration settling column experiments as shown in figure 2.3. The solid line represents the model results for column heights of 4, 2 and 1 metres. It shows an increasing settling velocity/concentration ratio, or increasing grain size diameter, assuming that $w_s \sim D$, with shear rate at small shear rates, and a decrease at large shear rates. Figure 2.3 shows a similar behaviour as Figure 2.2. The dashed line in figure 2.3 represents the settling velocity/concentration ratio under equilibrium conditions. At small shear rates flocs can not reach this equilibrium. According to figure 2.2 the floc size increases significantly at low shear stresses, resulting in increasing settling velocities. Flocs in such an environment will settle on the bed before they have reached their equilibrium size. Only when the water depth is large there is enough time for the flocs to coagulate and reach their equilibrium size. The residence time of the flocs thus becomes a limiting factor for size. At large shear stresses the flocs
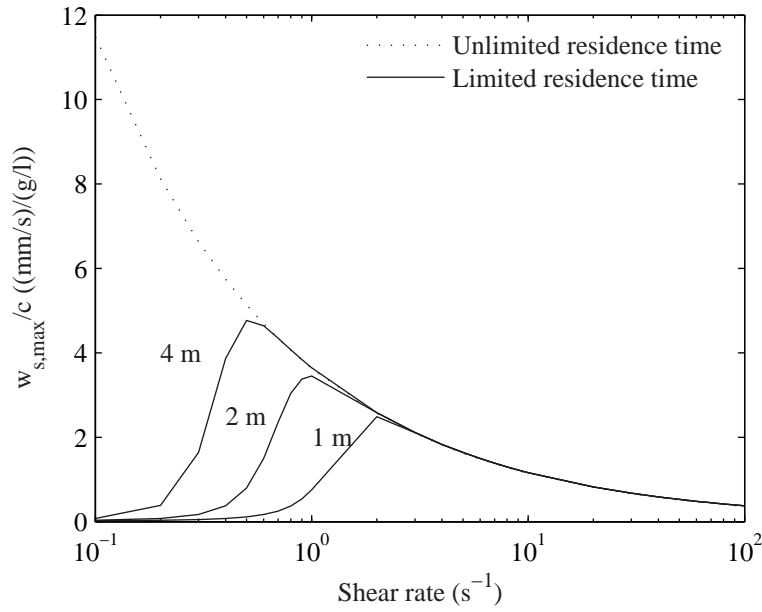
Figure 2.3. Variation of $w_{s,max}/c$ with shear rate (Winterwerp, 1998).

and thus the settling velocities remain smaller and the residence time of flocs in the water is enough to reach equilibrium.

2.1.3 Settling velocity

The settling velocity of a single particle in still water is given by $w_{s,0}$. Stokes found for spherical, massive particles (sand) in the Stokes' regime (particle Reynolds number $Re_p = \frac{w_{s,0}D}{\nu} < 1$):

$$w_{s,0} = \frac{(\rho_s - \rho_w)gD^2}{18\mu} \tag{2.1}$$

in which ρ_s is the density of the primary sediment particles, ρ_w the water density, g the acceleration of gravity, D the particle size, μ the dynamic viscosity and ν is the kinematic viscosity. However, this cannot be used for mud flocs, as they are not spherical and massive.

The settling velocity of mud flocs is a function of their size D and their differential density $\Delta\rho_f$, i.e. the excess density relative to water (ρ_s - ρ_w). Flocs have a relatively small $\Delta\rho_f$ due to flocculation and their high water and organic material content. Values for $\Delta\rho_f$ can amount up to a few tens of kg/m^3 (Winterwerp, 1998). Winterwerp (1998) found for mud flocs with a fractal structure an implicit formula for the settling velocity of single mud flocs in still water ($w_{s,0}$):

$$w_{s,0} = \frac{\alpha}{18\beta} \frac{(\rho_s - \rho_w)g}{\mu} D_p^{\,3-n_f} \frac{D^{n_f-1}}{1 + 0.15 Re_p^{\,0.687}} \tag{2.2}$$

Where α and β are shape factors of the flocs, D_p is the diameter of primary mud particles, n_f is the fractal dimension of mud flocs, which is based on $\Delta\rho_f$, and Re_p is the particle Reynolds number. $1 \leq n_f \leq 3$, but in general $n_f \approx 2$, which shows that the settling velocity is proportional with the floc diameter (D) and not with D^2 as in Stokes' formula. Furthermore, it is assumed that fluid flows around, and not through the particles. This in contrast to Johnson *et al.* (1996) who treated flocs as permeable particles, where the settling velocity is affected by the flow through pores of the flocs. Winterwerp (1999) however concluded, after reviewing literature on settling velocities of flocs, that flocs may be treated as porous, though impermeable entities.

2.1.4   Hindered settling

Hindered settling is caused by the influence of neighbouring particles on the settling velocity of an individual particle within a suspension (Winterwerp, 2002). Hindered settling in mud suspensions normally occurs when concentrations reach over a few kg/m^3. At lower concentrations particles settle with a settling velocity defined by Stokes, as described in equation 2.1 for sand or equation 2.2 for flocs.

Seven processes can be identified that affect the settling velocity of individual particles in a suspension (Winterwerp, 2002):

1. Return flow and wake formation. Falling particles create an upward directed return flow and a wake. The fall velocity of other particles in the near vicinity will be affected, decreasing the overall effective settling velocity of the suspension by a factor $(1 - \phi)$, where ϕ is the volumetric concentration of mud flocs.

2. Dynamic flow effect. The effect of neighbouring particles on the velocity gradients around a falling particle.

3. Particle-particle collisions. Collisions between particles cause additional stresses, decreasing the effective settling velocity of the suspension.

4. Particle-particle interaction. The attraction and repulsion of particles, where attraction may result in flocculation.

5. Viscosity. The effective viscosity increases with particle concentration. Each individual particle falls in the remainder of the suspension with increased viscosity, thus decreasing the effective settling velocity of all particles.

6. Buoyancy or reduced gravity. Individual particles settle in the remainder of the suspension with an increased bulk density, decreasing the effective settling velocity by a factor $(1 - \phi_p)$, where ϕ_p is the volumetric concentration of primary particles.

7. Cloud formation or settling convection. The tendency of particles to settle in groups, thereby actually increasing the settling velocity. This effect is beyond the present scope of this thesis.

All present models on hindered settling incorporate some of these processes.

Scott (1984) made an extensive review of hindered settling formulae and models. However, these were developed for massive, Euclidean particles (sand) and mostly based on Stokes' settling velocity for single particles. Therefore these models cannot be used directly for cohesive material.

The detailed review made by Scott (1984) was presented partly in a paper by Mandersloot *et al.* (1986). This author defined all hindered settling models, theoretical and empirical, as flow field models or viscosity function models. The flow field model is based on the theory of particle-particle interaction (nr. 3, 4). These models usually account wrongly for buoyancy as the density of the liquid and not the density of the total suspension is used to calculate buoyancy.

Viscosity function models are based on the superposition of the effects of buoyancy (nr. 6) and return flow (nr. 1), adding a suspension viscosity term to account for particle-particle interaction (nr. 4, 5). This suspension viscosity term tends to infinity for high concentrations. However, the resistance to flow through a particle assembly does not become infinite at high particle concentrations. At these high concentrations water can still flow through the particle assembly. Therefore viscosity function models do not work properly at very high concentrations. According to Mandersloot *et al.* (1986), introducing a suspension viscosity is physically questionable, because in hindered settling a swarm of particles descends as a whole without substantial mutual particle movement; the suspension is therefore not sheared in total. In fact, the only fluid dynamic phenomenon that affects a settling particle in a suspension (compared with single particle sedimentation) is an increase in the velocity gradient around the particles and thus the viscous force on a particle. As this increase in velocity gradient is caused by the presence of other particles, return flow through the space between the particles is generated (Mandersloot *et al.*, 1986).

Thacker & Lavelle (1977) define kinematic and dynamic effects that hinder settling. Kinematic effects are due to the upward flow of the fluid (nr. 1) and to the influence of the sediment on the hydrostatic pressure (nr. 6). Dynamic effects (nr. 2) are due to increases in drag force on the particles by turbulence, which increases with increasing concentrations, and due to random forces felt by particles due to asymmetries in the flow field.

Davis (1996) makes a summary of theoretical hindered settling models which involves solving the low-Reynolds number equations within a fluid cell encasing a representative particle. Characteristic of these models is that the particles are assumed to be configured in an ordered array. This in contrast to models that assume randomly distributed particles. The assumptions then made regarding the statistical structure of the suspension determine the kind of hindered settling model.

Most of the hindered settling models for sand are based on the well known formula by Richardson & Zaki (1954) in which the processes mentioned under nr. 1 and 6 are accounted for in an empirical way. Richardson & Zaki (1954) derived their formula from an extensive series of sedimentation and fluidization experiments with particles of a large variety in shape and Reynolds numbers. Examples of studies that are based on the

Richardson and Zaki type formulae are the experimental studies of Landman & White (1992) and the theoretical and numerical studies of Darcovich *et al.* (1996), Thacker & Lavelle (1977) and Buscall (1990), of which the latter two use a two-phase model.

When dealing with cohesive sediment, however, the models and proposed equations in Scott's (1984) review need to be adjusted as there is a fundamental difference between the hindered settling of sand and cohesive sediment. Volume effects are much more important for cohesive sediment. Also, there is a basic difference in viscosity effects; flocs are compressible, whereas sand is rigid. Furthermore, due to differences in shape and density, flocs do not have a constant settling velocity and their fragility facilitates break up. For hindered settling of mud flocs, Mehta (1986) suggested a modified form of the Richardson and Zaki formula:

$$w_s = w_{s,0}(1 - k\phi_p)^n \tag{2.3}$$

where w_s is the effective settling velocity, $w_{s,0}$ the settling velocity of a single particle in still water, k is an empirical parameter, ϕ_p the volumetric concentration of primary particles, $\phi_p = c/\rho_s$ in which c is the mass concentration and ρ_s the density of the sediment, and n is a function of the particle Reynolds number. The parameter n has been subject to discussion. According to the original experiments by Richardson & Zaki (1954) n should lie in between 2.5 and 5.5, depending on the particle Reynolds number. More recent research by Baldock *et al.* (2004) has indicated that the value of n for natural sand can differ significantly from the values determined by Richardson & Zaki (1954), with the hindered settling effect typically greater for sand than for spheres of equivalent size. They derive a relatively easy method to determine the value of n for sand, but it is not known whether it is suitable for mud as well.

Winterwerp (2002) reasoned that the rationale of Scott (1984) and Mandersloot *et al.* (1986) can be applied to cohesive sediments as well, but that equation 2.3 is probably not correct because:

- The viscosity of mud suspensions in the hindered settling regime does not scale with $(1 - a\phi_s)^{-b}$; it is therefore proposed to use the classical Einstein formula $\nu = \nu(1 + 2.5\phi)$.

- The buoyancy effect does not scale with $(1 - \phi)$, but with $(1 - \phi_p)$, where ϕ_p is the volumetric concentration of primary particles ($\phi_p = c/\rho_s$).

With the above mentioned, Winterwerp (2002) introduced a new formula for the hindered settling of mud flocs for $\phi \leq 1$:

$$w_s = w_{s,0}\frac{(1 - \phi)^m(1 - \phi_p)}{1 + 2.5\phi} \tag{2.4}$$

If $\phi > 1$ there is no hindered settling but consolidation. The factor $(1-\phi)$ in equation 2.4 accounts for the return-flow effect (nr. 1), $(1-\phi_p)$ accounts for the buoyancy effect (nr. 6) and $(1+2.5\phi)$ accounts for augmented viscosity (nr. 2,3,5). The exponent m is an empirical parameter to account for possible non-linear effects. When the return flow effect is linear, $(m = 1)$, only the volume effect of a suspension settling in a liquid is taken

into account. The downward flux of sediment is thus expected to create an equal upward flux of water. When non-linearity is taken into account this means that all the effects generated by a settling particle in a suspension (for example acceleration, deceleration of flow and the curvature of streamlines) are incorporated.

The volumetric concentration is related to the gelling concentration ($\phi = c/c_{gel}$), in which c_{gel} is the concentration at which flocs become space-filling and form a network structure, called a gel, and a measurable shear strength builds up. In this definition the volumetric concentration, ϕ, can thus become larger than unity when consolidation takes place and the flocs are squeezed. The volumetric concentration of primary particles can also be related to the gelling concentration, $\phi_p = c/\rho_s = c_{gel}\phi/\rho_s$.

Winterwerp (2002) tested equation 2.4 to existing data by fitting the model parameters and not actually using parameter values derived from data. A proper fit was obtained, using reasonable values for c_{gel}, as can be seen in figure 2.4. Note that different $w_{s,0}$ values are used.
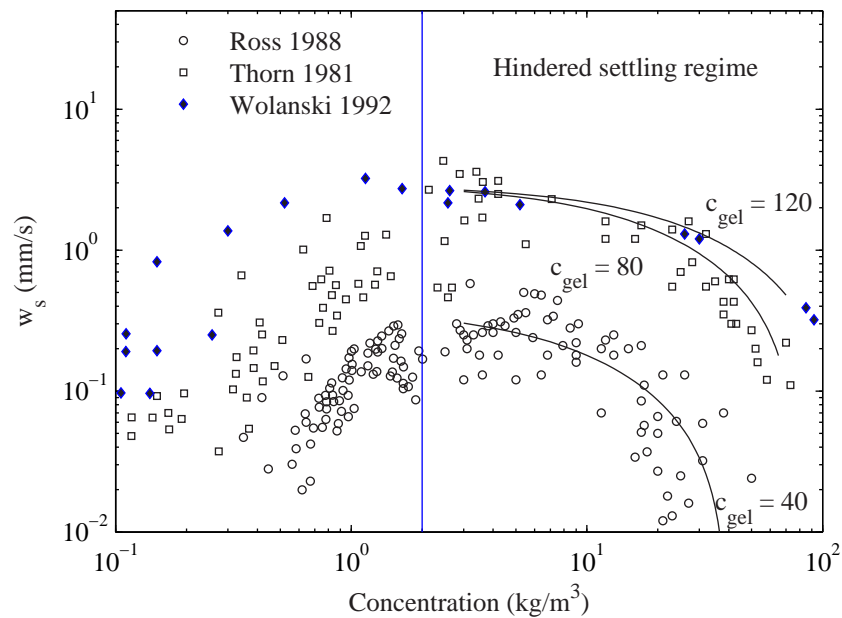

Figure 2.4. Comparison of equation 2.4 (with $m = 1$) with experimental data (Winterwerp, 1999).

The problem with many hindered settling experiments is that settling velocities are determined by visual observations of the settling of the interface only. Often this proves to be a difficult and subjective method as it is hard to determine an interface when it is smeared out into a more gradual concentration gradient because of segregation and possibly also because of non-homogeneous return flow effects. This gradient in concentration also results in a gradient in settling velocity, with the larger particles settling faster then the smaller particles. It is therefore important to use a narrow grain or floc size distribution.

Hulsey (1961) carried out experiments with equal sized glass spheres in settling tubes

to study the difference in settling velocity between the faster and slower settling particles. He found that the velocity of the fastest settling particles increased and the velocity of the slowest settling particles decreased, for larger clouds of particles. This he ascribed to the fact that the fast particles settle as a group in the so-called settling convection regime where most water flows around the particle group and not through them, decreasing the shear. Particles higher up in the vertical are retarded by the return flow and turbulence produced by the settling particles lower in the vertical. Hulsey (1961) states furthermore that grains falling in a turbulent system do not achieve the velocity they would have in still water without other particles; rather they achieve settling velocities characteristic only of the particular system in which they settle.

Another point in accurately predicting settling velocities of mud flocs is that often the permeability and density of flocs is not known. Johnson *et al.* (1996) showed experimentally that fractal aggregates composed of inorganic microspheres can settle on average 4 - 8.3 times faster than predicted for impermeable flocs. Johnson *et al.* (1996) explain this to be due to the heterogeneous distribution of primary particles in a fractal aggregate, assuming that flow through particles occurs. However, it is questionable whether flow through flocs increases the settling velocity, as flow through flocs increases the area that is affected by friction (Winterwerp & Van Kesteren, 2004). Other experiments (Moudgil & Vasudevan, 1988; Stolzenbach & Elimelich, 1994) have indicated that flow through flocs will be small or non-existent and that fractal aggregates are hardly permeable at fractal dimensions beyond $n_f = 2$ (Gregory, 1997). Therefore, we assume that flocs may be treated as porous, though impermeable entities.

2.1.5 Segregation

Larger particles in a suspension tend to settle faster than smaller particles, leading to a gradient in grain size. This is called sorting or segregation. Torfs *et al.* (1996) studied the occurrence of segregation in mud-sand mixtures by means of analysing data of earlier experiments. They found that in some mud-sand mixtures sand had fallen through the mud matrix and was collected at the bottom of the column. Figure 2.5 shows the size grading of the bottom and top layer of an experiment with Hong Kong mud ($c_0 = 1$ - 3 kg/m^3, $D_{50sand} = 230$ μm) before and after the input of sand. In the top panel the suspension contains no sand while in the lower panel the suspension contains 66% sand. The size grading indicates clear segregation between the top and the bottom of the bed for both tests. Furthermore there was increased segregation for the 66% sand tests where the bottom millimetre of the bed consisted entirely of sand (Torfs *et al.*, 1996). They concluded that the occurrence of segregation depends on a number of factors, such as the type of mud (mineralogical and chemical composition, organic content and biological processes) and the initial input density, as segregation occurs for initial mud concentrations below the gelling point. Segregation in the mud-only experiments was attributed to strong, compact flocs that sink rapidly to the bottom of the bed (Torfs *et al.*, 1996).
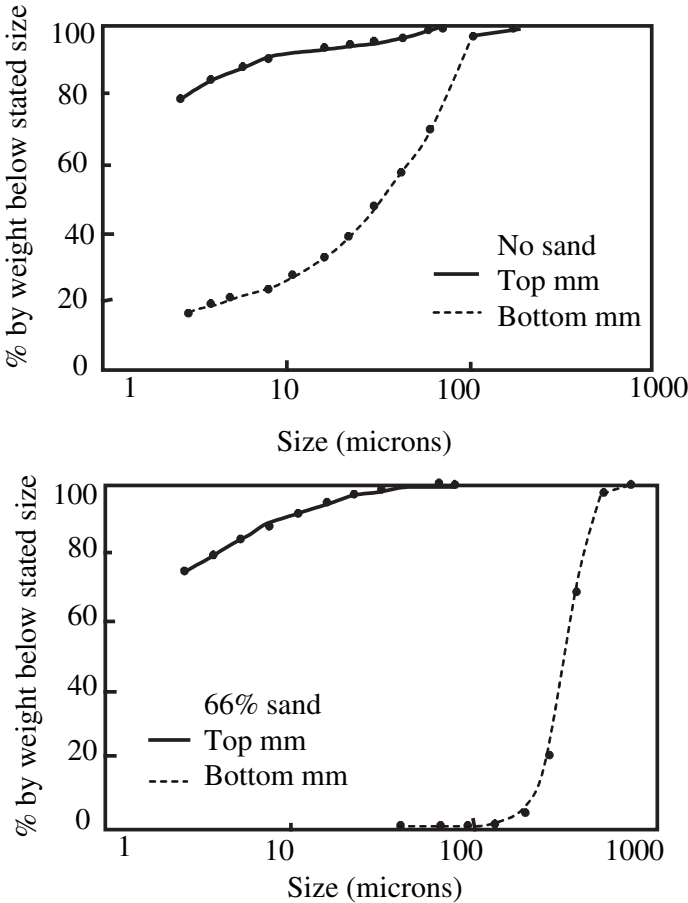
Figure 2.5. Size grading of the top and bottom millimetre of the bed before and after a single input of sand (Torfs *et al.*, 1996).

2.1.6 Consolidation

When mud flocs settle, the flocs that arrive first are squeezed by the flocs that settle on top of them. Pore water is driven out of the flocs and out of the space between the flocs. This process is known as self-weight consolidation (Terzaghi, 1943). It demonstrates the transition from a fluid-supported suspension to a soil, characterised by a change from a state in which pore-fluid pressures are equal to the vertical total stress, to a state defined by the existence of effective stress, at which pore-fluid pressures are less than the total vertical stress (Sills, 1998). Note that effective stress is a mathematical concept and not a real stress, defined by the difference between the total stress and the pore water pressure (Sills, 1998; Winterwerp & Van Kesteren, 2004). In figure 2.6 a vertical concentration profile with its corresponding pressure distributions is given. The concentration profile consists of a fluid supported part, the hindered settling phase, and a grain supported part, the consolidation phase. The hindered settling phase is characterised by equal pore and total pressures, while in the consolidation phase the pore pressures are smaller than the total pressure, indicating the presence of effective stresses. In figure 2.6 b, consolidation starts at $P = 0.17$ kPa, indicated by the development of effective stresses. This value corresponds in figure 2.6 a to a density of around 1200 kg/m^3. In soil mechanics this density is called the structural density.

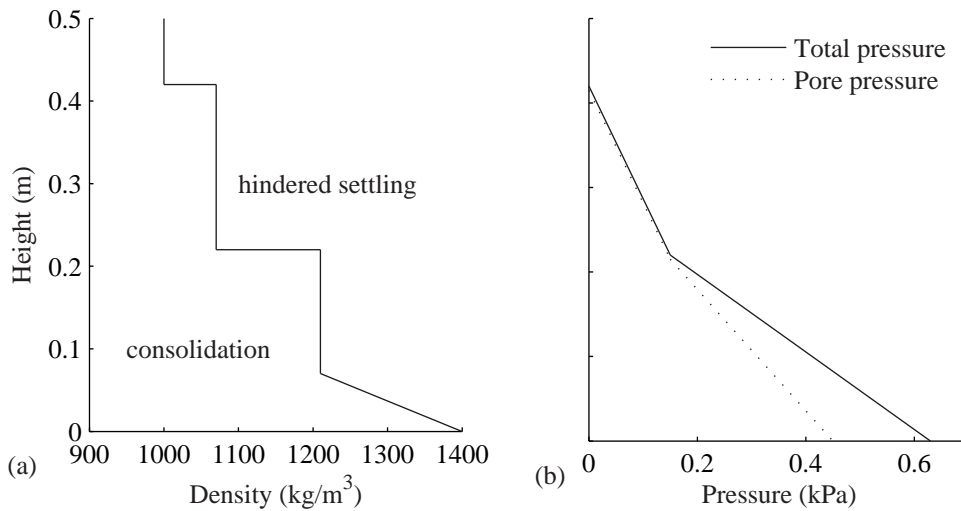**Figure 2.6.** Sketch of density profile and its corresponding pressure distribution at one stage in the settling and consolidation process, based on (Been, 1980) and (Sills, 1998)

2.1.7 Settling and hindered settling of mud-sand mixtures

Mono-dispersed particles in the hindered settling phase have a more or less uniform settling velocity. The same is true in the consolidation phase, although the settling rate is

lower. In the case of poly-dispersed particles, such as in mud-sand mixtures, there is a difference in the behaviour between those two phases. In the hindered settling phase there is segregation when the sand particles settle faster than the mud flocs. In the consolidation phase, however, sand particles are arrested in the mud matrix that has gained strength and all particles settle as one.

Wang *et al.* (1995) were one of the few to analyse the behaviour of the settling of non-cohesive sediment in clay suspensions. They propose an equation based on the Richardson & Zaki (1954) and Maude & Whitmore (1958) formule:

$$\frac{w_s^s}{w_{s,0}^s} = (1 - \phi_p^s)^n (1 - \phi_p^m)^{2.5} \tag{2.5}$$

in which w_s^s is the hindered settling velocity of the sand through the mud suspension, $w_{s,0}^s$ is the Stokes settling velocity of sand, ϕ_p^s the particle volume concentration of sand, ϕ_p^m the particle volume concentration of mud and n is a function of the particle Reynolds number, as in the Richardson & Zaki (1954) formula. They performed experiments with large amounts of quartz sand, plastic beads and gravel in both dilute and concentrated mud suspensions. For the dilute suspensions the model followed the experiments well, although with much higher values of n (i.e., $n \approx 8$) than suggested by Richardson & Zaki (1954). However, for high initial concentrations of the mud suspension the sediment finer than a critical diameter did not settle because the sand particles were arrested in the mud matrix. The critical diameter for this condition depends on the yield stress of the suspension and the specific weight of the sand particles. Therefore, sand particles coarser than the critical diameter did settle in the highly concentrated mud suspension. Wang *et al.* (1995) concluded that their model works well for the hindered settling of sand in dilute mud suspensions but deviates from the experiments if the mud concentration is so high that the critical diameter approaches the median diameter of the particles. The data set of Wang *et al.* (1995) cannot be used in this research as we try to determine the behaviour within highly concentrated mud suspensions with a low sand content, while Wang *et al.* (1995) deals with hindered settling in low mud concentrations (the hindered settling is caused by the large concentration of sand grains), and hindered settling in mud concentrations beyond the gelling concentration.

Volume effects are important in the hindered settling phase. For suspensions in which $\phi^s << \phi^m$, the return flow effect and viscosity effect are mainly determined by the mud fraction. Winterwerp & Van Kesteren (2004) derived a model to determine the settling velocity of both the mud and sand fraction separately:

$$w_s^m = w_{s,0}^m \frac{(1 - \phi^m - \phi_p^s)^m (1 - \phi_p^m - \phi_p^s)}{1 + 2.5\phi^m} \tag{2.6a}$$

$$w_s^s = (w_{s,0}^s - \phi^m w_{s,0}^m) \frac{(1 - \phi^m - \phi_p^s)^m}{(1 - \phi^m)} \frac{(1 - \phi_p^m - \phi_p^s)}{(1 + 2.5\phi^m)} \tag{2.6b}$$

The superscripts m and s define the mud and sand fraction respectively. Both buoyancy and augmented viscosity are accounted for in this model, as is the non-linear return

flow effect. At present this model has, however, not been tested as no suitable data are available. One goal of the present research is to create such data sets and at a later stage in this research this model will be tested upon them. As a first step, equation 2.6a is tested on mud-only experiments. If successful, both equation 2.6a and 2.6b will be tested on a mud-sand data set.

2.2 Theories of sedimentation

2.2.1 Kynch's Theory

Sedimentation of highly concentrated suspensions was analytically studied by Kynch (1951). He introduced an empirical relationship between settling velocity and local sediment concentration by assuming that at any point in a suspension the settling velocity of particles depends only on the local concentration of particles. This implies that the settling process can be determined from a continuity equation. In this section, Kynch's theory, with some further elaborations by Kranenburg (1992), is described.

First the vertical particle transport flux (S) is introduced:

$$S = w_s \phi \tag{2.7}$$

in which w_s is the effective settling velocity. The frame of reference is given in figure 2.7, where ϕ_0 is the initial volumetric concentration. The effect of hindered settling is introduced by assuming that the settling velocity is a decreasing function of the local sediment concentration,

$$w_s = w_{s,0} f(\phi) \tag{2.8}$$

where $w_{s,0}$ is the settling velocity of a single particle in still water and $f(\phi)$ is a function that describes the effect of the concentration on the settling velocity, and $f(0)=1$ and
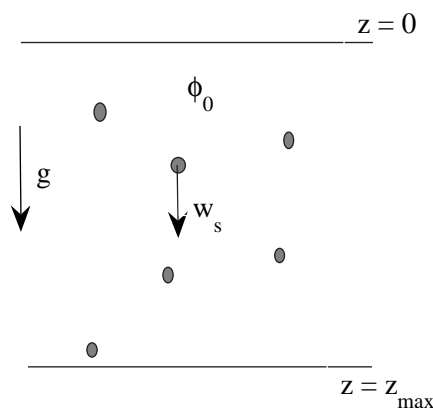

Figure 2.7. Frame of reference.

$f(1)=0$. The vertical, one-dimensional volume balance for a settling suspension can then be written as:

$$\frac{\partial \phi}{\partial t} + \frac{\partial S}{\partial z} = 0 \tag{2.9}$$

where t is time and z is the vertical coordinate, positive downward. When equation 2.7, 2.8 and 2.9 are combined, this leads to the following equation:

$$\frac{\partial \phi}{\partial t} + w_{s,0}F(\phi)\frac{\partial \phi}{\partial z} = 0 \tag{2.10}$$

where

$$F(\phi) = \frac{\mathrm{d}}{\mathrm{d}\phi}[\phi f(\phi)] \tag{2.11}$$

Equation 2.10 is a 1-D wave equation. In this case it describes the settling of a cohesive sediment suspension in still water. It can be used for settling in the hindered settling phase and in the first part of the consolidation phase where effective stresses are small and the diffusion term is negligible. This will be explained further in Section 2.2.2. The simple wave equation is hyperbolic and its solution allows for the formation of shocks. It can be solved by integrating along characteristic lines in the (z,t) plane. These characteristic lines are given by:

$$\frac{\mathrm{d}z}{\mathrm{d}t} = w_{s,o}F(\phi) = C_c \tag{2.12}$$

presenting lines of equal concentration, where C_c is the celerity (wave speed). The height of the characteristics in time is given by:

$$z(t) = z_0(\phi) + w_{s,0}F(\phi)t \tag{2.13}$$

where $z_0(\phi)$ is the initial height of a specific characteristic. When characteristics converge and cross there will be a jump in concentration, called an interface. Two characteristic lines converge if $\frac{\mathrm{d}z}{\mathrm{d}z_0}$ decreases with time (figure 2.8). Differentiating equation 2.13 gives:

$$\frac{\mathrm{d}z}{\mathrm{d}z_0} = 1 + w_{s,0}\frac{\mathrm{d}F}{\mathrm{d}\phi}\frac{\mathrm{d}\phi}{\mathrm{d}z_0}t \tag{2.14}$$

As an interface develops when characteristic paths converge, equation 2.14 implies that an interface will therefore develop when $\frac{\mathrm{d}F}{\mathrm{d}\phi} < 0$, as $\frac{\mathrm{d}\phi}{\mathrm{d}z_0}$ is in general not negative. In settling columns, an interface will always develop between the water above the suspension and the settling suspension. As this upper interface is always present (in a mono-dispersed suspension), and a lower interface will develop when characteristics in the suspension cross, it can be concluded that when:

$$\frac{\mathrm{d}F}{\mathrm{d}\phi} < 0 \tag{2.15}$$

two interfaces develop and when

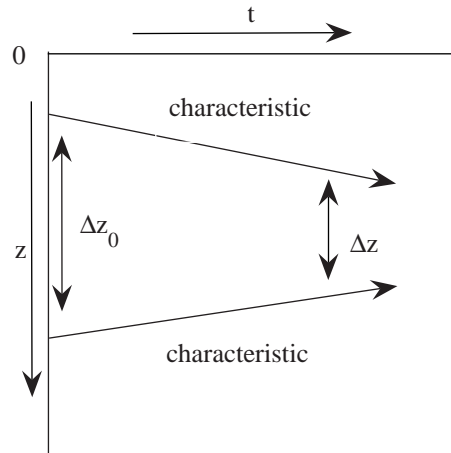$$\frac{\mathrm{d}F}{\mathrm{d}\phi} > 0 \tag{2.16}$$

Figure 2.8. Two converging characteristics.

one interface develops. In the latter case the concentration within the suspension increases gradually as there is no interface in the suspension. These two types of settling may both exist, depending on the initial concentration. For suspensions that can settle at both modes there is a concentration, ϕ_{cr}, at which the behaviour changes from settling with two interfaces to settling with one interface. It is obvious that any hindered settling model should be able to account for this behaviour.

So we conclude that the interference between characteristics can result in a jump in concentration or a gradual change in concentration. A jump in concentration is called an interface and it can form a regular shock or a compound shock wave. These occur when the characteristic lines cross from both sides (figure 2.9 a) or from one side (figure 2.9 b), respectively. A gradual change in concentration, in which no interface is present as the characteristics diverge, is called a rarefaction wave (figure 2.9 c). The upper interface in
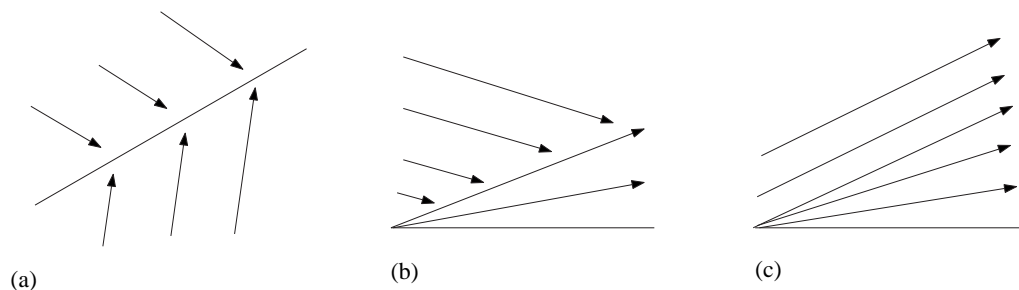

Figure 2.9. Three possible types of characteristic wave paths. (a): Regular type; (b): Compound type; and (c): Rarefaction type (After Bartholomeeusen *et al.*, 2003).

a settling suspension consists generally of a regular shock wave. In the suspension itself all three types of waves are, theoretically, possible. A regular or compound shock wave in the case of $dF/d\phi < 0$, and a rarefaction wave in the case of $dF/d\phi > 0$. A regular shock wave is, however, highly unlikely to occur. In experimental situations there is, if a lower interface is present, generally a gradual increase from the shock towards the gelling concentration (Toorman, 1992), indicating a compound shock wave.

Whether compound, regular or rarefaction waves occur depends on the flux function ($S(\phi)$) and the position of the initial volumetric concentration on the flux function. Bartholomeeusen *et al.* (2003) and Bustos *et al.* (1999) show that the speed of the shock wave, s, is determined by the Rankine Hugoniot Jump Condition:

$$s = \frac{S(\phi_u) - S(\phi_d)}{\phi_u - \phi_d} \tag{2.17}$$

and that a regular or compound shock occurs when Oleinik's Jump Entropy condition is fulfilled (Bustos *et al.*, 1999):

$$\frac{S(\phi) - S(\phi_u)}{\phi - \phi_u} \geq s \geq \frac{S(\phi) - S(\phi_d)}{\phi - \phi_d}$$
$$\text{or}$$
$$w_{s,0} F(\phi_u) \geq s \geq w_{s,0} F(\phi_d) \tag{2.18}$$

with ϕ_u and ϕ_d the volumetric concentrations just above and just below the shock respectively. When equation 2.18 is not fulfilled there will be a gradual transition of concentration (rarefaction wave, figure 2.9 c).

Kynch (1951) analysed three types of flux density functions (S): a concave function, a function with one inflection point and a function with two inflection points. Bustos *et al.* (1999) distinguish seven different types of sedimentation within these three types of flux functions. They state that a concave flux density function is purely theoretical, that two modes of sedimentation exist for flux density functions with one inflection point and the remaining four modes of sedimentation only exist for two inflection points. The flux functions with two inflection points have modes that are similar to the flux functions with one inflection point, but the second inflection point produces an additional discontinuity or interface (Bürger & Tory, 2000). We focus on the first three modes of sedimentation as given in Bustos *et al.* (1999). Definition sketches of these three modes are shown in figure 2.10 and are explained below.

- MS-1: Two regular shock waves (sharp interfaces). The concentration jumps from zero to ϕ_0 and changes abruptly from ϕ_0 to ϕ_{max}, where ϕ_{max} is the volumetric concentration of a consolidated soil. This mode is purely theoretical.

- MS-2: A regular shock wave followed by a compound shock wave and a rarefaction wave. The concentration jumps from zero to ϕ_0 and changes suddenly from ϕ_0 and then increases gradually to ϕ_{max}.

- MS-3: A regular shock wave and a rarefaction wave. The concentration jumps from zero to ϕ_0 and increases gradually from ϕ_0 to ϕ_{max}.

This figure shows that the slope of the hindered settling area (S1) and thus the actual settling velocity of the suspension, is derived from the flux function by drawing a line from the origin to $S(\phi_0)$. The slope of the second interface (compound shock wave C1 in figure 2.10 b) is derived by taking the tangent to the flux function from $S(\phi_0)$, while the slopes of the characteristics can be determined by taking the tangent at $S(0)$, $S(\phi_0)$ and $S(\phi_{max})$ respectively. In figure 2.10, a represents the inflection point of S, indicating the volumetric concentration (ϕ_{cr}) at which the settling behaviour changes from settling with two interfaces to settling with one interface. For both MS-1 and MS-2 $\phi_0 < \phi_a$, indicating
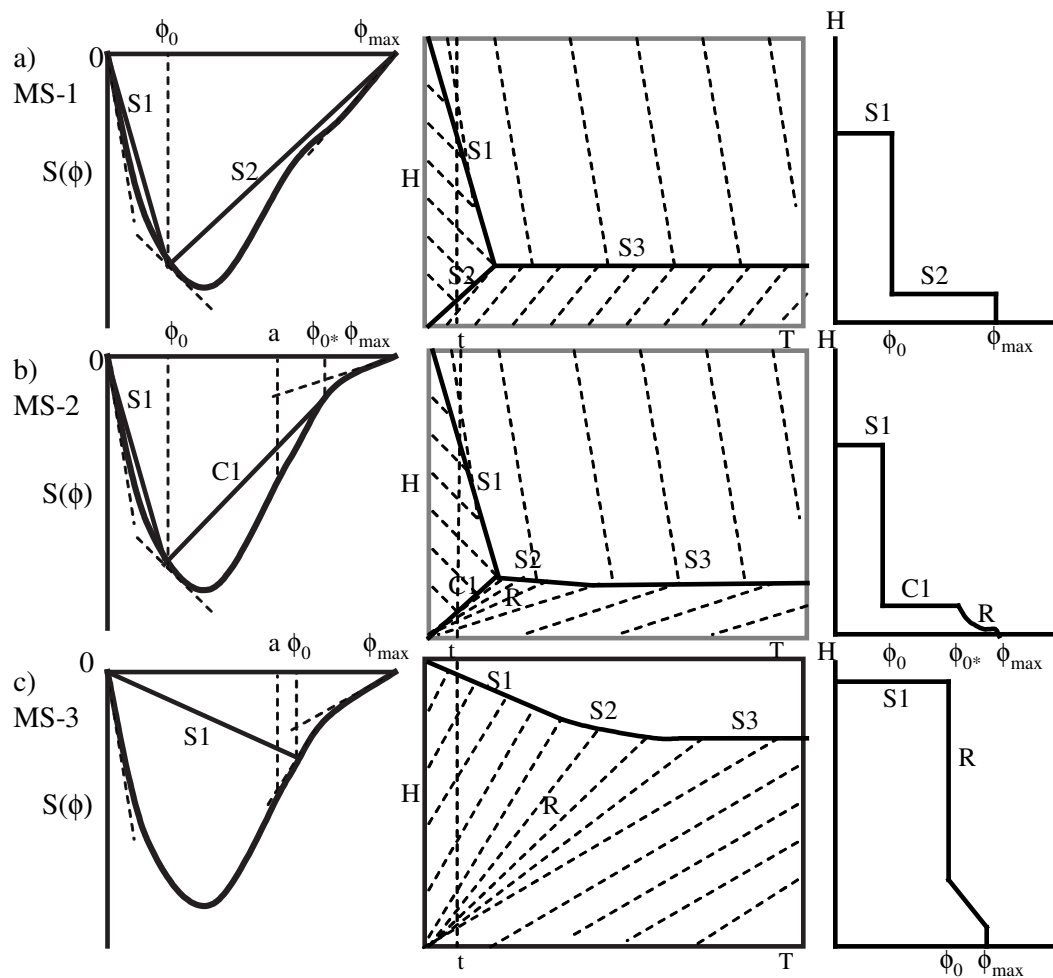

Figure 2.10. Modes of sedimentation, showing the flux plot, the settling plot with characteristics and shock lines and a representative concentration profile at time $t = t^*$. Chords in the flux plots and settling plots with the same slopes are marked by the same symbols, S is regular shockwave, C is compound shockwave and R is rarefaction wave (Bürger & Tory, 2000).

two interfaces, while for MS-3 $\phi_0 > \phi_a$, indicating one interface. However, MS-1 types, where a regular shock occurs within the suspension, are highly unlikely to occur. In the MS-1 types the characteristics do not form a fan. This means that the suspension jumps immediately to a consolidated soil. The other two modes, MS-2 and MS-3, do occur in settling suspensions.

2.2.2   From theory to application

The ultimate purpose of this research is to derive a formulation for the settling behaviour of sediment in complex 3D models. For this purpose, an "integral" advection-diffusion equation was derived (Winterwerp & Van Kesteren, 2004) that accounts for both the (hindered) settling and consolidation regime and which can be applied from the water surface into the bed. This advection-diffusion equation for hindered settling and consolidation of a suspension reads:

$$\frac{\partial \phi_p}{\partial t} = \frac{\partial}{\partial z}\left(\Xi_s \phi_p\right) + \frac{\partial}{\partial z}\left((D_s + \Gamma_T + \Gamma_c)\frac{\partial \phi_p}{\partial z}\right) \tag{2.19}$$

where ϕ_p $(= c/\rho_s)$ is the volumetric primary particle concentration of the solids fraction, Ξ_s is the settling function (Winterwerp & Van Kesteren, 2004), D_s is the molecular diffusion coefficient, Γ_c is the diffusion component (i.e. consolidation coefficient) in the consolidation formula and Γ_T is the eddy diffusivity in which fractal theory has been used. The advection-diffusion equation can be rewritten as:

$$\frac{\partial \phi_p}{\partial t} = \frac{\partial}{\partial z}\left[\Xi_s \phi_p + (D_s + \Gamma_T + \Gamma_c)\frac{\partial \phi_p}{\partial z}\right] = \frac{\partial}{\partial z}\left[\text{Flux}(\phi_p)\right] \tag{2.20}$$

The settling function in the advection term consists of two parts:

$$\Xi_s = w_{s,eff} + \frac{f_c}{1 + \eta f_c} \tag{2.21}$$

in which the first term is the particle flux in the hindered settling regime and the second term the particle flux in the consolidation regime with $w_{s,eff}$ is the effective settling velocity, η is a heuristic parameter to obtain a smooth transition between the descriptions for hindered settling and permeability and

$$f_c = \frac{\rho_s - \rho_w}{\rho_w} k \phi_p \tag{2.22}$$

with ρ_s is the solids density, ρ_w is the density of water and k is the permeability.

   The diffusion term in equation 2.20 describes consolidation when the effects of effective stress and permeability are dominant, while the consolidation part in the advection term describes early consolidation when the effect of permeability is dominant. The flux in equation 2.20 can thus be divided into three phases, namely a hindered settling phase, a phase where the effects of permeability are dominant and a phase where the effects of
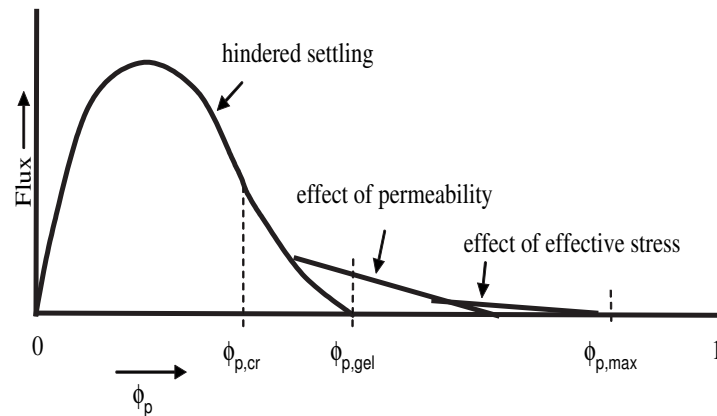
Figure 2.11. A sketch of the flux in equation 2.20 as a function of ϕ_p. Three process are incorporated in the flux: hindered settling, the effect of permeability and the effect of effective stress. For clarity, the joint effect of effective stress and permeability, as modelled in the diffusion term, is referred to as the effect of effective stress only.

effective stress are dominant. The latter two comprise consolidation. Of course, these regimes may overlap partly. A similar kind of division is made by Lester *et al.* (2005).

The complete advection-diffusion equation cannot be solved with Kynch's method. However, when the diffusion term in equation 2.20 is small, only the settling function is left, and the equation reduces to the simple wave equation which can be solved with the method of characteristics. The first stage of consolidation, where permeability effects are important, is still incorporated in this equation and can thus be solved, c.q. analysed, with this same method of characteristics that was described in the previous section.

Figure 2.11 shows a sketch of the complete flux function of equation 2.20. The hindered settling part ends at $\phi_{p,gel}$ where the flux, if we only account for the hindered settling flux, is 0. The definition of $\phi_{p,gel}$ that is used in this research comprises nothing more than that at that concentration the hindered settling function yields $w_{s,eff} = 0$. By incorporating the effects of consolidation (both permeability and effective stress), the settling flux reduces slower, becoming 0 at $\phi_{p,max}$ only, i.e. the most dense packing. ϕ_{cr} depicts the (first) inflexion point of the flux function and indicates the change between settling with two interfaces to settling with one interface.

Permeability effects start to become important around $\phi_{p,gel}$ from just before the end of the hindered settling phase till the beginning of consolidation phase where effective stresses are important. This implies the existence of 5 stages: a hindered settling area, an area where hindered settling overlaps with the effects of permeability, an area where permeability effects are dominant, an area where the effects of permeability overlap with the effects of effective stress and an area where effective stress is dominant (figure 2.11). In the latter three cases we are dealing with consolidation. In the second stage we are dealing with hindered settling combined with the permeability effects of starting consolidation. This is the area which we refer to as the fluid mud phase (we realise that this is not a
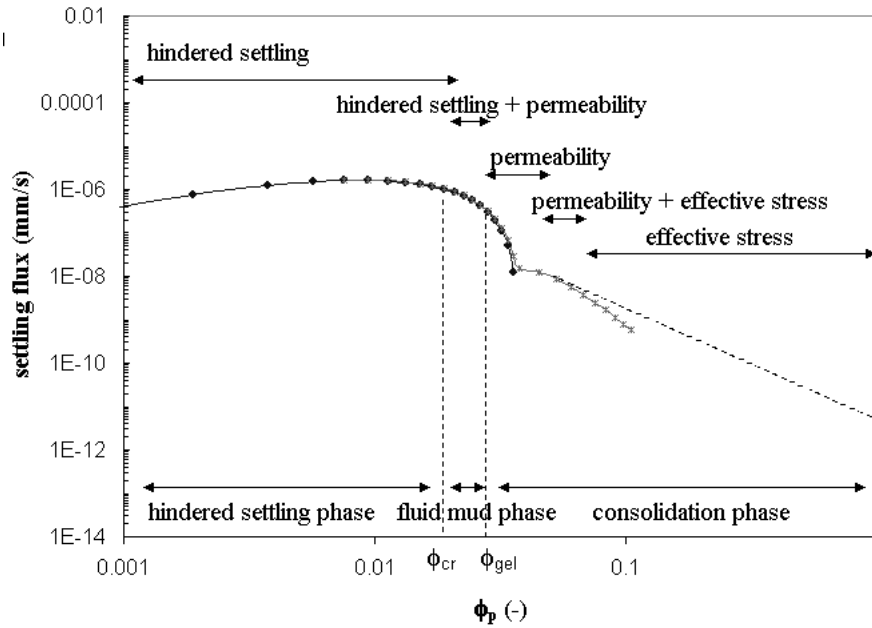
Figure 2.12. Double logarithmic plot of the settling flux against ϕ_p.

common definition for fluid mud). In theory, hindered settling takes place in this area as $\phi_p < \phi_{p,gel}$. In reality, the effects of permeability influence the settling behaviour when ϕ_p approaches $\phi_{p,gel}$ and Darcy's law becomes relevant. The 5 stages can be reduced to 3 phases: the hindered settling phase, the fluid mud phase and the consolidation phase, based on the behaviour within the 5 stages.

As said, here we define the change between hindered settling and consolidation with $\phi_{p,gel}$. In soil mechanics the change from hindered settling to consolidation is set at the concentration where a measurable strength builds up. We appreciate that effective stresses may develop at $\phi_p < \phi_{p,gel}$. However, it can be shown (Winterwerp & Van Kesteren, 2004) that at $\phi_{p,gel}$, the effective stress ≈ 1 Pa, which amounts to a few tenth promille of the total stress in the bed. Therefore, we distinguish between ϕ_{gel}, which marks the transition between hindered settling and consolidation, and ϕ_{struc}, which marks the onset of a (measurable) effective stress.

These 5 separate stages and 3 phases are again shown in figure 2.12 where a log-log plot of the complete settling flux against volumetric particle concentration is given, based on data presented in Winterwerp & Van Kesteren (2004). It shows an area with hindered settling, followed and overlapped by an area of early consolidation where permeability is important, followed and overlapped by an area of consolidation where the effect of effective stress is important, followed by an area where only effective stress is important.

The types of sedimentation in figure 2.10 are shown again in 2.13 but now with the definitions that will be used in this thesis. The equations are all related to the volumetric floc concentration (ϕ) instead of ϕ_p and in this research we define $\phi = 1$ at c_{gel}, implying that ϕ can become larger than unity when consolidation takes place. Instead of the often
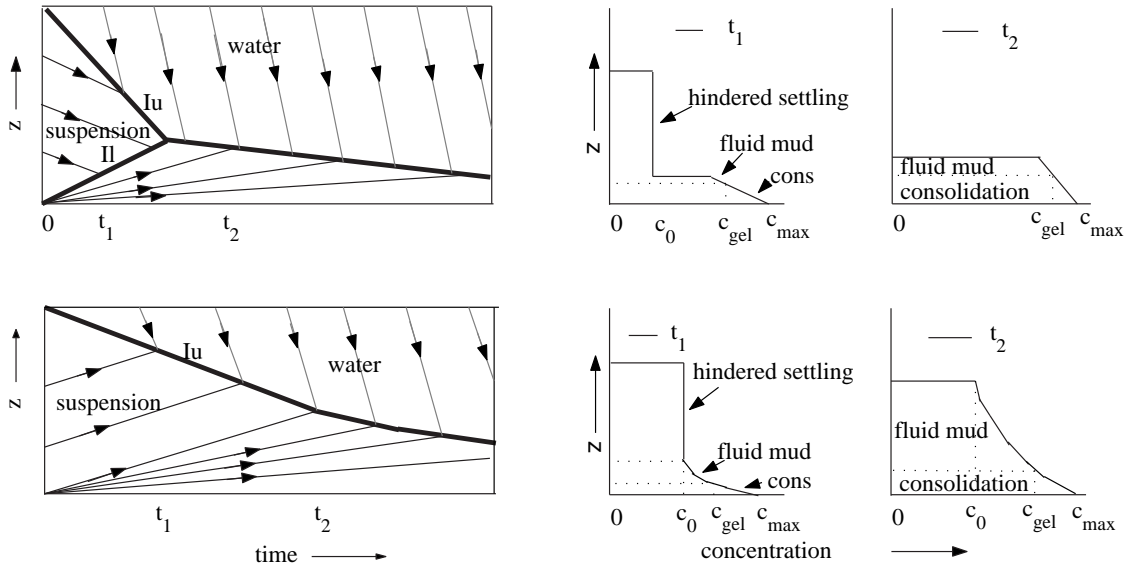
Figure 2.13. The two different settling behaviours for uniform initial concentration distributions according to Kynch. Characteristic lines (marked with arrows), interfaces (Iu = upper interface, Il = lower interface) and concentration distributions at two time levels. Adjusted from (Kranenburg, 1992).

used structural density ρ_{struc} we choose to use c_{gel} as the division between hindered settling and consolidation, as reasoned above.

In the top panel $\phi_0 < \phi_{cr}$ and $dF/d\phi < 0$, which means there are two interfaces. The interfaces are indicated by the converging characteristics. The upper interface is a regular shock, while the lower interface is a compound shock (see also figure 2.9 a and b), later followed by a rarefaction wave. As explained before, we refer to the area above the compound shock as the hindered settling phase and below, at $\phi < 1$ as fluid mud phase and at $\phi > 1$ as consolidation phase. Figure 2.13 shows that three different phases are defined, but only two processes. Hindered settling takes place in the hindered settling and in the fluid mud phase, while consolidation takes place in the consolidation phase.

In the lower panel $\phi_{cr} < \phi_0 < \phi_{gel}$. The characteristic lines intersect with each other to form an upper interface (regular shock). In the suspension itself the characteristics do not intersect and a rarefaction wave is formed (see also figure 2.9 c). The area in which the characteristic lines are parallel to each other is still the hindered settling phase. Lower in the suspension the concentration increases gradually, which is indicated by the diverging characteristics. This is the start of the fluid mud phase, which changes to the consolidation phase when the concentration becomes larger than the gelling concentration.

The hindered settling function $f(\phi)$ in equation 2.8 can be specified now, and by applying the theory mentioned in section 2.2.1, the behaviour according to different hindered settling functions can be predicted. Figure 2.14 shows the behaviour of two different hindered settling functions (f, as given by equation 2.4 and 2.3) and their derivative, F. For equation 2.4, $m = 1$, and for equation 2.3, $n = 4$. In both cases, f decreases monotonically
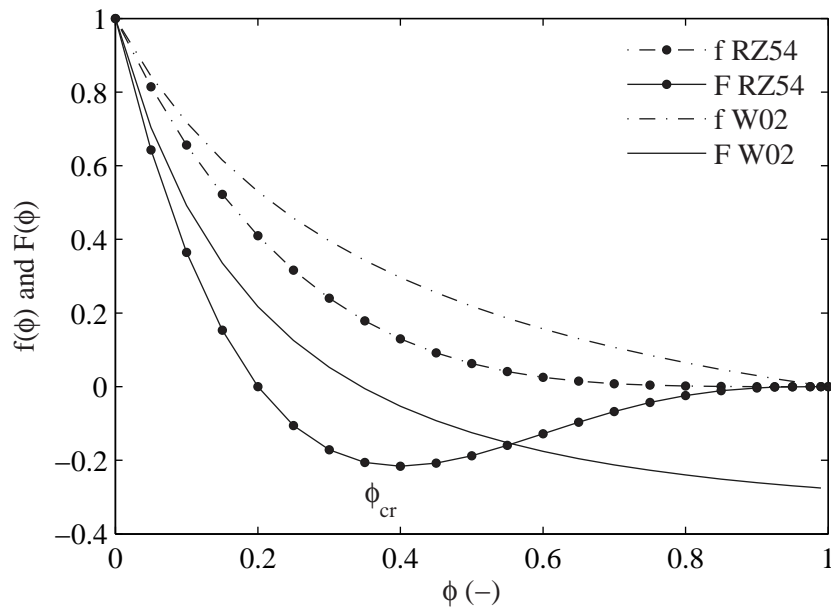
Figure 2.14. Variation of hindered settling functions f and F with ϕ for equation 2.3(RZ54) ($k = 1$, n $= 4$) and equation 2.4 (W02) ($m = 1$), after Kranenburg (1992) and Winterwerp & Van Kesteren (2004).

with ϕ. Its derivative F, however, behaves differently for both cases. For equation 2.3, F has a minimum at a volumetric concentration ϕ_{cr}. From equation 2.15 and 2.16 it can be seen that this indicates the change in sign of $\frac{\mathrm{d}F}{\mathrm{d}\phi}$, and thus, the change from the occurrence of two interfaces in a settling suspension to the occurrence of one interface. Equation 2.4 does not have such a minimum. This means that equation 2.15 is always valid and all settling suspensions are expected to develop two interfaces during settling according to equation 2.4.

We will use this theory to analyse the experimental data in Chapters 3 and 4. Furthermore, we will develop a proper model that accounts for the above described theory by allowing both types of settling.

3

Hindered settling of mud

3.1 Introduction

In Chapter 2 background information on mud was given and theories on the settling of highly concentrated suspensions were introduced. With these theories we analysed the settling behaviour of cohesive sediment suspensions analytically. In this chapter settling experiments on highly concentrated suspensions are described and analysed, and specific characteristics of the suspensions are derived. For the analysis, Kynch's theory of a settling suspension is applied. The derived characteristics and parameter values shall be used in the model in Chapter 5.

3.2 Experimental set-up

3.2.1 Experiments

The settling experiments on mud alone were performed in the laboratory of the Environmental Fluid Mechanics Section at Delft University of Technology, using acrylic columns with a height of 40 cm and a diameter of 7 cm. The suspensions were prepared with kaolinite, a clay mineral with relatively low cohesion. The mineral was diluted with salt water ($\rho = 1003$ kg/m^3) to a suspension with a concentration of about 100 - 120 kg/m^3. A 12-litre tank was filled with this mixture which was stirred thoroughly for at least 2 hours every day during at least two weeks, in order for the kaolinite suspension to reach a steady chemical state (de Wit, 1992).

Sixteen experiments with varying initial conditions was carried out in two series. The second series of experiments was performed two months later than the first series, but with the same initially prepared suspension. For every experiment a sample was taken from the tank and diluted with salt water to the desired initial concentration, whereafter it was poured in one of the settling columns and mixed thoroughly before allowing it to settle.

3.2.2   Settling of the interface

For various initial sediment concentrations the lowering of the interface of the kaolinite suspensions in the settling columns was measured. Before every experiment, the suspension was stirred gently, with a minimum disturbance of the flocs, but thoroughly enough to create a homogeneous mixture. Thereafter, the measurements started immediately. During the experiments the settling of the interface was observed visually. The height of the interface was recorded at an interval of one minute. Once the settling slowed the recording time step was increased to 5 minutes. The measurements led to settling curves for the different suspensions. Possible lower interfaces, the bed interfaces, could not be detected visually. Their development in time is thus not available.

3.2.3   Concentration profiles

Sediment concentrations were measured by means of a conductivity probe developed by Delft Hydraulics. The principle of the conductivity probe is based on the fact that the conductivity of a sediment mixture decreases when the sediment concentration increases. The probe has four electrodes and is supplied with an alternating current to eliminate polarisation effects.

The aim was to measure the concentration at several heights during the settling and consolidation phase. Measuring concentration profiles in the vertical is a destructive process as the probe damages the structure of the suspension and bed. Therefore it was decided that every experiment should be repeated several times with the concentration measured at different heights. For the experiments in the first series, three different levels were selected for every experiment, depending on the initial concentration and the expected level at which a bed structure would be formed. For the experiments in the second series, four different levels were selected. In general one measurement was done in the top layer, one or two in the middle part and one 5-10 cm above the bottom of the column.

A calibration was performed before every measurement. To calibrate the probe the suspension had to settle first. Then, with a pipette, two samples were taken from the settled sediment and one from the clear water above. The samples were placed in a small jar. The conductivity was measured and the density of the suspensions was determined with an Anton Paar density meter. Thereafter, the settled suspension in the settling column was mixed thoroughly and another sample was drawn from the suspension. From this sample, the density and conductivity were determined as well, whereafter calibration curves were drawn for each experiment. Calibration before every experiment was necessary as the probe is sensitive to temperature changes and different amounts of solutes in the water. It is noted that during the experiments, which had a duration of approximately one hour, the temperature in the settling column always increased. This, as a result, increased the conductivity, leading to an under-estimation of the concentration. The maximum under-estimation of the concentration data used in this analysis is about 5 kg/m^3. Furthermore, due to the settings of the software of the conductivity probe, the measured concentrations have a resolution of $\pm$ 2 kg/m^3. However, because the initial

concentration for every experiment is known exactly and the shape of the calibration profile is very much the same within one experiment, the actual error is estimated to lie within a range of ± 5 kg/m^3. The same method as described above was used to measure the consolidated bed profiles. The bed profiles could only be measured once, as the penetration of the conductivity probe destroyed the bed structure.

3.3 Results

3.3.1 Settling curves

For all sixteen experiments the effective settling velocity of the suspension is determined (table 3.1). The effective settling velocity can be derived from the first derivative of the initial settling curves. All settling curves are shown in figure 3.1. Kynch (1951) described two distinct types of settling curves (figure 2.13) which can be recognised in figure 3.1 as well. The first type of settling curve in figure 2.13 is indicated by a profile with a steep hindered settling part followed by an inflection point and a less steep consolidation part with two interfaces. In figure 3.1 the curves with initial concentrations up to 50 - 70 kg/m^3 show that kind of behaviour. The upper interface in figure 2.13 is the actual settling curve in figure 3.1, while the lower interface in figure 2.13 is represented by an imaginary line from the origin to the point of contraction (the inflection point) in figure 3.1.
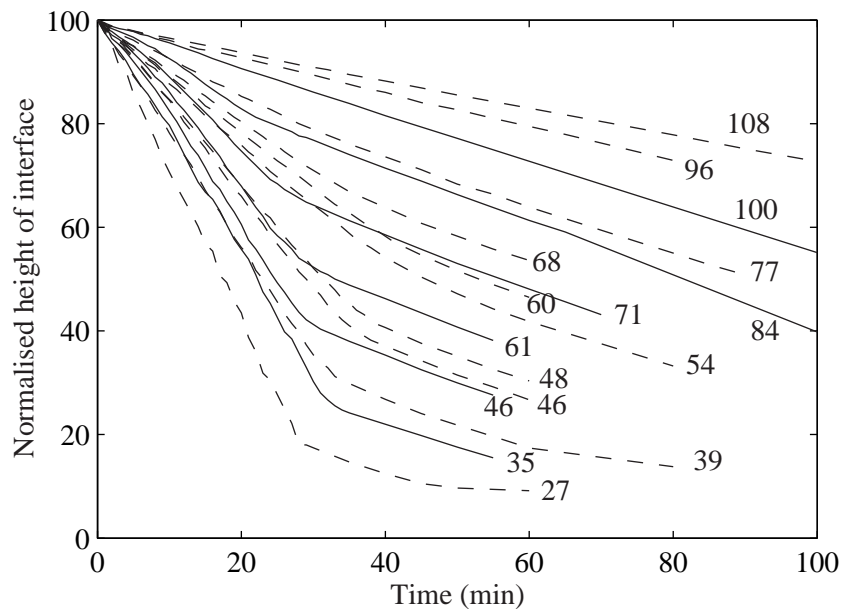

Figure 3.1. Normalised settling curves for different initial kaolinite concentrations. Solid lines represent Series 1, dashed lines represent Series 2. Numbers indicate the initial concentration (kg/m^3). The initial height varied between 34 and 37 cm.

The second type of settling curve in figure 2.13 is indicated by a gently sloping, curved line. This type has only one interface, the upper interface, and according to the curves in figure 3.1, this behaviour occurs when the initial concentration is larger than 50 - 70 kg/m^3. In this case there is either a short hindered settling phase followed by consolidation ($\phi_{cr} < \phi_0 < \phi_{gel}$) or consolidation from the start ($\phi_0 > \phi_{gel}$).

Besides the settling velocity, the fractal dimension, n_f, can be derived from the settling profiles (table 3.1). The fractal dimension of a mud floc can be any number between 1 and 3. Very elongated flocs will have a n_f close to 1, while in the case of fully massive cubicle particles $n_f = 3$. The fractal dimension can straightforwardly be determined from the measured settling interfaces versus time plots on double logarithmic scales as shown in Merckelbach (2000). This author found values of $n_f \approx 2.75$ for natural consolidating mud. For our experiments the fractal dimensions are much lower.

The effective settling velocities of the suspensions and other experimentally derived parameters are given in Table 3.1. Only the velocities of the part above the point of contraction are elaborated as this research focuses on the hindered settling phase.

Table 3.1. All experiments with their initial concentration, effective settling velocity, gelling concentration and fractal dimension.

Id	c_0 (kg/m^3)	w_s (mm/s)	c_{gel} (kg/m^3)	n_f
30kol	35	0.134	66	2.31
40kol	46	0.111	83	2.38
50kol	61	0.071	87	2.45
60kol	71	0.058	90	2.43
70kol	84	0.052	-	2.36
80kol	100	0.028	-	2.51
10tt	27	0.170	-	2.61
20tt	39	0.133	80	2.36
30tt	46	0.101	67	2.37
40tt	48	0.096	77	2.40
50tt	68	0.067	88	2.53
55tt	54	0.075	85	2.37
60tt	77	0.059	-	2.43
70tt	60	0.044	83	2.46
80tt	96	0.022	-	2.60
90tt	108	0.019	-	2.62

3.3.2   Gelling concentration

The gelling concentration (c_{gel}) is an important property. It indicates when particles in a suspension start to come in contact with each other and build up a framework. This means that the suspension starts to gain strength and consolidates. It thus indicates the change between a phase where particles settle individually, to a phase where particles form part of a suspension that settles homogeneously. It is difficult to determine the gelling concentration and two methods can be used to derive it. In general, gelling concentration is determined on the basis of the mass balance of the settling profile and from average concentrations above and below the lower interface. This method gives an approximation of the gelling concentration as it only gives accurate results when there is no consolidation. The gelling concentration with this method is given by:

$$hc_0 = \int_0^{h(t)} cdz = \int_0^{\delta_1} cdz + \int_{\delta_1}^{h} cdz \approx c_{\text{gel}}\delta_1 + c_2\delta_2 \tag{3.1}$$

leading to:

$$c_{\text{gel}} = \frac{c_0 h - c_2\delta_2}{\delta_1} \tag{3.2}$$

in which c_0 is the initial concentration, h is the initial height, c_2 is the concentration in the area from the upper interface to the shock or lower interface (figure 3.2, in which $c_2 = c_0$, thus c_2 is constant over δ_2), δ_2 is the height from the top interface to the lower interface at time t_1, δ_1 is the height from the lower interface to the bottom of the column at time t_1 and c_{gel} is the concentration between the 2nd interface and the bottom (assumed to be constant over δ_1). This means that the calculated c_{gel} is approximated by the average concentration over δ_1. In figure 2.13, top panel, it can be seen that the characteristic lines in that area form a fan and the concentration increases towards the bed. In reality, the gelling concentration is reached at the top of the δ_1 layer, and its representation by an average value is not accurate. With this method a gelling concentration of 109 ± 8 kg/m^3
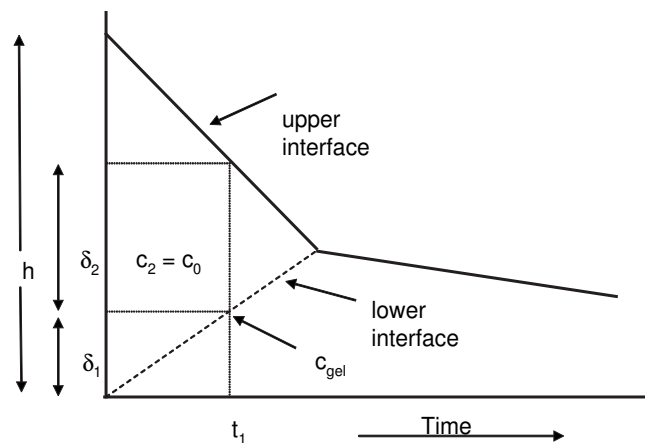

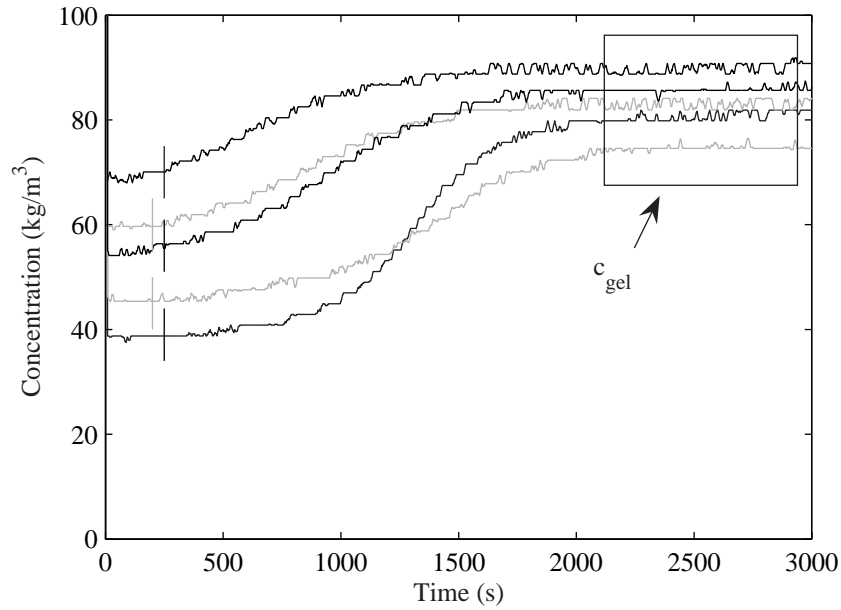**Figure 3.2.**   Determining the gelling concentration from a settling curve.

Figure 3.3. Concentration time series for experiments with different initial concentrations. At t=0 from top to bottom: c_0=68, 60, 54, 48, 39 kg/m³; the vertical lines represent the estimated experimental error.

is obtained for the experiments. The actual value of c_{gel} will be lower, as the concentration of the suspension in layer δ_1 is affected by consolidation.

A second method to obtain c_{gel} is to use measured concentration profiles. It was found that a conductivity meter, placed a few centimeters above the bottom of the column, could be used for this purpose. Some of the concentration time series measured are shown in figure 3.3. In these profiles the concentration increases gradually in time until the gelling concentration is reached (boxed area in figure 3.3), where the rise stops. At this point the mud flocs are in contact with each other and consolidation starts, which is a slow process. The gelling concentration has been derived from this method for most of the experiments, except for the ones in which the initial concentration was already higher than the gelling concentration, or for the experiments in which the conductivity probe was placed too high. From the measurements with the conductivity meter a mean gelling concentration of 81 ± 8 kg/m³ is obtained, which is lower than the value of the previous method.

Gelling concentrations determined with the conductivity probe are shown in figure 3.4. A trend of increasing gelling concentration for increasing initial concentration is visible. This was expected, as higher concentrations result in larger flocs and the gelling concentration depends on floc size. Other factors that influence the floc size and thus the gelling concentration are history effects, flow effects, the type of sediment and the type of environment (e.g. salt water or the availability of organic material). Figure 3.4 shows, and it is acknowledged that, the gelling concentration is not a constant. However, our final goal is to model the settling behaviour. For predictability it is easier to use a mean
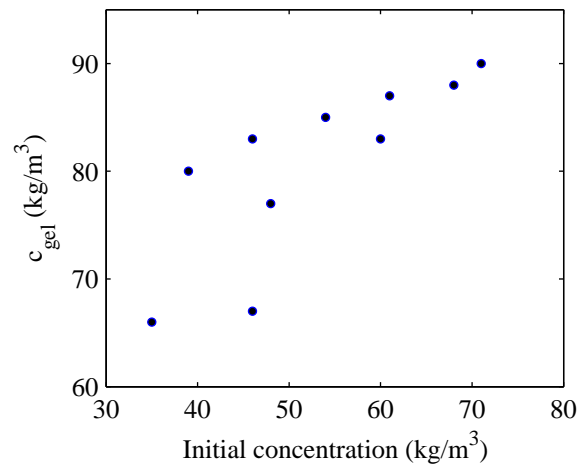
Figure 3.4. Measured gelling concentrations.

gelling concentration. In this research, the mean gelling concentration that was derived with the second method ($c_{gel} = 81$ kg/m^3) will be used. The maximum and minimum gelling concentrations can be used to determine the sensitivity. For more advanced model results, the gelling concentration can be made dependent on the floc size. The latter is beyond the scope of this research.

3.3.3 Characteristics

Kynch's theory of a settling suspension, in which hindered settling is described as a hyperbolic problem, is explained in Chapter 2. A hyperbolic problem can be solved with the method of characteristics. Inherent to this method is that it allows for the formation of shocks (interfaces). This theory is used for the analysis of the experimental results in order to see whether shocks will occur during settling. A first step is to draw characteristic lines from the data. In the section of application (section 3.3.5) the experimentally drawn characteristics are compared to those drawn according to the theory.

In figure 3.5 six settling curves are shown with their characteristics. These characteristics are based on experimental results. The conductivity meter was used to determine the concentration at three or four different heights in the settling suspension and in the bed, whereafter points of equal concentration could be connected through characteristics. A distinction can be made between figure 3.5 a, b, c and figure 3.5 d, e, f. In the first three there is a steep first part of the settling curve, followed by a point of contraction and a less steep part. We infer that these figures indicate two interfaces. The upper interface (regular shock wave), is presented by the dot-dashed line, while a lower interface (compound shock wave) is found where the characteristic lines converge. Hindered settling takes place in between the upper and lower interfaces while hindered settling followed by consolidation, or only consolidation, takes place between the lower interface and the bottom of the column.
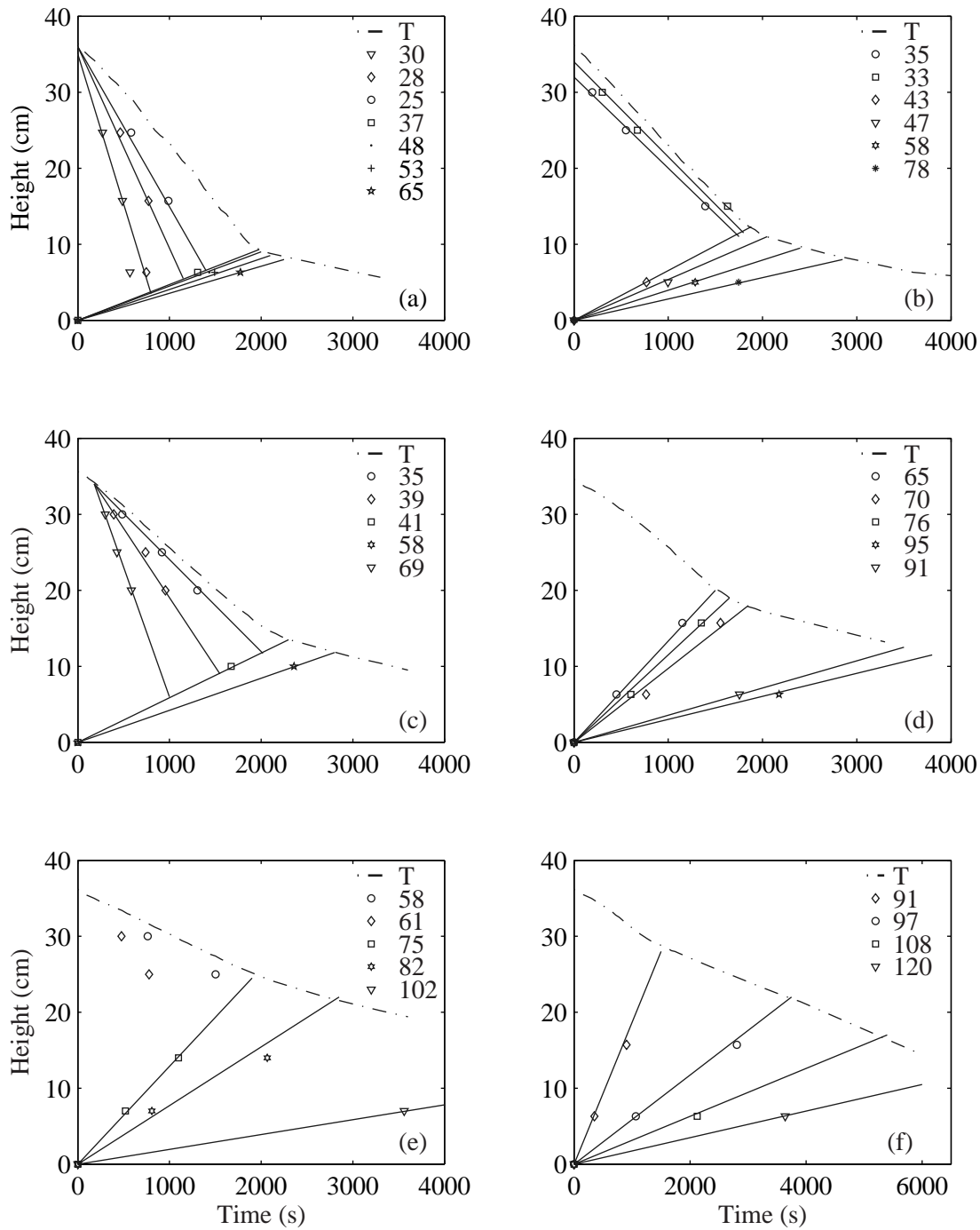
Figure 3.5. Settling curves of experiments: (a) 30kol ($c_0 = 35$ kg/m^3),(b) 20tt ($c_0 = 39$ kg/m^3), (c) 30tt ($c_0 = 46$ kg/m^3), (d) 50kol ($c_0 = 61$ kg/m^3), (e) 50tt ($c_0 = 68$ kg/m^3) and (f) 70kol ($c_0 = 84$ kg/m^3) with characteristic lines. T represents the upper interface and the numbers indicate the concentration in kg/m^3.

Normally it is not possible to draw characteristics based on data in the hindered settling phase of a settling plot. According to the theory for mono-dispersed suspensions, in which no segregation occurs, the concentration in this area should be the same everywhere. This means that the direction of characteristics can only be determined analytically. In the cases presented here, the concentration decreases slightly near the upper interface. This makes it possible to draw characteristics. The decrease in concentration might be due to segregation, diffusion and/or wall effects. The direction of characteristics in the hindered settling phase is therefore more an indication of trend, they can be drawn but their direction is not always unambiguous.

Beneath the lower interface the characteristics show an increase in concentration with time, which agrees with theory. At first the characteristics represent concentrations that are lower than the gelling concentration which gradually increases to concentrations beyond c_{gel}. This gradual change towards consolidation after a lower interface has been recognised before (Toorman & Berlamont, 1991; Toorman, 1992) and was indicated as a succession of the hindered settling phase. However, in Chapter 2 we have defined the gradual increase in concentration from the hindered settling phase to the consolidation phase as the fluid mud phase. Thus, the presence of a lower interface indicates the start of a fluid mud phase ($\phi < 1$) or the start of consolidation ($\phi > 1$).

Figure 3.5 d,e and f have a different appearance. Their settling curves are more gradual and do not have a distinct point of contraction. In figure 3.5 e the data points in the hindered settling phase indicate some segregation, but in none of the cases there is a clear sign of a lower interface. The characteristics have a fan-like structure, indicating a rarefaction wave, and the settling process consists of:

- hindered settling with one interface ($\phi_0 > \phi_{cr}$), followed by consolidation or

- consolidation only ($\phi_0 > 1$, $c_0 > c_{gel}$)

In figure 3.5 d and f, the initial volumetric concentration is 0.84 and 0.75 respectively, indicating settling with one interface. In figure 3.5 e, $\phi_0 = 1.04$, which is larger than the gelling concentration. In this case there is no hindered settling but consolidation from the start.

From the analysis with characteristics we can conclude that there can be one or two interfaces (regular shock or compound shock waves) within the settling suspension if $\phi_0 < 1$. If $\phi_0 > 1$ there is no hindered settling, but only consolidation and two shocks will never develop.

3.3.4   Concentration profiles

The concentration time series can be used to further examine the possible occurrence of shocks and settling behaviour in general. Some examples of concentration time series are shown in figure 3.6. They were measured with a conductivity probe positioned at various heights above the bed. For these results the same measuring accuracy as indicated before, *i.e.* 5 kg/m^3 on either side of the data values, is valid.
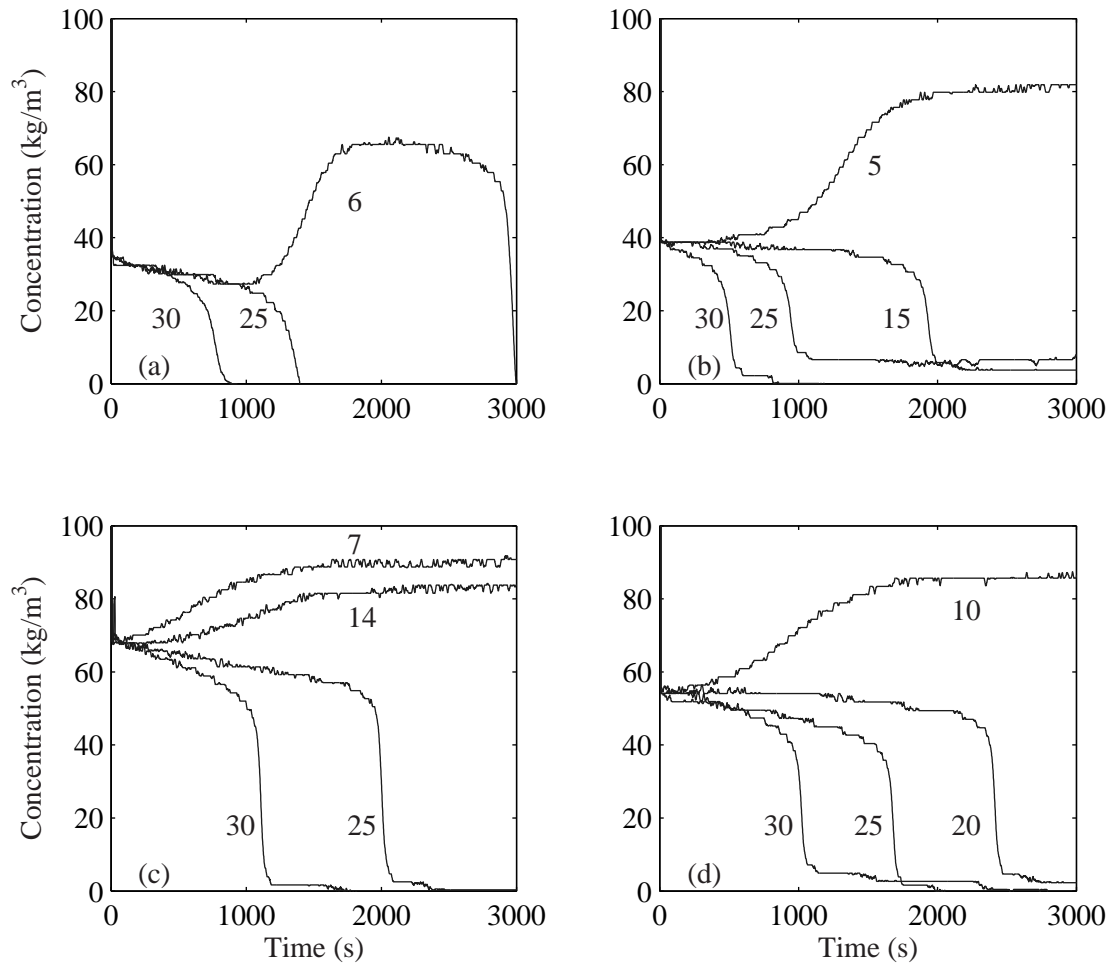
Figure 3.6. Concentration time series at selected heights above the bottom. (a) Experiment 30kol, c_0 = 35 kg/m³ (b) Experiment 20tt, c_0 = 39 kg/m³ (c) Experiment 50tt, c_0 = 68 kg/m³ (d) Experiment 55tt, c_0 = 54 kg/m³. The numbers indicate the height of the probe in cm above the bottom of the column.

In all figures the passage of the upper interface is evident. These interfaces are represented by the fast decrease from the initial concentration to a concentration close to zero. The probes that were positioned lower in the column, between 5 and 14 cm from the bed, do not show a decrease in concentration but an increase, indicating the presence of a lower rising interface, or a gradual increase in concentration. The 6 cm line in figure 3.6 a shows a sharp increase towards the gelling concentration. In this case there is a lower interface present, indicated by a fast increasing concentration towards the gelling concentration. Around $t = 3000$ s the two interfaces have merged and settle again as one, causing the sharp decrease in concentration towards the end.

Figure 3.6 b shows a more gradual increase in concentration towards the gelling concentration while in figure 3.6 c and d this increase is even more gradual. In Kynch's theory (figure 2.13) the two types of settling are indicated by (1) a lower interface, represented by

a compound shock and a sharp increase in concentration, and (2) no lower interface, only a gradual increase in concentration, a rarefaction wave. The differences between figure 3.6 a on one hand and c,d on the other, indicate that in the settling process one or two interfaces may develop. This is consistent with figure 3.5, which also shows settling with either one or two interfaces.

3.3.5 Application of Kynch's theory

In Section 2.2 it is explained that the occurrence of interfaces can be inferred from $\mathrm{d}F/\mathrm{d}\phi$. Two interfaces are expected when $\frac{\mathrm{d}F}{\mathrm{d}\phi} < 0$, while one interface is expected when $\frac{\mathrm{d}F}{\mathrm{d}\phi} > 0$. Thus every hindered settling model should be able to account for both types of behaviour. The equation for hindered settling as given by Winterwerp (2002) and Winterwerp & Van Kesteren (2004) (equation 2.4) can yield two interfaces if the return flow effect is non-linear ($m > 1$). The value of m can be determined empirically from the experimental results in Section 3.3.3 and 3.3.4, and from observations in the settling column. It was found that the settling behaviour in the experiments changes when $0.43 < \phi < 0.68$, *i.e.* $\frac{\mathrm{d}F}{\mathrm{d}\phi}$ changes in sign. Hence, this gives the critical concentration $0.43 < \phi_{cr} < 0.68$. F is given by:

$$F(\phi) = (\phi f(\phi))' = \frac{(1-\phi)^m \left(1 - \frac{c_{\mathrm{gel}}\phi}{\rho_s}\right)}{1 + 2.5\phi} - \phi \frac{(1-\phi)^m m \left(1 - \frac{c_{\mathrm{gel}}\phi}{\rho_s}\right)}{(1-\phi)(1+2.5\phi)} +$$
$$-\phi \frac{(1-\phi)^m c_{\mathrm{gel}}}{\rho(1+2.5\phi)} - 2.5\phi \frac{(1-\phi)^m \left(1 - \frac{c_{\mathrm{gel}}\phi}{\rho_s}\right)}{(1+2.5\phi)^2} \qquad (3.3)$$

As $\mathrm{d}F/\mathrm{d}\phi = 0$ at $\phi = \phi_{cr}$, the minimum in $F(\phi)$ is derived by differentiating $F(\phi)$ and we find:

$$m = \frac{1}{2} \frac{5\phi_{cr}^2 - 2\phi_{cr} + 4 + \sqrt{25\phi_{cr}^4 + 60\phi_{cr}^3 - 116\phi_{cr}^2 + 64\phi_{cr} + 16}}{\phi_{cr}(2 + 5\phi_{cr})} \qquad (3.4)$$

from which we find $1.4 < m < 2.6$ with an average of $m = 2$ for $0.43 < \phi_{cr} < 0.68$. In figure 3.7 the function F (equation 2.4) is shown for $m = 1$, the experimentally determined average $m = 2$, and its upper and lower boundaries ($m = 1.4$ and $m = 2.6$). For $m = 1$, F decreases monotonically with ϕ, but for $m > 1$, F depicts a minimum. From figure 3.7 it is clear that the settling behaviour changes when $m > 1$, while for $m = 1.4$ to 2.6 only ϕ_{cr} changes but not the settling behaviour.

The experimentally obtained value for m and the proposed hindered settling equation can be tested against available data sets and can be used to analyse, together with Kynch's theory, the experiments and the occurrence of shocks.

In figure 3.8 we compare two cases of hindered settling equation 2.4 ($m = 2$ and $m = 1$, but with same c_{gel}, see also figure 2.4) with data from literature. A good fit for $m = 2$ is obtained when the gelling concentration is set to 60, 90 and 120 kg/m^3 for the different data sets respectively. These are reasonable values and it indicates that the proposed equation with $m = 2$ is a good predictor.
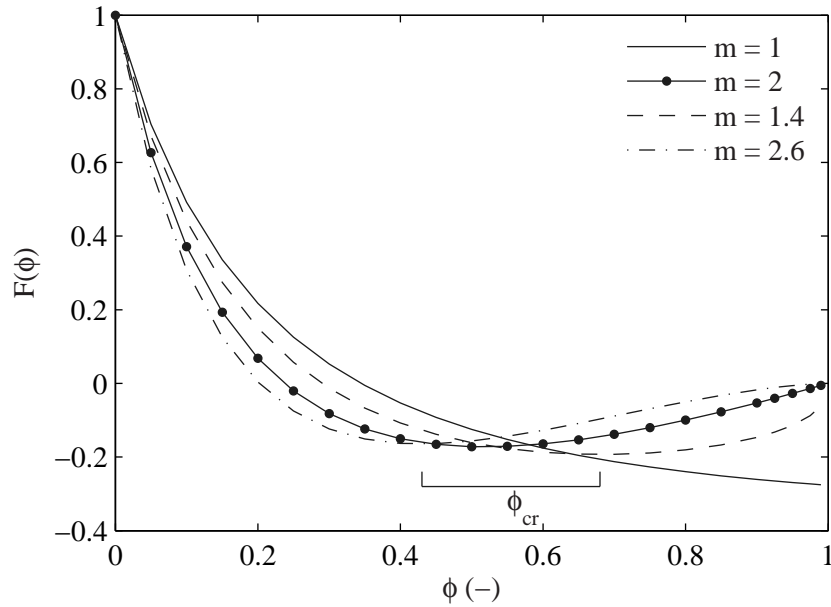
Figure 3.7. Variation of F with ϕ for equation 2.4 with $m = 1$, $m = 2$, $m = 1.4$ and $m = 2.6$.
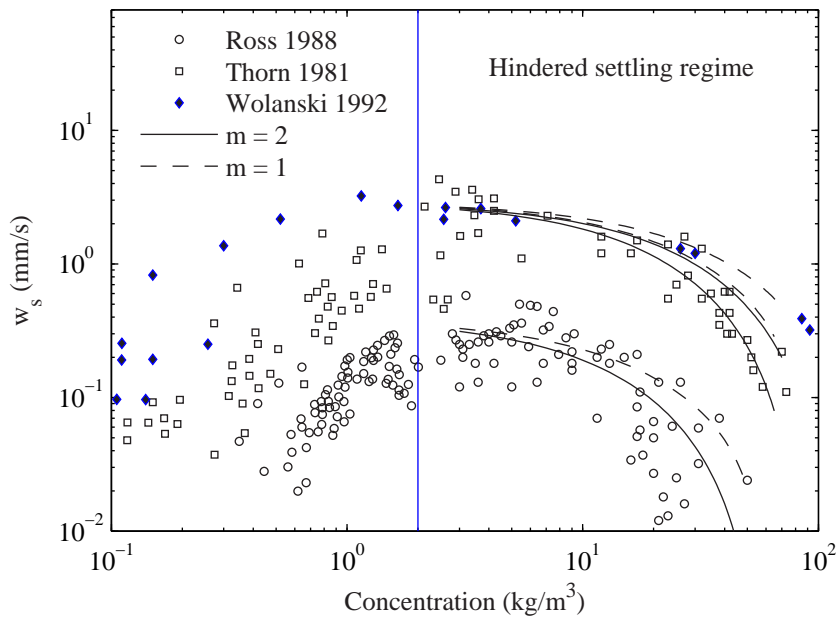

Figure 3.8. Fit of hindered settling equation 2.4 with $m = 2$ (solid line) and $m = 1$ (dashed line) to experimental data. c_{gel}: Ross (1988) = 60 kg/m^3, Thorn (1981) = 90 kg/m^3, Wolanski (1992) = 120 kg/m^3.

From the case with $m = 1$, where the same gelling concentrations are used, it is clear that the predicted effective settling velocities are not much different for both cases. This indicates that care should be taken when applying this method. Both $m = 1$ and $m = 2$ predict approximately the same effective settling velocity but an entirely different type of settling behaviour, which has consequences for the consolidation behaviour thereafter.

The behaviour of a suspension according to a specific hindered settling function can be predicted with the flux function of that hindered settling function. From this flux function the upper and possible lower interfaces and characteristics can be derived as explained in figure 2.10. The flux function of equation 2.7 with w_s from equation 2.4 is given by:

$$S(\phi) = \phi \left(w_{s,0} \frac{(1 - \phi)^m (1 - \phi_p)}{1 + 2.5\phi} \right) \tag{3.5}$$

The location of $\phi = \phi_0$ on this flux function determines the shape of the settling profile and the angle of the characteristics (Bustos *et al.*, 1999). In figures 3.9 and 3.10 some examples are given in which we vary ϕ_0 as in the experiments. On the left hand side in figures 3.9 and 3.10 the flux functions are shown from which the existence of the interfaces and angle of characteristics were derived. The flux is divided by its maximum value (S_{max}) for normalisation. On the right hand side of figures 3.9 and 3.10, analytical settling profiles are drawn with the interfaces and characteristics derived from the flux functions.

The precise determination of the different angles will be described shortly; more information can be found in (Bustos *et al.*, 1999). The angle of the upper interface (I1) is given by the line from $S(\phi_0)$ towards the origin that is tangent to the flux function. The angle of the lower interface (I2) is given by the line from $S(\phi_0)$ towards S_{max} that is tangent to the flux function. ϕ_* is the concentration at which the lower interface, I2, becomes tangent to the flux curve. In all cases the characteristics in water (C1) and at the start of the consolidation phase (C3) are given by the tangent to the flux function at its origin and at its end, respectively. Because the flux function is the same for every plot, these characteristics are also the same for every plot. In contrast, the characteristics in the hindered settling regime are given by the tangent at $S(\phi_0)$ and thus are different for every initial concentration.

The flux function is only valid in the area $0 < \phi < 1$. Therefore, only the first consolidation characteristic (C3), at which $\phi = 1$, is shown with a solid line in the settling profiles, thereby giving an indication of the start of consolidation. In the consolidation phase itself, the consolidation equation, a parabolic equation, does not yield characteristics. However, early in the consolidation phase, the effects of permeability $>>$ the effects of effective stress, thus the advective term remains large compared to the diffusion term and the hindered settling equation, which does yield characteristics, gives a reasonable approximation (see Section 2.2.2). The characteristics in this area are therefore indicated with dotted lines. The settling of the bed due to consolidation is incorporated by using a simple exponential function in the consolidation phase in the settling profiles of figures 3.9 and 3.10.

Figures 3.9 a, c, e and 3.10 g and their corresponding settling profiles have a similar appearance. In all these cases there are two interfaces, a top interface which represents

a regular shock and a lower interface which represents a compound shock. The main difference is the slope of the characteristics in the hindered settling phase, which changes from negative to positive when ϕ_0 passes the maximum of the flux function.

In figures 3.10 i and k, and their corresponding settling profiles, there is only one upper interface. Now the position of ϕ_0 on S has moved beyond the inflexion point, and $\frac{\mathrm{d}F}{\mathrm{d}\phi} > 0$. In the settling curves the characteristics diverge and the concentration increases gradually from the hindered settling phase (C2) towards the consolidation phase (C3), indicating the presence of a rarefaction wave.

The relative times $t1$ and $t2$ indicate when the entire suspension has changed from the hindered settling phase to the fluid mud phase and from the fluid mud phase to the consolidation phase, respectively.

The theoretical settling profiles in figures 3.9 and 3.10 can be compared with the experimental profiles in figures 3.5. Some of the initial volumetric concentrations in the flux functions are the same as the volumetric concentrations in the experiments. Figures 3.9 d and f and 3.10 h, j and l correspond to figures 3.5 a, b, c, d and e respectively. The main behaviour predicted with the theory is the same as the behaviour in the experimental examples. Figures 3.9 d and f and 3.10 h predict two interfaces, as are observed in figures 3.5 a, b and c, while figures 3.10 j and l predict one interface, as observed in figures 3.5 d and e.

The characteristics in the hindered settling phase (C2) can only be drawn theoretically (tangent to the flux function), because the concentration in the hindered settling phase should be constant. As explained before, the decrease in concentration in the experimentally derived characteristics in this phase is probably due to segregation, diffusion and/or wall effects. In the theory these factors are not included. Hence, a difference in direction of the characteristics between the theoretical plots and the experimental plots may occur, which is actually the case for figures 3.5 b, c and figures 3.9 f and 3.10 h.

The sharp inflexion point occurring in the cases with two interfaces indicates the change from the hindered settling phase to fluid mud phase, also referred to as point of contraction in soil mechanics. The height at which this occurs is almost similar in the experimental and predicted results. This means that the flux function predicts the shape of the upper interface (I1) rather well. In contrast, it is not clear whether the shape of the lower interface (I2) is predicted well, as the experimental settling curves in figure 3.5 are distorted in the horizontal direction.

A different predicted settling behaviour, with steeper or less steep interfaces, can be expected if other flux functions are used. In Bustos *et al.* (1999) and Bürger & Tory (2000) some examples of different flux functions are given. As the settling profiles in figure 3.9 and 3.10 correspond well to the measured settling profiles in figure 3.5, it can be concluded that equation 2.4 predicts the settling behaviour well. This is further elaborated in Chapter 5.
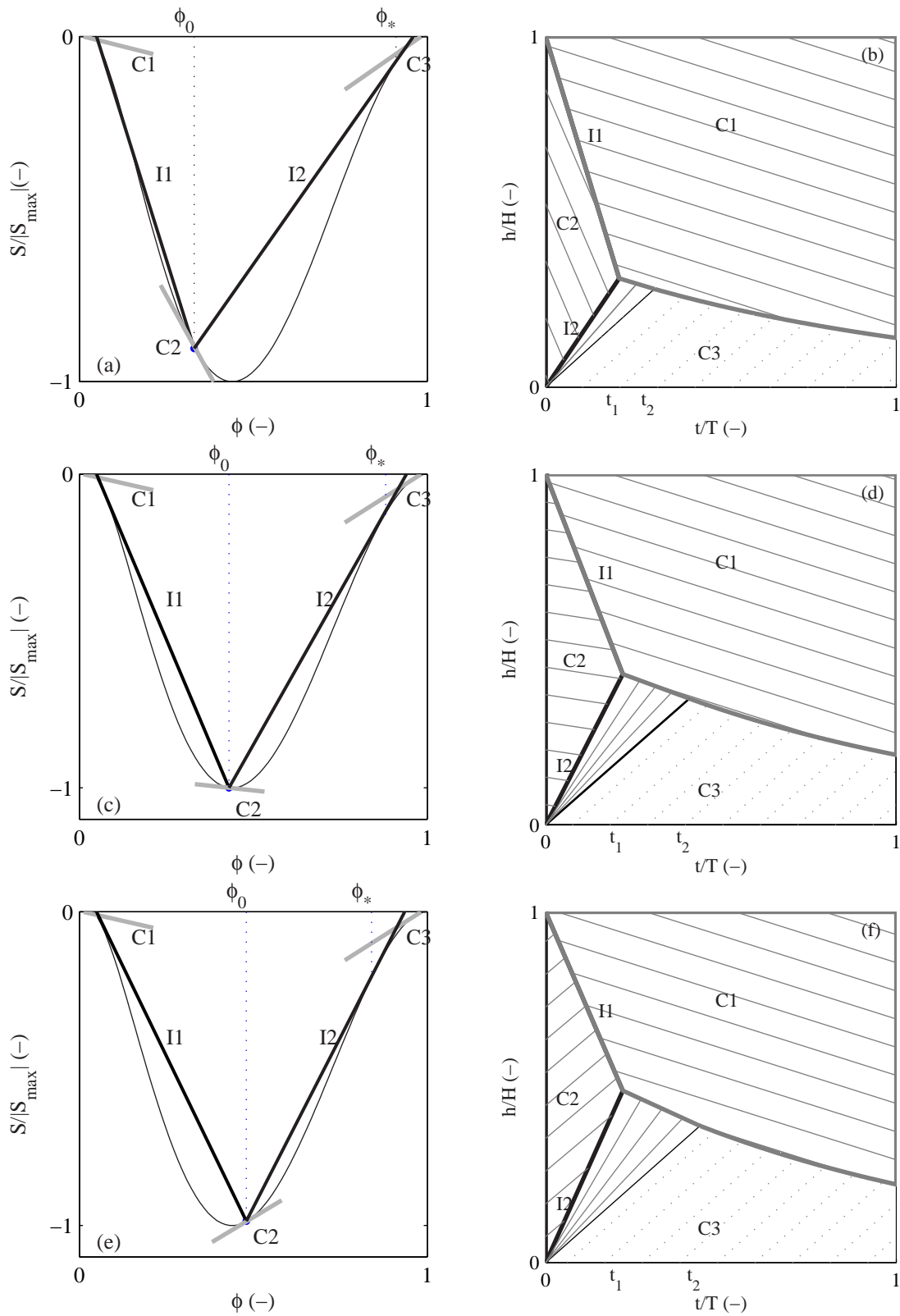
Figure 3.9. Flux functions and settling profiles for $\phi_0 = 0.33$, $\phi_0 = 0.43$ and $\phi_0 = 0.48$.
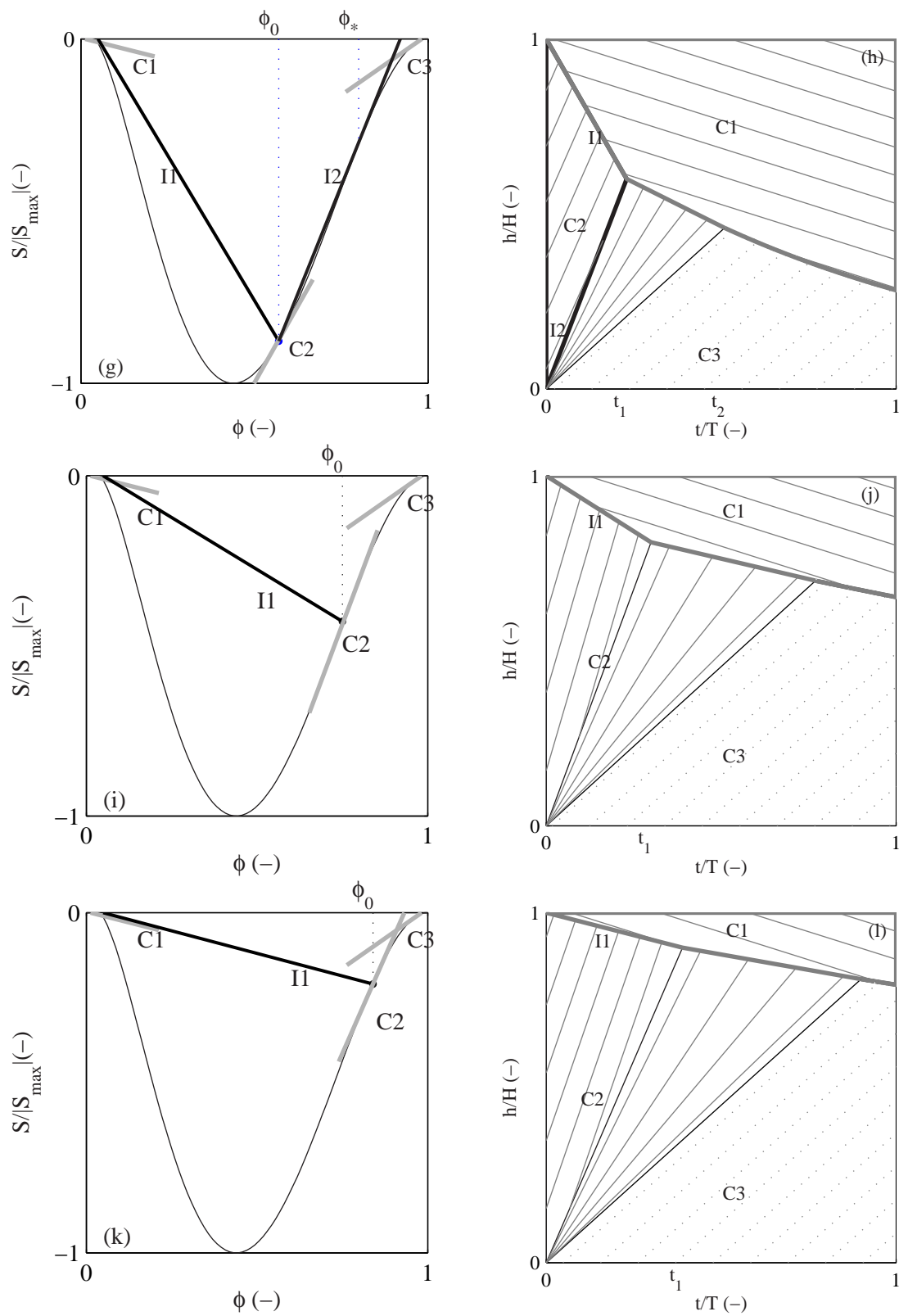
Figure 3.10. Flux functions and settling profiles for $\phi_0 = 0.57$, $\phi_0 = 0.75$ and $\phi_0 = 0.84$.

3.3.6   Bed profiles

At the end of the experiments the columns were left to consolidate for approximately 7 days. Thereafter, the density of the bed profile was measured with the conductivity meter. In table 3.2 the experimental data are given, while in figure 3.11 the corresponding concentration profiles are shown.
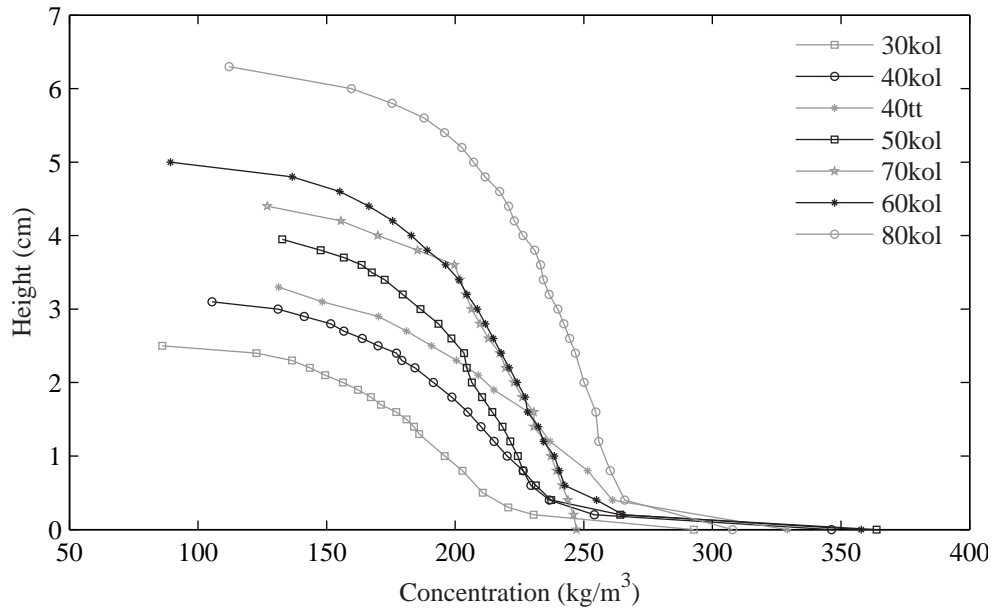

Figure 3.11. Concentration profiles of consolidated kaolinite for several experiments. The markers represent data points.

Table 3.2. Properties of the concentration profiles with h_0 is the initial height of the suspension ansd h_e the height of the sediment layer after the indicated number of days.

Id	c_0 (g/l)	h_0 (m)	h_e (m)	Duration (days)
30kol	35	0.367	0.025	7
40kol	46	0.337	0.031	7
50kol	61	0.346	0.04	7
60kol	71	0.364	0.05	8
70kol	84	0.362	0.054	7
80kol	100	0.363	0.063	11
40tt	48	0.359	0.035	10

The profiles have a typical convex form. This illustrates a strong downward increase in concentration in the surface part of the bed, followed by a much slower increase in

concentration in the rest of the bed. Close to the bottom the profiles in most cases become more concave, which can be an indication of segregation. The strong increase in concentration in the last two millimeters is an artefact of the instrument, resulting from interference of the column with the magnetic field of the conductivity meter.

In the bed, self weight consolidation increases the density. The most upper part of the surface layer is, however, not subject to self weight consolidation and thus should remain at the gelling concentration infinitely. The concentration near the water-bed interface measures between 80 and 130 kg/m^3. A comparison with the gelling concentrations in table 3.1 shows that these are in fair agreement, especially when taken into account that measuring the concentration at the top of a bed layer with a conductivity probe is not very accurate.

3.4   Concluding remarks

In this chapter experimental results on highly concentrated mud suspensions were presented and analysed. Simple techniques such as visual observations of the settling interface and concentration measurements with a conductivity probe were found to perform well and produce good data. With the data, settling velocities and gelling concentrations could be determined and characteristics could be drawn. The settling behaviour was further analysed with Kynch's theory of a settling suspension. This theory was found to be applicable. The suspensions in the experiments were found to develop one or two interfaces during settling, depending on the initial concentration. Beyond a critical initial volumetric concentration the settling behaviour changed from developing two interfaces to one interface. This was validated with the flux functions and characteristics resulting from Kynch's theory.

4

Hindered settling of mud-sand mixtures

4.1   Introduction

In the previous chapter the hindered settling of highly concentrated mud suspensions was discussed. In practice, such suspensions often contain small amounts of sand. In this chapter, the behaviour and settling velocity of these highly concentrated mud-sand mixtures is examined for both the total suspension and for the fractions separately. A challenging objective, as, to the author's knowledge, no comparable data sets on the subject are available. This implies that there is no standard on how to measure the behaviour in these suspensions. Therefore, we use a combination of techniques, consisting of visual observations, X-ray density profiles and particle tracking velocimetry. The experiments were performed in the Soil Mechanics Laboratory at the Engineering Department of Oxford University; the experimental set-up and results are described in this chapter.

4.2   Experimental set-up

4.2.1   Sediment preparation

Mud

The experiments were carried out with natural mud, dredged by the Harbour Authority of Rotterdam from the Calland-Beer Channel in the Port of Rotterdam. More than 200 liters of mud were brought on shore and transported to Delft University of Technology. In the Laboratory for Environmental Fluid Mechanics in Delft all sand present was removed by diluting the mud, mixing it and letting it settle to segregate. We used sediment from the top layer only, which consisted of virtually pure mud. The mud was stored in a dark place before it was shipped to Oxford University, where the experiments took place. In order to prevent bacterial growth, the mud was kept at 4 °C during the period in which the experiments occurred.

For every experiment a different initial mud concentration was used, ranging from 11 to 76 kg/m^3, but all suspensions were prepared in the same manner. Half a day before the start of an experiment mud was diluted with salt water (5 ppt) to the desired density. This mixture was stirred overnight in order to regain room temperature.

Sand

Two types of quartz sand were used in the experiments. A light coloured sand with D_{50} = 110 μm and a silversand with D_{50} = 360 μm. Both sands have a narrow grain size distribution (figure 4.1), and no further sieving was needed. The small grain size was
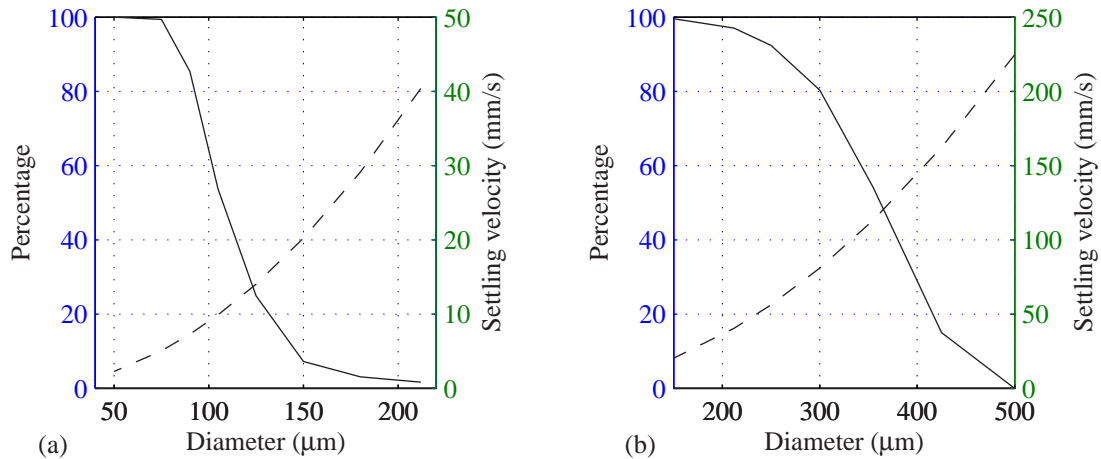

Figure 4.1. Grain size distribution (solid line) and settling velocity (dashed line) for (a) fine sand and (b) coarse sand.

chosen on the basis of its expected settling velocity in water. This settling velocity needs to be low in order for the settling particles to be detected with a camera. In general, small amounts of sand were used in the experiments (5-20 gram sand per 19 liter mud).

4.2.2   Experimental equipment

Settling column

Four settling columns were used in the experiments (figure 4.2). The columns were made of acrylic and had a height of about 1.9 metre and an inner diameter of 100 mm. All four columns consisted of three or four segments to facilitate the handling of the almost 2 metre tall column. At the bottom of the columns a removable plug was placed. All columns were mounted on a rig that was custom built for easy use of the X-ray density profiler.

Sand dispersal system

A sand dispersal system (figure 4.3) could be mounted on top of the columns, increasing the columns' height by 214 mm. The sand dispersal system consisted of a perspex base with a diameter of 440 mm in which a stainless steel dispersal system was placed, on
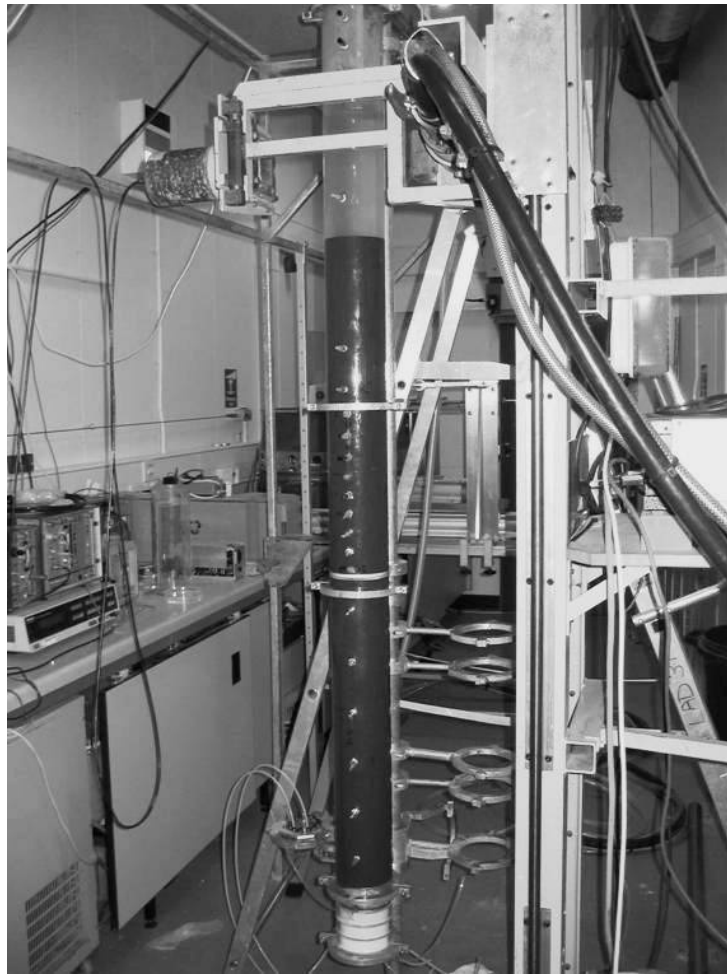
Figure 4.2. The settling column, filled with mud, surrounded by the X-ray device.

which the sand was placed. The dispersal system had remotely controlled Venetian blinds which could be opened rapidly. After opening, the blinds shook for a few seconds in order to release all sand placed in the dispersal system.

X-ray device

A non-destructive X-ray technique, developed by Been (1980), was used to measure density profiles in these experiments (figure 4.2). The specifics of the device, its use and accuracy are described in detail by Sills (1997) and Been (1980). Here, the main principles of the X-ray technique are given.

The X-ray device produces a collimated beam of X-rays passing through the settling column. Its signal at the opposite side of the column is detected with a sodium iodide crystal and photomultiplier assembly. A count rate (N) is measured, which relates to
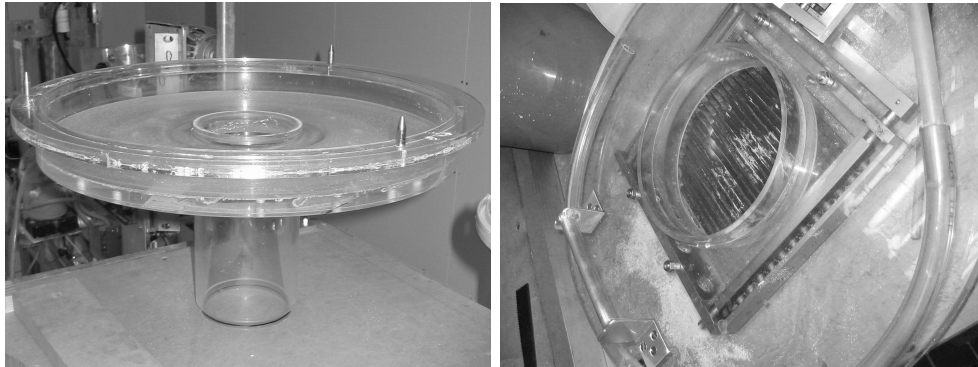
Figure 4.3. The perspex base (left) for the sand dispersal with Venetian blinds (right).

density (ρ) according to:

$$N = N_0 e^{-k\rho} \tag{4.1}$$

in which N_0 is a reference value and k an empirical parameter. Both N_0 and k can be determined by either using calibration samples, or through the principle of conservation of mass. With the second method, the initial concentration, and thus total mass, of the suspension should be known. Then the density profiles can be adjusted to match this initial mass over the volume of the suspension.

For our experiments sand is added to the system at a later stage, so the latter method cannot be applied. Therefore, calibration samples are needed. Normally, the sediment in the calibration samples should be the same as the sediment in the column. In our case it was difficult to fulfill this requirement as the relatively low density of the suspension, and the long duration of the experiments, would cause the suspended material in the calibration samples to settle before the experiment had finished. Therefore, calibration samples made of plastic were used. The density of these samples was adjusted by adding various amounts of sand. From X-ray density measurements of the plastic samples, three mud samples with known density and one water sample, the count rate of the plastic samples could be related to a mud density.

The accuracy of the density measurements is estimated to be ± 2 kg/m³ at a resolution of ± 1 mm (Sills, 1997). For every experiment, profiles were measured both downward and upward. This way uncertainties due to shifts in X-ray voltage were minimized.

PTV and PIV measurements

Particle Tracking Velocimetry (PTV) and Particle Image Velocimetry (PIV) are techniques by which the velocity of particles can be determined from video images. It is a non-intrusive optical technique, which is applicable in sediment-laden flow without disturbing the flow. Furthermore, it is a field technique, allowing synoptic measurements over an area (Raffel *et al.*, 1998). In general, this technique is used to determine and measure flow structures and tracer particles have to be added to trace the flow. In this research, the sand grains and mud flocs are the tracer particles. PTV is mostly used in

case of low particle density, while PIV is used in case of medium to high particle density. Both techniques are explained briefly in here.

With PTV, two successive images are compared with each other. The velocity of the particles follows from the distance these particles have travelled between the successive images (figure 4.4). The accuracy of the method increases with increasing number of particles and images.
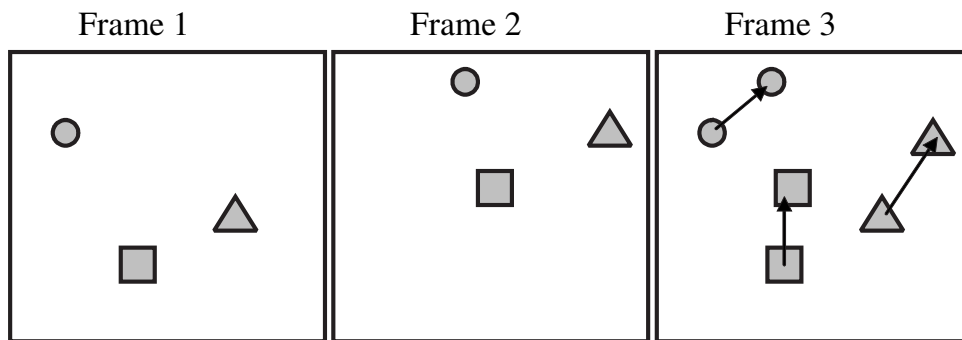

Figure 4.4. Example of PTV method.

PIV is based on pattern recognition. Every image is divided in blocks with a user-defined grid size (figure 4.5). The pattern of particles in each grid cell is compared to the particle patterns in the succeeding image. The distance between the two matching grid cells is then a measure for the velocity.
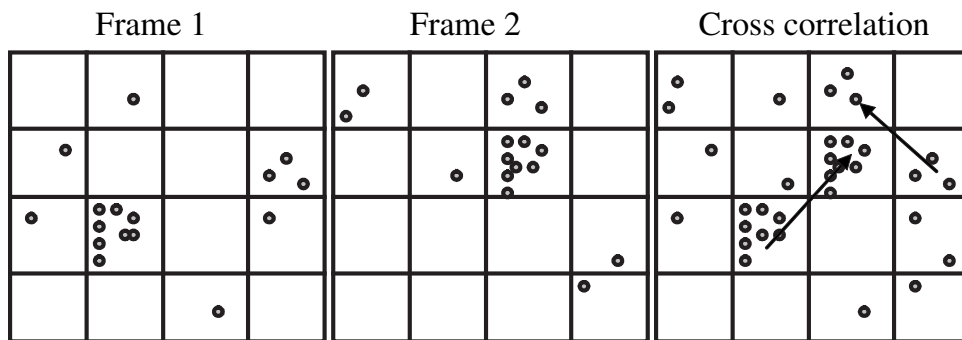

Figure 4.5. Example of PIV method.

PIV/PTV equipment

We used a JAI-CV10 video camera to capture images for the PIV/PTV measurements. This is a progressive scan, or non-interlaced, camera, meaning there is no time delay between capturing alternate lines of pixels, an important prerequisite for PIV/PTV measurements. The camera had a resolution of 948×576 pixels.

The camera was operated from, and images were captured directly by a frame grabber board. This board allowed the capture of monochrome images of 2000 × 2000 pixel resolution at 30 frames per second. For this research, the resolution was set to 636 × 480 pixels.

In general, good illumination is one of the most important factors in PIV/PTV measurements. In a first set-up, a laser-diode was used to create a vertical light sheet through the column with the mud suspension,which proved to be rather impermeable to light. Therefore, we externally illuminated an area close to the wall. This allowed capturing of good video images. Unfortunately, only particles close to the wall could be observed with this method. The set up during the particle tracking measurements is shown in figure 4.6.

Figure 4.6. Set-up of light and camera for the PTV and PIV measurements.

Because of the low particle density of the sand grains, PTV was used to determine the settling velocity of sand particles. Post-processing of the images was, however, needed before successive frames could be compared to each other. For this purpose, the mud fraction was filtered out of the images by subtracting the mean background light intensity in the images. Thereafter, the velocities were determined by using cross-correlation.

The mud fraction had a much larger particle density. Therefore its velocity was determined with PIV. First, the sand particles had to be filtered out, a difficult process that could not be performed completely satisfactory, and, as a result, the accuracy of the PIV measurements is not too high (accuracy within a range of 0.6 mm/s). The velocities were determined by using a multi-pass cross-correlation method with a window size ranging from 64 × 64 pixels to 16 × 16 pixels and a 50% overlap.

Experimental procedure

It is not possible to make a homogeneous mud-sand mixture below the gelling point, to pour this in a 2 metre column and then to start settling experiments with uniform initial conditions. Therefore, an alternative method was applied by which sand was topped on a homogeneous suspension of mud. The experiments were performed with high concentrations of mud (11 - 76 kg/m^3) and small amounts of sand (5 - 20 gram per measurement), implying that the suspension settling and sand settling are both mainly determined by the volume effects of the mud fraction. To fill the column completely with a mud suspension, 19 liters of mud at the desired concentration were needed per experiment. This mud was prepared the day before and its density was determined with a portable density meter, developed by Anton Paar. The X-ray had to be warmed up for 20 minutes, whereafter the experiment could start. The suspension was quickly poured into the column and the X-ray was started as soon as possible (in general within 2 minutes). The start of the X-ray is taken as $t = 0$, i.e. the start of the measurement. The X-ray traversing speed was set to 2 mm/s and as a result an X-ray scan, both down and up, of the mud suspension took about 35 minutes. After one X-ray scan, the camera was put in place, a calibration picture was shot and the sand was released from the Venetian blinds. The camera was started when sand began to pass the camera. In most cases a second and sometimes third sand input was performed, together with a corresponding video. In other cases, several videos were made of one sand input. In general, three or four video films per experiment were made of the settling sand grains. Each video had a length of approximately 1 minute and a rate of 30 frames per second, leading to about 2000 frames per video and about 6000 frames per experiment. For the PTV/PIV every fifth frame was used. Because of the low quality of some videos, the data had to be reduced further to about 500 - 1000 frames per experiment. The number of sand grains that could be detected in each frame ranged from just a few to, in exceptional cases, a maximum of about twenty, giving a total amount of 2500 - 5000 velocity measurements per experiment.

Following the measurements with the video camera, as many X-ray scans as possible were made during the day. This methodology enabled us to observe the settling of the interface through time and the density development in the mud layer. In the following three to four days, one X-ray scan was made every day.

In total 27 experiments were performed. The first experiments were done in the Environmental Fluid Mechanics Laboratory in Delft. For these experiments the same small columns as the ones described in Chapter 3 were used. They are called SC1 - SC6 and they were performed to test some typical properties of the mud. The actual experiments were performed in the Soil Mechanics Laboratory at the University of Oxford in columns with a height of 2 meter and they are called Ox1 - Ox21. The first five experiments in this Ox-series were performed with mud only, while in experiment Ox6 to Ox21 mud and sand was used. During every Ox-experiment, a series of X-ray density profiles and PIV/PTV measurements were made. The different series are identified by the letters a, b, c etc., while an extra letter is added when the X-ray was moving down (d) or moving up (u).

4.3   Results

All experiments and measurement methods are presented in Table 4.1. Both concentration and density are given in this table. From now on we shall mostly use concentration instead of density to characterise the experiments.

Table 4.1.   All experiments and measurements.

Id	Concentration (kg/m^3)	Density (kg/m^3)	X-ray scans	PTV/PIV
SC1	26	1019		
SC2	47	1032		
SC3	34	1024		
SC4	41	1028		
SC5	21	1016		
SC6	19	1015		
Ox1	19	1015		
Ox2	23	1018		
Ox3	35	1025		
Ox4	53	1036		
Ox5	62	1042		
Ox6	19	1015	a-d	x
Ox7	21	1016	a-f	x
Ox8	55	1037	a-i	x
Ox9	0	1003	-	x
Ox10	76	1050	a-f	x
Ox11	32	1023	a-f	x
Ox12	40	1028	a-h	x
Ox13	35	1019	a-g	x
Ox14	11	1010	a-c	x
Ox15	21	1016	a-h	x
Ox16	15	1012	a-f	x
Ox17	31	1022	a-f	x
Ox18	41	1028	a-f	x
Ox19	18	1014	a-g	x
Ox20	37	1026	a-c	x
Ox21	47	1032	a-b	x

4.3.1 Phemenological description

During the settling of the suspension and the consolidation that followed, many features and processes were visually observed and are described in this section.

Hindered settling phase

When the mud is introduced into the column, it immediately starts to settle slowly. After a few minutes the disturbance, created during the infill, has ceased and the mud settles in a quiescent way. When the sand is introduced, the suspension is again disturbed greatly, causing the sand grains to flow randomly in all directions. After the cessation of this initial disturbance, the sand starts to settle down more uniformly (figure 4.7). First, the grains settle through the clear water layer on top of the already settling mud suspension. Upon reaching the interface between water and mud suspension, the impact of the sand on the mud interface causes a strong wavy movement in the upper part ($\pm$ 5 cm) of the mud suspension. This is remarkable as the sand volumetric concentration is very low compared to the mud volumetric concentration.

The sand particles can be followed properly throughout the entire column. Just before the first sand particles start to pass a certain level, a sudden increase in movement of the mud suspension is recorded. During the time the sand passes, a strong upward directed return flow is observed, and sometimes an increased downward flow. These processes do not occur throughout the column. From visual observations it was observed that the areas of induced flow shift, seemingly randomly, through the column.
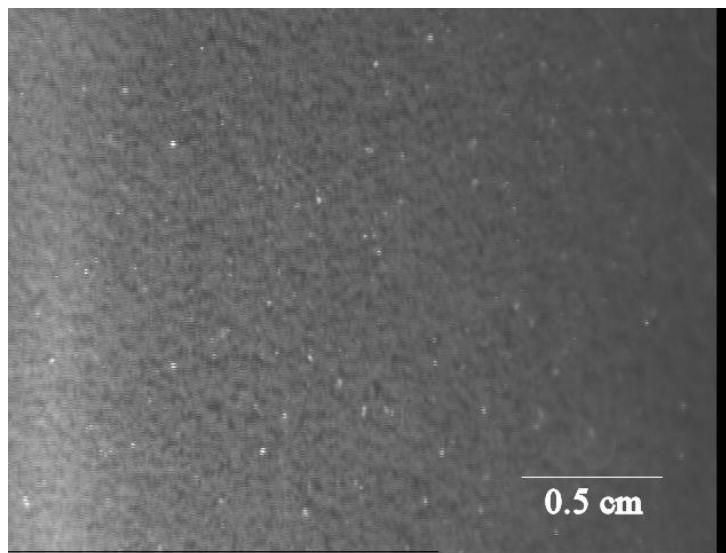

Figure 4.7. Sand grains (light coloured dots) settling through mud flocs in a highly concentrated mud suspension ($c_0 = 31$ kg/m^3).

Consolidation phase

When the mud suspension gains some strength and starts to consolidate, water is expelled through small dewatering channels. These channels are formed during settling and disappear again when most water is expelled from the soil. It was observed that not only water is expelled through these channels, but that sand grains follow these channels as well to settle towards the base of the column (figure 4.8). Lower in the column, consolidation has progressed and the larger dewatering channels are closed, leaving open only very small (diameter $\pm$ 0.1 mm) drainage paths. The sand grains are arrested by the mud matrix and pockets of sand develop, filling up the dewatering channels (figure 4.9).
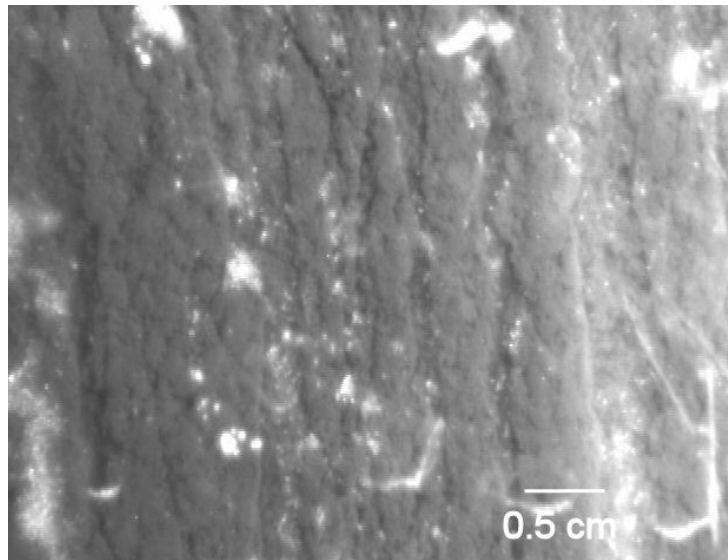

Figure 4.8. Sand grains use the dewatering channels in a consolidating mud. Scale is not accurate.

It was expected that sand would be arrested when the mud had reached a certain strength. This thus would lead to sand layers in the mud. The existence of dewatering channels through which sand grains travel, however, shows that sand can travel much further and faster than expected. As a result, not one single layer of sand is formed in the mud matrix, but many sand pockets are formed, at different heights in the column.

All these observations were done close to the wall of the column and may have been affected by wall effects. Therefore, the distribution of the sand in the cross section was analysed. Three columns were left to consolidate for 4 more months, whereafter the bottom plug was carefully taken out, giving the opportunity to see the lowest bed layer in the column. Figure 4.10 shows that sand patches and grains, the lighter areas in the picture, are found throughout the bottom slice. This suggests that the sand particles settle more or less uniformly over the entire cross section and we infer that wall effects are not too important.
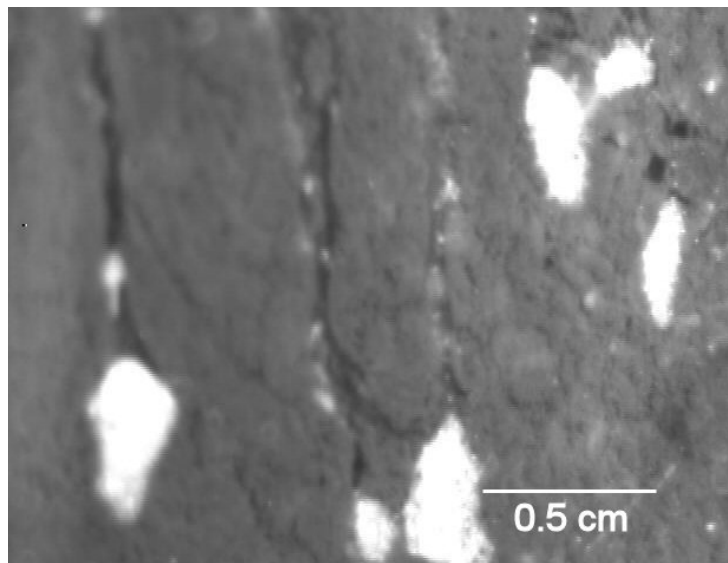
Figure 4.9. Sand pockets are created at the end of dewatering channels in consolidating mud. Scale is not accurate.
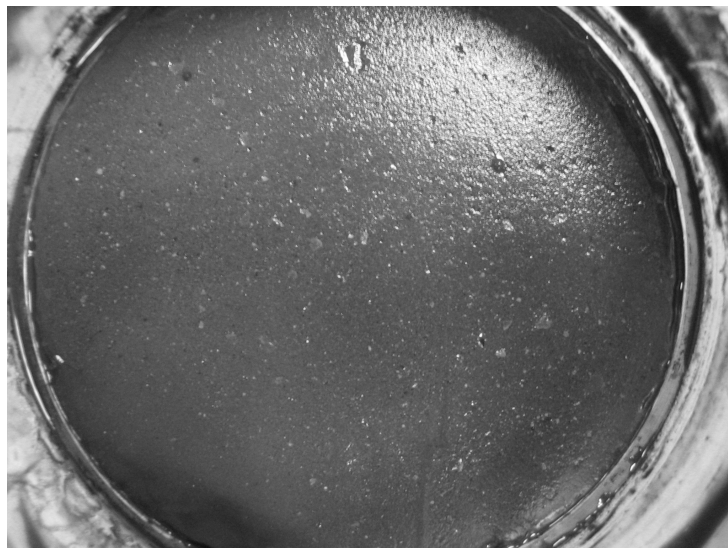

Figure 4.10. Slice of consolidated mud. Light speckle indicates sand pockets.

4.3.2 Suspension settling velocity

The effective settling velocity of suspensions can be determined from the lowering of the interface in time. As in the experiments $\phi^s << \phi^m$, it is expected that the influence of sand on the suspensions settling velocity is not too large and that the suspensions settling velocity is mainly determined by volume effects due to mud concentration. Suspension settling velocities are determined for both the small columns in the SC-experiments and the large columns in the Ox-experiments for the steepest part of the settling profile (hindered settling phase), by taking the tangent to the settling profile. In figure 4.11 the settling curves of 6 SC-experiments are given. For these experiments the same mud as in the Ox-experiments was used, and the different initial concentrations were produced by diluting the dense suspension with salt water ($\rho = 1003$ kg/m^3). All profiles show a hindered settling phase, followed by a "fluid mud" phase and consolidation phase. Furthermore, an increase in initial concentration shows a decrease in the concave shape of the settling profile. This means that towards a higher initial concentration, the effective settling velocity decreases as a result of hindering, till the concentration becomes so large that the initial conditions are within the consolidation regime. The latter process is not observed in figure 4.11, because only relatively low initial concentrations were used.

The settling profiles of the experiments in the large columns (Ox1 - Ox21) are presented in two different graphs in figure 4.12, because of the time span of the experiments. In general, an experiment is continued for 3 - 4 days. In figure 4.12 a only the hindered settling and fluid mud phases of the experiments are shown, while in figure 4.12 b results up to $t = 6000$ minutes are shown. Both figures 4.11 and 4.12 show settling curves with an
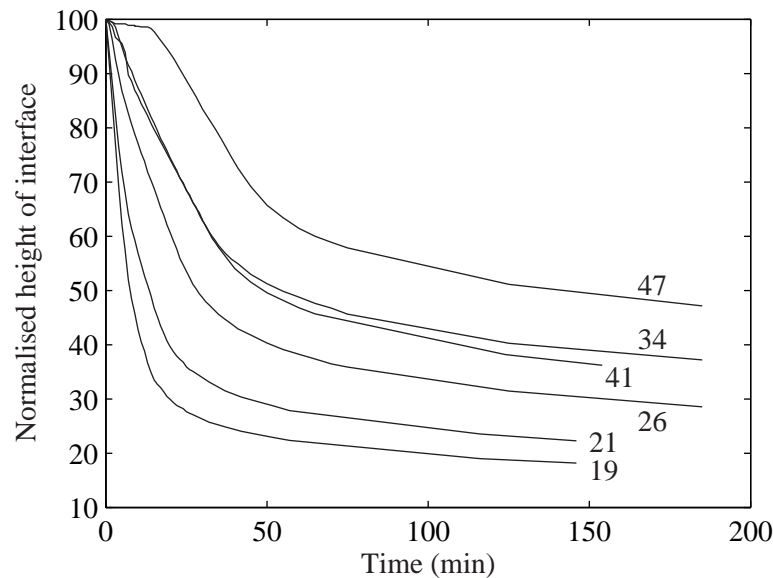

Figure 4.11.   Normalised settling curves of mud suspensions in small columns (SC-series). The numbers indicate the initial mud concentration (kg/m^3).
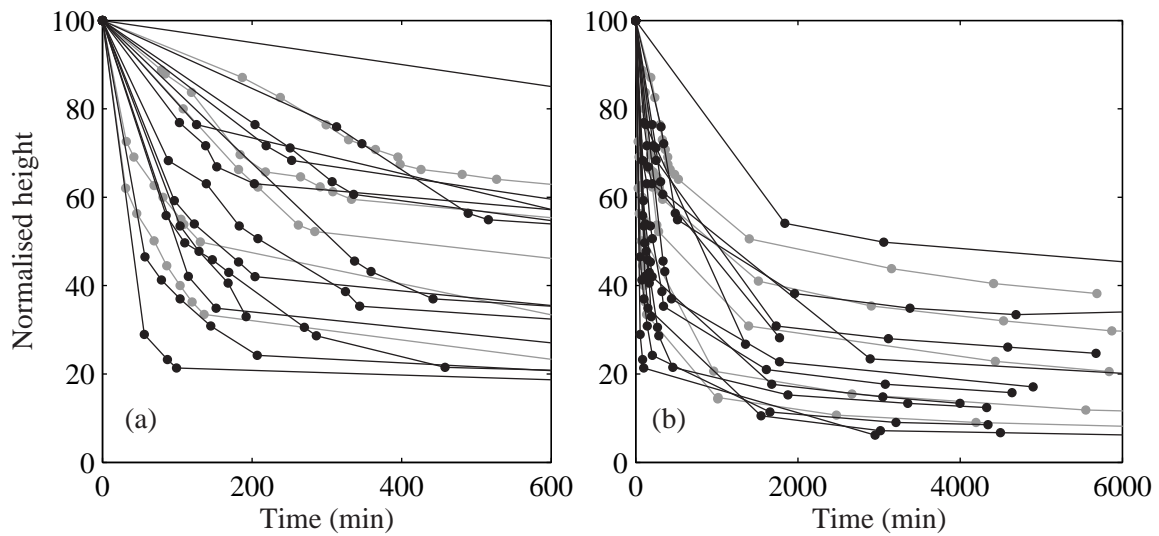
Figure 4.12. Normalised settling curves of mud suspensions in large columns (Ox-series): (a) the first 600 minutes and (b) the first 6000 minutes. Grey colours represent Ox1 - Ox5, black colours represent Ox6 - Ox21.

initially steep profile followed by a less steep profile. In the case of figure 4.12 b, the less steep profile is further followed by an almost flat curve, characteristic for consolidation.

In a double logarithmic plot (figure 4.13) the consolidation phase can easily be identified by the angle of the settling curves. In the consolidation regime the height of the bed decreases with the square root of time, as presented by the triangle in figure 4.13. For the performed experiments, consolidation starts after about 100 - 500 minutes.

The calculated settling velocities for experiments with mud only, experiments with mud-sand mixtures and for the SC-experiments, are presented in figure 4.14. In Table 4.2 the value of the suspension settling velocity for each experiment is given, ranging between 10^{-5} and 10^{-4} m/s.

The data points in figure 4.14 show a more or less exponential decline in settling velocity with increasing initial concentration. Furthermore, the settling velocities of the suspensions in the SC-experiments appear to be slightly larger than the settling velocities in the Ox-experiments. This can result from different experimental procedures, such as storage time and preparation of the mud, but also from differences in wall effects between small and large columns. Within the Ox-experiments, the settling velocities of suspensions with mud-only are more or less the same as the velocities of the suspensions with mud-sand mixtures. This confirms our hypothesis that the effective settling velocity of mixed suspensions is only slightly affected by an addition of a small amount of sand, and that the suspensions settling velocity may be modelled with an equation that is based on that for mud.
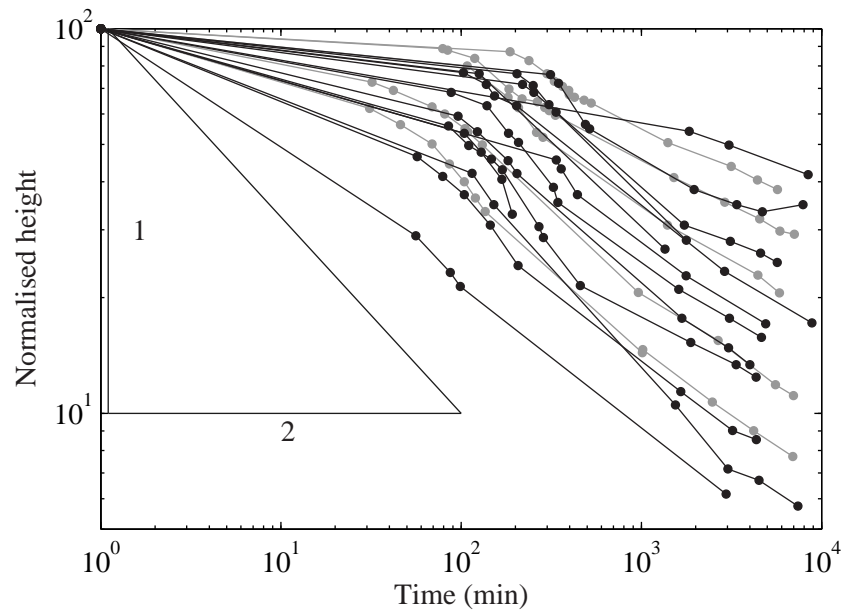
Figure 4.13. Double logarithmic plot of the measured settling curves.
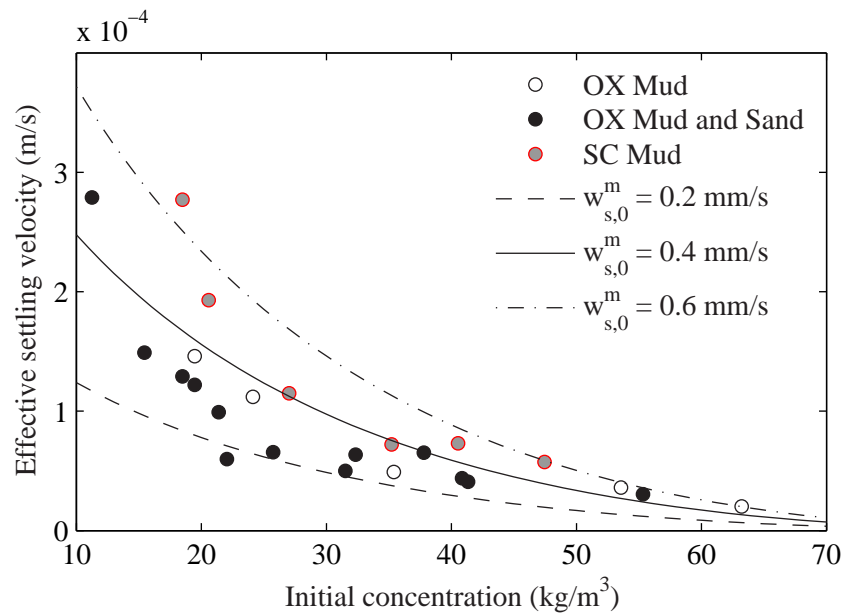

Figure 4.14. Suspension settling velocities at different initial concentrations for SC-experiments and Ox-experiments. The lines represent equation 4.2a, with $c_{gel} = 91$ kg/m^3 and $w_{s,0}^m$ as indicated.

Table 4.2. Effective suspension settling velocities for all experiments

Id	Concentration (kg/m^3)	Density (kg/m^3)	Settling velocity (m/s)
			$\times 10^{-4}$
SC1	26	1019	1.15
SC2	47	1032	0.58
SC3	34	1024	0.72
SC4	41	1028	0.73
SC5	21	1016	1.93
SC6	19	1015	2.77
Ox1	19	1015	1.46
Ox2	23	1018	1.12
Ox3	35	1025	0.49
Ox4	53	1036	0.36
Ox5	62	1042	0.20
Ox6	19	1015	1.22
Ox7	21	1016	0.99
Ox8	55	1037	0.31
Ox9	0	1003	-
Ox10	76	1050	-
Ox11	32	1023	0.63
Ox12	40	1028	0.44
Ox13	35	1019	0.66
Ox14	11	1010	2.79
Ox15	21	1016	0.60
Ox16	15	1012	1.49
Ox17	31	1022	0.50
Ox18	41	1028	0.41
Ox19	18	1014	1.29
Ox20	37	1026	0.65
Ox21	47	1032	-

Winterwerp & Van Kesteren (2004) derived a model to determine the settling velocity of different fractions in highly concentrated suspensions, as given in Chapter 2, equation 2.6a and 2.6b. In our experiments $\phi_p^s <<< \phi_p^m$, reducing equation 2.6 to:

$$w_s^m = w_{s,0}^m \frac{(1 - \phi^m)^2 (1 - \phi_p^m)}{1 + 2.5 \phi^m} \tag{4.2a}$$

$$w_s^s = (w_{s,0}^s - \phi^m w_{s,0}^m) \frac{(1 - \phi^m)^2 (1 - \phi_p^m)}{1 + 2.5 \phi^m} \tag{4.2b}$$

in which the superscripts s and m represent the sand and mud fraction respectively. Equation 4.2a, with $c_{gel} = 91$ kg/m^3 and $w_{s,0}$ is 0.2, 0.4 and 0.6 mm/s, is plotted in figure 4.14, representing the data fairly well. The SC-experiments data points are best represented by $w_{s,0} = 0.4$ - 0.6 mm/s, while for the Ox-experiments $w_{s,0} = 0.2$ - 0.4 mm/s is more appropriate, indicating a smaller primary floc size in the Ox-experiments.

4.3.3   Gelling concentration

The SC-experiments were initially performed to determine the gelling concentration of the mud as this determines the range of concentrations to be used in the Ox-experiments. In Chapter 3 the gelling concentration of kaolinite suspensions was determined with a conductivity meter, positioned a few centimetres from the bottom. This same method, in the same columns with a height of 40 cm and a diameter of 7 cm, was used for the SC-experiments. The derived gelling concentrations are given in table 4.3 (SC4 - SC6) and the concentration time series are shown in figure 4.15.

The conductivity meter was calibrated before and after every experiment. Therefore, a single experiment has two concentration profiles, one obtained with the first calibration line and one obtained with the second line. Figure 4.15 shows that a large inaccuracy ($\pm$ 20 kg/m^3) can occur, either due to temperature shifts or other factors, such as suspension inhomogeneity and measuring errors. Only for the experiment with $c_0 = 21$ kg/m^3, both calibration lines were equal, yielding one concentration profile and one gelling concentration.

The concentration profiles in figure 4.15 were measured 5 cm above the bed and they show a rise in concentration with time until the gelling concentration is reached (Dankers $et\ al.$, 2006). From these concentration profiles a mean gelling concentration of 91 $\pm$ 13 kg/m^3 is obtained.

At a later stage the gelling concentration was also derived from the mud-only Ox-experiments. For these experiments it is assumed that the concentration at the top of a consolidated bed profile always represents the gelling concentration because self-weight consolidation is small in the upper layer. The gelling concentrations derived with this method are given in table 4.3 (Ox1 - Ox5), yielding a mean gelling concentration of 121 $\pm$ 18 kg/m^3. The difference in gelling concentration between the two methods is attributed to history effects and preparation and residence time before a sample is used. The material used in the Ox-experiments, for example, is mixed thoroughly.

Table 4.3. Gelling concentrations obtained from concentration profiles and X-ray profiles.

Id	c_0 (kg/m^3)	c_{gel} (kg/m^3)											
Conc. profile		1	2										
SC4	41	103	108										
SC5	21	80											
SC6	19	102	71										
X-ray profile		fd	fu	gd	gu	hd	hu	id	iu	jd	ju	kd	ku
Ox1	19	126	128	116	94	144	145						
Ox2	23	102	100	104	116	125	127						
Ox3	35	99	87	102	104	106	111						
Ox4	53			103	106	117	126	127	133	142	142	162	154
Ox5	62					114	110	117	126	133	136	149	137
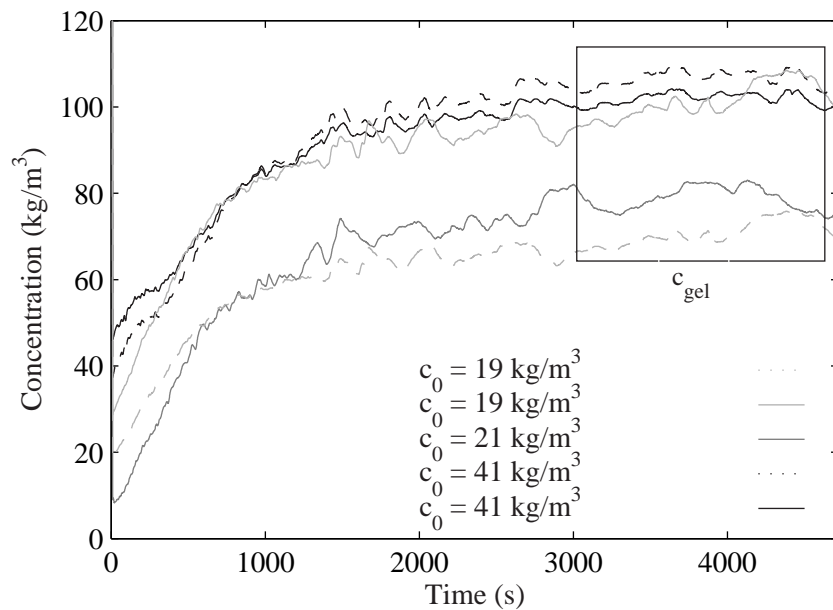
Figure 4.15. Concentration profiles at a height of 5 cm above the bed for different initial concentrations. Solid lines indicate calibration before experiment and dotted lines indicate calibration after experiment.

During mixing, flocs break up, leading to a smaller overall floc size and a larger gelling concentration. Furthermore, two different methods are used, both with their own inaccuracy.

In table 4.4 gelling concentrations from earlier experiments with mud (Buscall *et al.*, 1988; Odd & Cooper, 1989; Toorman, 1992; Williams & Williams, 1989) and bauxite mining waste (Sills, 1998) are presented as solid-phase volumetric gelling concentration ($\phi_{gel} = c_{gel}/\rho_s$) with corresponding mass concentration (c_{gel}) and bulk density (ρ_{gel}), assuming saline water ($\rho = 1030$ kg/m^3) and $\rho_s = 2650$ kg/m^3 for the mud experiments and $\rho_s = 3470$ kg/m^3 for the bauxite experiment. The values in table 4.3 correspond well with the values in table 4.4.

Table 4.4. Summary of gelling concentrations from literature.

Name	ϕ_{gel} (-)	c_{gel} (kg/m^3)	ρ_{gel} (kg/m^3)
Buscall *et al.* (1988)	0.02-0.05	50-130	1050-1100
Odd & Cooper (1989)	0.03	80	1070
Toorman (1992)	0.05	130	1100
Williams & Williams (1989)	0.01-0.07	30-180	1040-1130
Sills (1998)	0.08	280	1200

4.3.4   Characteristic lines

The shape and direction of characteristics are an indication of the type of behaviour within a suspension. They can be derived from points of equal concentration, to be determined from successive X-ray concentration profiles. This technique could only be used in the mud-only Ox-experiments as in the mud-sand experiments the presence of a second fraction invalidates the theory. The characteristics for the mud-only experiments are shown in figure 4.16. It was only possible to draw characteristic lines in the fluid mud phase and early consolidation phase. In the hindered settling phase the concentration should be equal to the initial concentration. In all plots of figure 4.16, the characteristic lines show an increasing concentration with time, indicating the possible presence of a lower interface. In figure 4.16 d and e there is, however, a decrease in concentration beyond 6000 and 4000 seconds respectively. This indicates that the consolidation phase is reached and the sediment is being compressed.

All Ox1-6 experiments have initial concentrations well below the gelling concentration, hence, there is never consolidation from the start. Whether there will be one or two interfaces is difficult to judge from figure 4.16, especially as there are no experimental results on the direction of characteristics in the hindered settling phase.
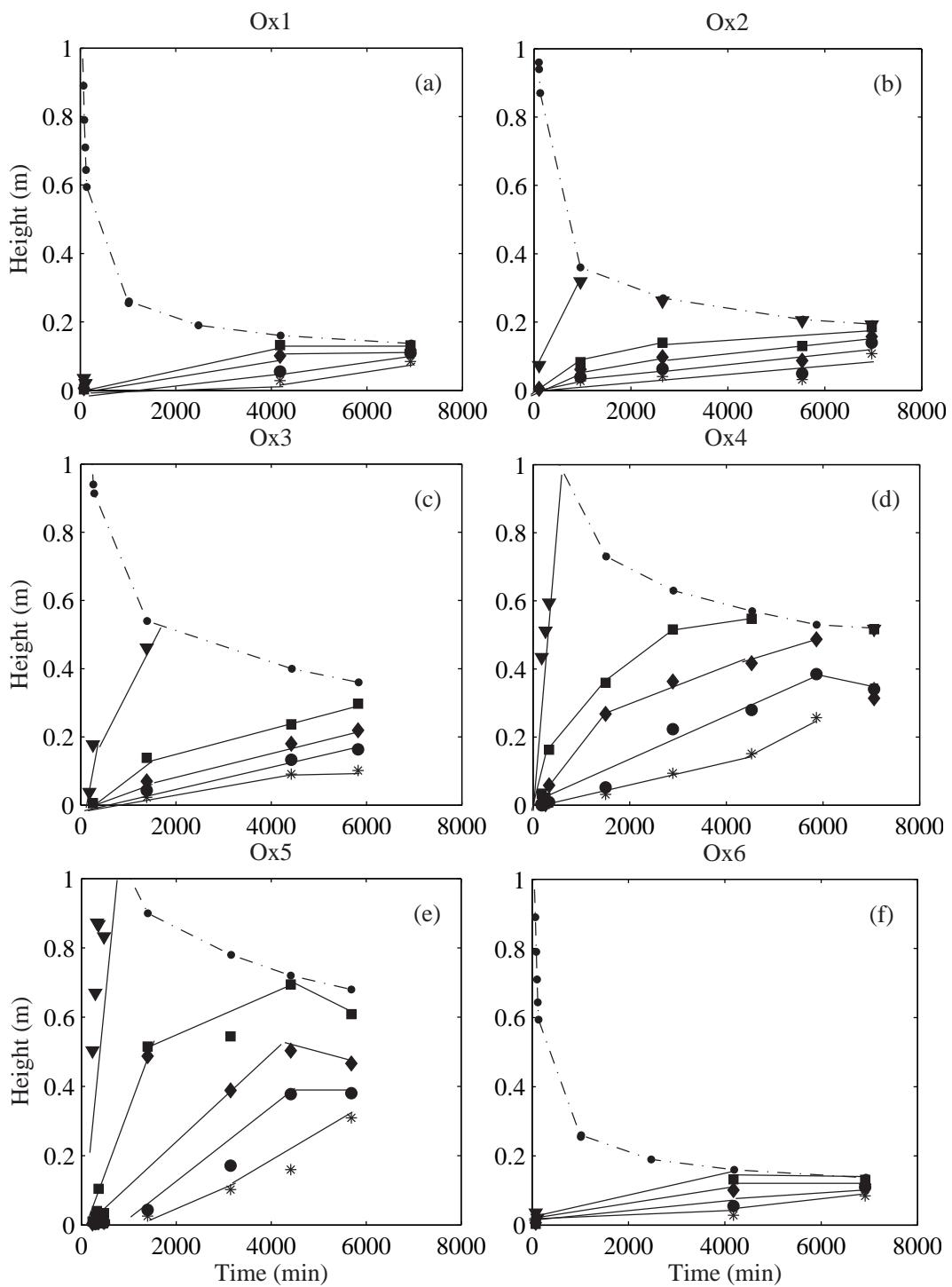
Figure 4.16. Points of equal concentration in the fluid mud and early consolidation phase. Concentrations: $80 < \blacktriangledown < 85$ kg/m^3, $120 < \blacksquare < 125$ kg/m^3, $135 < \blacklozenge < 140$ kg/m^3, $150 < \bullet < 155$ kg/m^3, $165 < * < 170$ kg/m^3.

4.3.5   Concentration profiles

Another way to study the possible occurrence of interfaces is from vertical concentration profiles. We used an X-ray profiler to measure undisturbed concentration profiles. For every measurement the X-ray was traversed along the column from top to bottom and back.

Figure 4.17 shows settling profiles of mud-only experiments Ox1 - Ox5. The concentration is calculated from the count rate by means of conservation of mass, described in section 4.2.2, which is the most accurate calibration method. All figures show a constant
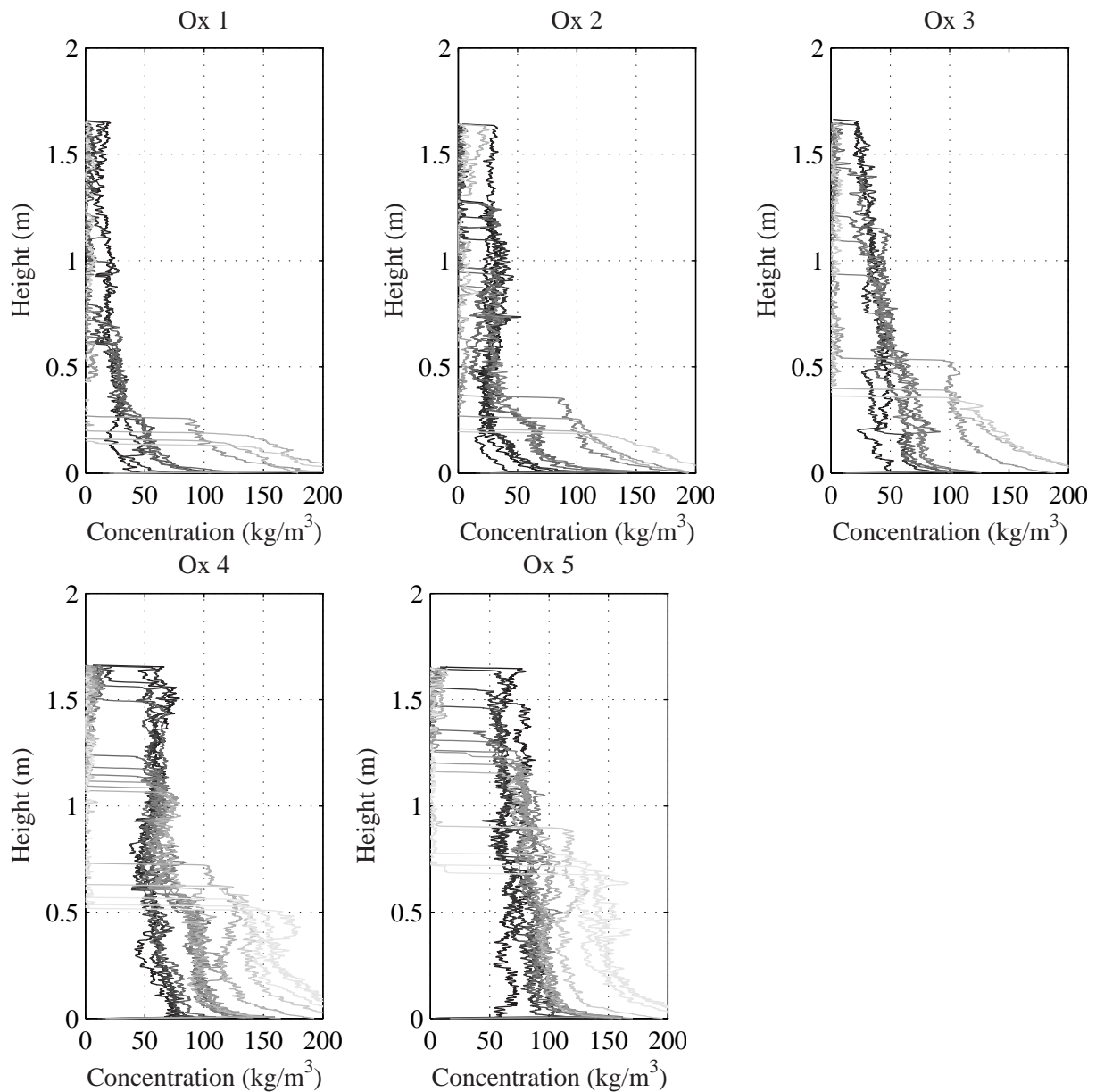

Figure 4.17.   Concentration profiles of mud-only Ox-experiments.

settling velocity of the upper interface in the hindered settling phase. In the fluid mud and consolidation phase, the upper interface settles much slower.

In figure 4.18 the profiles of experiment Ox4 are plotted separately for more details on the settling and the formation of interfaces. Effects of segregation and settling are already visible during the first few hours in figure 4.18. Close to the bottom of the column the concentration increases gradually in the downward direction. An upper interface is visible from $t = 1{:}00$ [hr:mm] onward, while a lower interface can be detected from measurement Ox4ddown until measurement Ox4gdown. This lower interface moves slowly upward in time until it meets the upper interface in Ox4hdown. The initial concentration in experiment Ox4 is 53 kg/m^3, well below the gelling concentration, and the occurrence of two interfaces is to be expected. The concentration profiles in experiment Ox1 - Ox5 (figure 4.17) show a similar behaviour, as do results from Sills (1998) for experiments with bauxite mining waste.

In experiments Ox6 - Ox21 sand was topped on the mud suspension after the first X-ray profile measurement. In this case the concentration could not be calibrated with the conservation of mass method. Instead, calibration samples were used and the regression lines obtained from these calibration were used to calculate the concentration from the X-ray count rate, giving a less accurate calibration method. Another inaccuracy ensues from the segments that build up a column. When the segments are not completely in line, the X-ray travels through less mass, resulting in negative concentrations and less accurate measurements. This effect can be seen, for example, in figure 4.19 in Ox13fdown, by a decrease in concentration between 0.5 and 1 meter.

Figures 4.19 and 4.20 show concentration profiles for the series Ox13 ($c_0 = 25$ kg/m^3), Ox16 ($c_0 = 15$ kg/m^3) and Ox18 ($c_0 = 41$ kg/m^3). Contrary to the behaviour of the mud-only experiments in figures 4.17 and 4.18, figures 4.19 and 4.20 show only an upper interface.

First, we will discuss figure 4.19. From Ox13bdown onwards there is a distinct upper interface between the clear water layer and the mud-sand suspension. Sand was injected into the system after Ox13adown in three separate suppletions of 5 gram fine sand ($D_{50} = 110$ μm), 20 gram coarse sand ($D_{50} = 360$ μm) and again 5 gram fine sand. The increase in concentration towards the bottom of the column can be explained by consolidation and segregation of sand and dense mud flocs. The settling of sand causes a strong return flow, as explained before. We hypothesize that upon the release of sand, the structure of the mud suspension is strongly disturbed, and a possible lower interface is destroyed. After the disturbance a new lower interface does not seem to develop again.

The concentration profiles show that the initial concentration has a strong influence on the settling of the interface. With a change in initial concentration from 15 kg/m^3 (Ox16) to 25 kg/m^3 (Ox13) and 41 kg/m^3 (Ox18), the settling velocity of the interface decreases with 66 % and 72 % respectively (see figures 4.19 and 4.20).

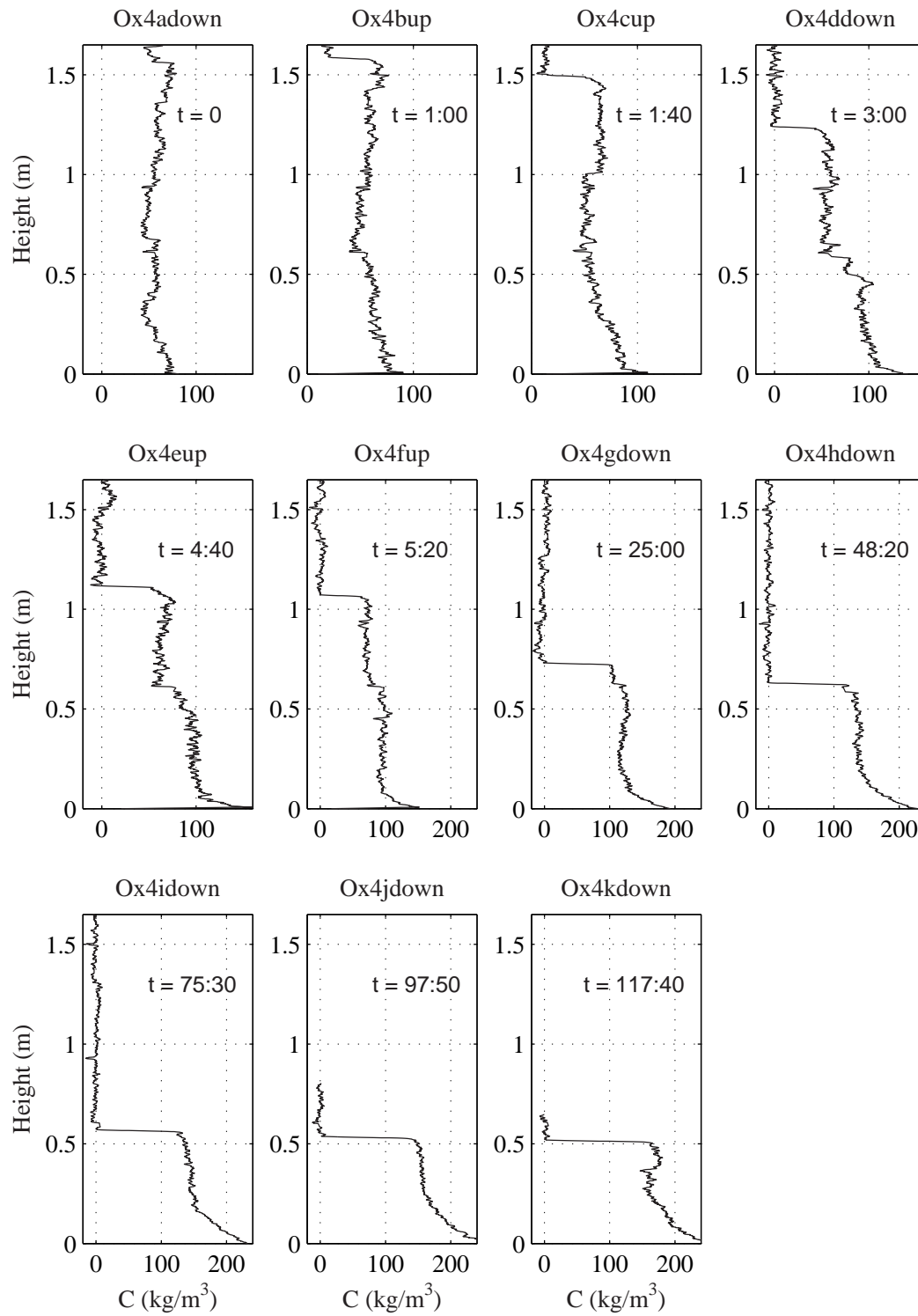**Figure 4.18.** Single concentration profiles of experiment Ox4 with $c_0 = 53$ kg/m^3 ($\rho_0 = 1036$ kg/m^3) at various times from start of the experiment (hh:mm).

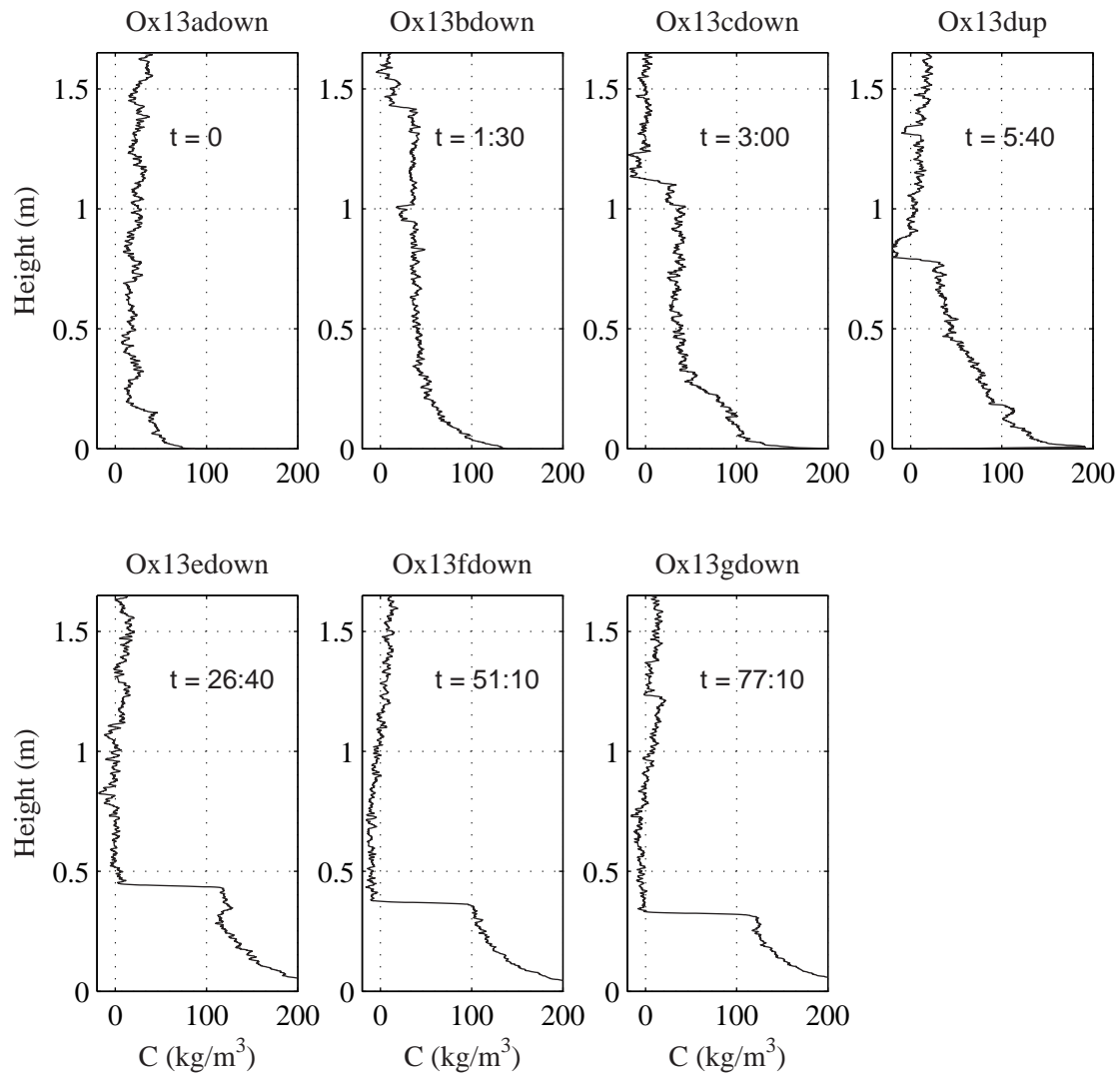**Figure 4.19.** Single concentration profiles of experiment Ox13 with $c_0 = 25$ kg/m^3 ($\rho_0 = 1019$ kg/m^3) at various times from start of the experiment (hh:mm).
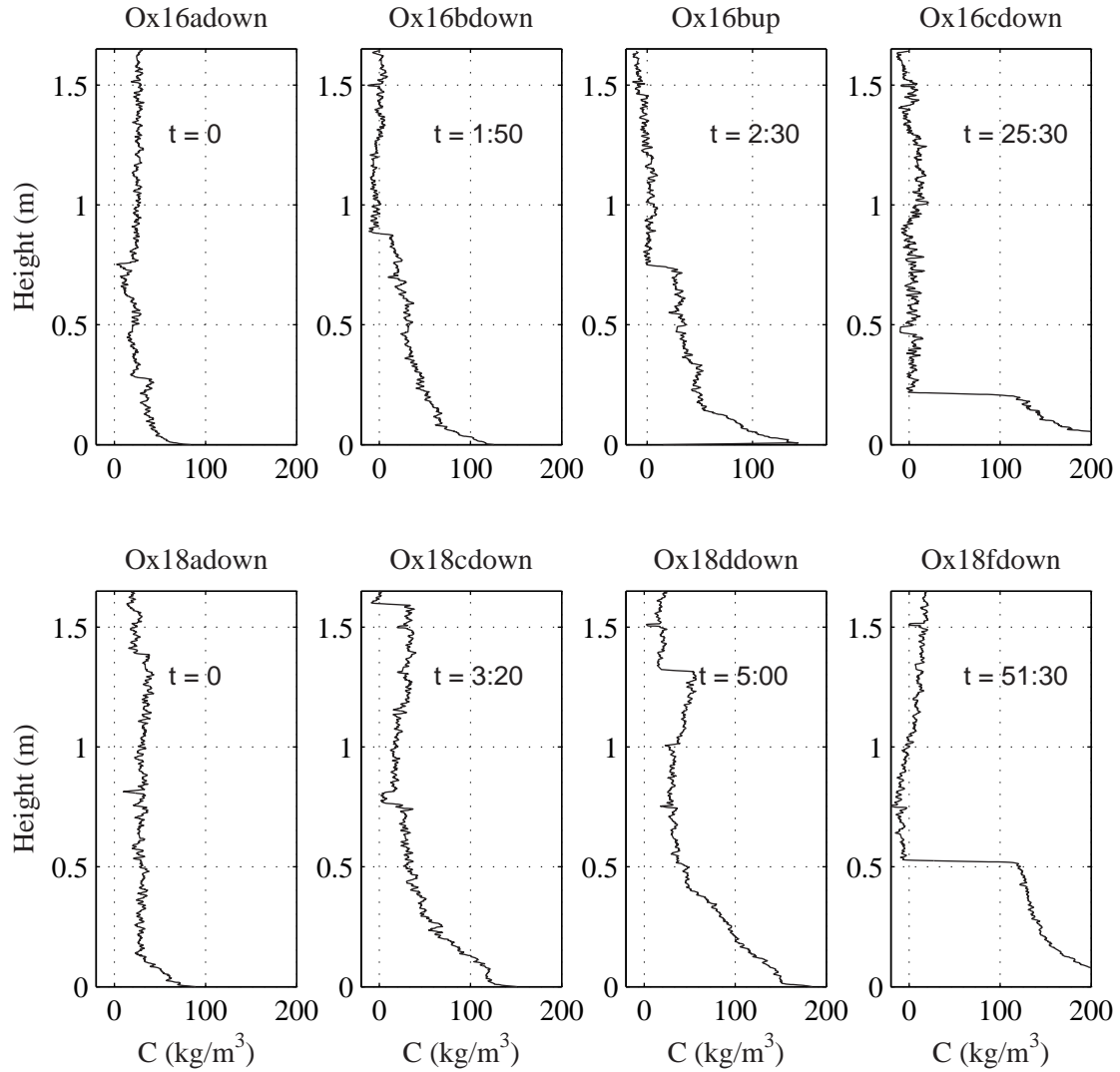
Figure 4.20. Single concentration profiles of experiment Ox16 with $c_0 = 15$ kg/m^3 ($\rho_0 = 1012$ kg/m^3) and Ox18 with $c_0 = 41$ kg/m^3 ($\rho_0 = 1028$ kg/m^3) at various times from start of the experiment (hh:mm).

In both the mud-only experiments and the mud-sand experiments the concentration profiles after 3 to 4 days (figure 4.21) have a similar appearance. The bed profiles are typically concave, indicating the presence of advection (permeability effects). This indicates that the material is in the early consolidation phase. In figure 4.21, Ox7 and Ox8, the concave shape is also due to segregated sand.

Overall, the measured concentration profiles for the mud-sand experiments do not clearly reveal the presence of two interfaces, contrary to the mud-only experiments. As said, this may be due to destruction of the developing lower interface by the sand grains. Unfortunately, this cannot be validated from the current data set.
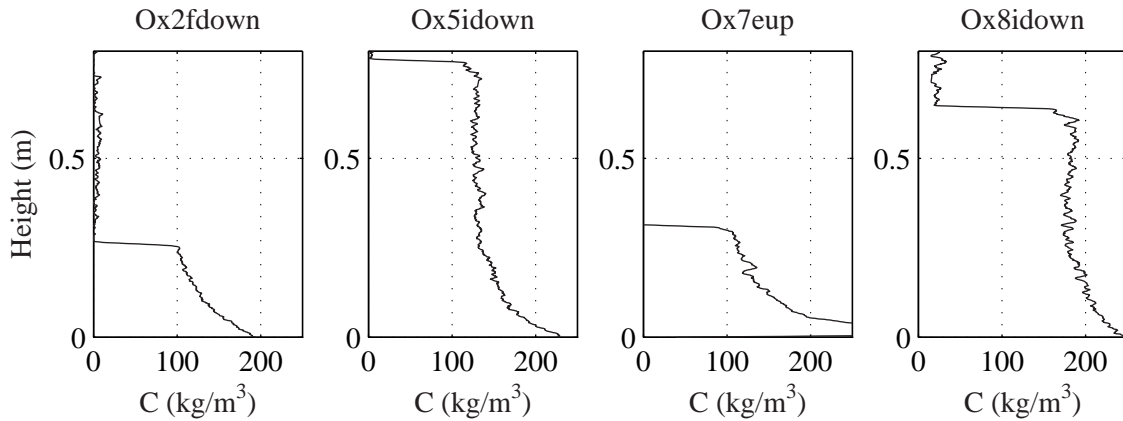
Figure 4.21. Concentration profiles at the end of experiment Ox2 ($c_0 = 23$ kg/m^3), Ox5 ($c_0 = 62$ kg/m^3), Ox7 ($c_0 = 21$ kg/m^3) and Ox8 ($c_0 = 55$ kg/m^3).

4.3.6   Sand settling in a mud suspension

The settling velocity of sand particles within a highly concentrated mud suspension is difficult to determine, as instruments placed in the suspension disturb the velocity field. One option is to use an optical method, which detects the particles close to the wall of the column only. In this research PTV and PIV techniques were used.

Because of the low particle density of sand grains in the experiments PTV was used to determine the settling velocity of the sand grains (w_s^s). All experiments in which sand velocities are determined are presented in table 4.5. The sand velocities were measured approximately 1 meter below the input level. It is therefore expected that the measured settling velocities are the equilibrium velocities.

Due to the observed flow of mud, which increased or decreased the settling velocity of sand grains, meaningful data can only be obtained when the measured sand settling velocities are corrected for the mud flow, giving a sand settling velocity ($w_{s,eff}^s$) relative to the mud flow. Because of the high particle density of the mud, PIV, which uses pattern recognition, was used to determine mud flow. For compatibility with the PTV results, the same frames as for the PTV measurements were used for the PIV measurements. The calculated PIV velocities of the mud (w_z, positive in upward direction) were placed on a grid and interpolated yielding a mud velocity in every grid cell of the frame. An example of two calculated vector plots and their corresponding interpolated velocity fields is shown in figure 4.22. The white area between X = 15 and X = 20 in the vector plots is an area with no data because of light reflection.

In the vector plots an area with strong upward flow can be identified (upward flow velocity $w_z \leq 2$ mm/s). Where upward (light colour in interpolated plot) and downward (dark colour in interpolated plot) flow meet, the downward flow is deflected. Apparently the upward flow is not stationary, as its area in the measuring window increases with time, as shown in figure 4.22. This type of behaviour, with narrow areas in which the suspension flows upward in an otherwise settling suspension, was observed during both the experiments with kaolinite and with natural mud. The specific case in figure 4.22 shows

Table 4.5. Settling velocities of sand determined with PTV and PIV. $\overline{w_s^s}$ gives the mean settling velocities of the sand grains and their standard deviation, $\overline{w_{s,eff}^s}$ gives the mean effective settling velocities of the sand grains (with respect to the mud flow) and their standard deviations.

| Id	c_0 (kg/m^3)	Sand input (gram)	$\overline{w_s^s}$ (mm/s)		$\overline{w_{s,eff}^s}$ (mm/s)	
			mean	std	mean	std
Ox7	21	20 fine	2.50	1.64	2.48	1.64
			1.50	1.14	1.48	1.14
Total			1.98	1.49	1.95	1.49
Ox11	32	20 fine	1.82	1.76	1.83	1.77
			1.74	1.42	1.74	1.42
Total			1.77	1.56	1.77	1.57
Ox11	32	5 coarse	1.41	1.45	1.40	1.45
Ox12	40	20 fine	2.24	2.13	2.22	2.12
		5 coarse	2.93	2.62	2.90	2.60
		5 coarse	3.95	3.57	3.91	3.58
Ox13	25	5 fine	3.10	2.05	3.08	2.05
		20 fine	2.89	1.78	2.88	1.79
		5 coarse	1.66	1.46	1.64	1.48
Ox14	11	20 fine	2.35	1.74	2.40	1.75
Ox15	21	5 fine	0.84	1.31	0.81	1.33
		20 fine	2.74	1.74	2.74	1.74
		20 fine	1.69	1.31	1.68	1.31
Ox16	15	5 fine	3.55	2.60	3.54	2.60
		20 fine	3.35	2.40	3.33	2.40
Ox17	31	5 fine	4.20	2.22	4.21	2.21
		20 fine	2.73	1.57	2.74	1.58
			2.24	2.15	2.24	2.15
Total			2.88	1.71	2.90	1.72
Ox18	41	5 fine	1.66	1.51	1.67	1.52
		20 fine	3.05	2.26	3.05	2.26
Ox19	18	5 fine	1.99	1.41	1.99	1.41
		20 fine	2.68	1.67	2.68	1.67
Ox20	37	20 fine	1.46	1.39	1.45	1.39
		20 fine	2.29	1.65	2.28	1.67
Ox21	47	20 fine	1.06	0.84	1.04	0.84
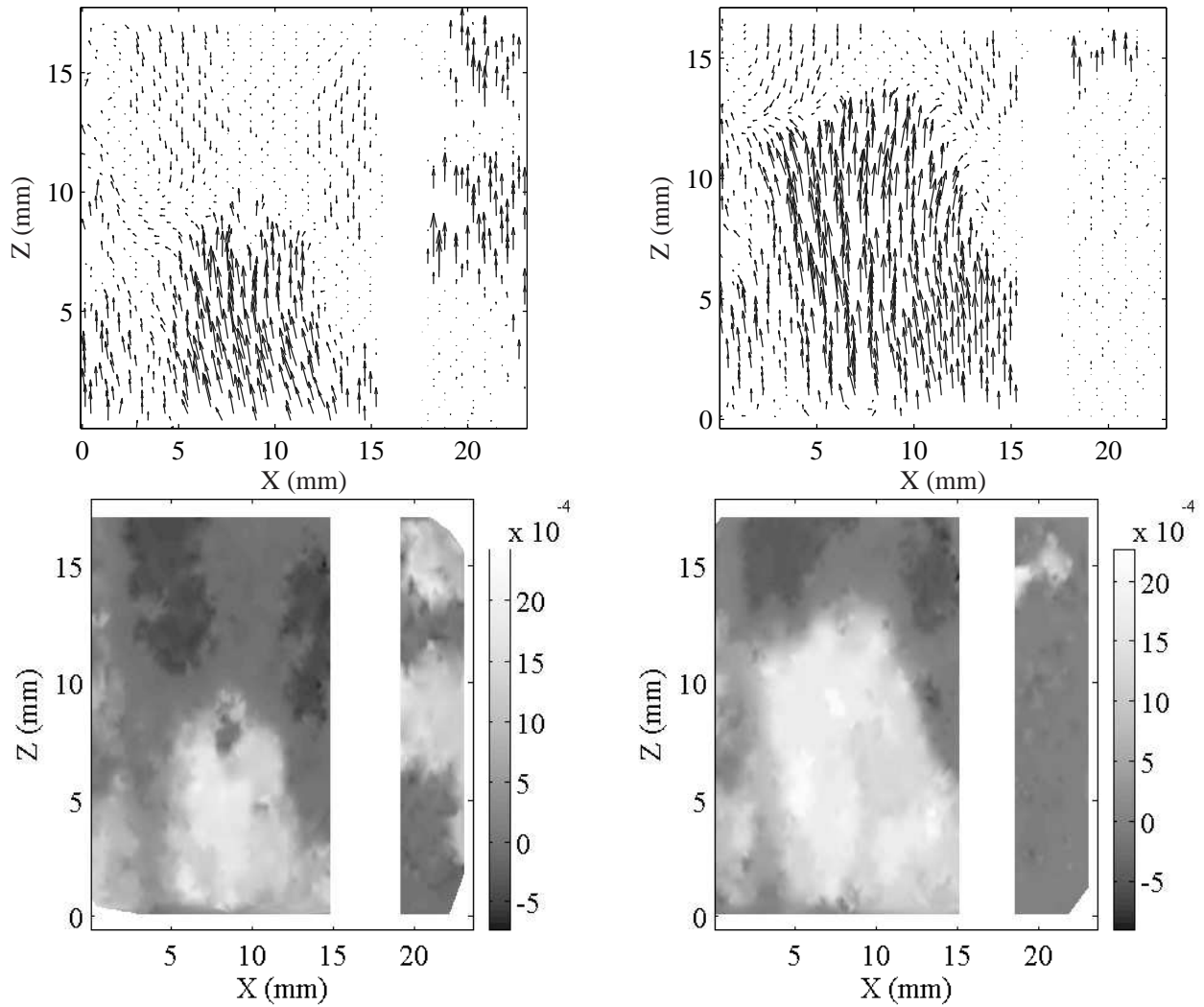
Figure 4.22. Vector plots for mud flow from PIV measurements (every fourth vector plotted) for two successive frames (0.5 seconds after each other) and their interpolated w_z magnitude fields. The velocity is given in m/s, with w_z positive in upward direction.

an up-flowing area with a width of 1 cm, but from visual observations we can conclude that the width can be a factor 5 larger. Although this type of behaviour occurs in both mud-only and sand-mud settling, it is expected to be more distinct in the latter due to the much larger density of sand grains compared to mud flocs.

The interpolated w_z fields in figure 4.22 give a good average representation of the corresponding vector fields. Therefore these interpolated velocity fields can be used to correct the PTV sand velocity, resulting in an effective settling velocity for sand particles settling through the mud suspension ($w^s_{s,eff}$).

In table 4.5 the mean effective settling velocities of the sand grains ($\overline{w^s_{s,eff}}$) per experiment are given. This table shows that $\overline{w^s_{s,eff}}$ does not significantly differ from $\overline{w^s_s}$, implying that the presence of irregular mud flow does not affect the mean settling velocity of the sand grains too much. Apparently, some grains are moving up while others are moving down, thereby cancelling out the effect of return flow.

Figure 4.23 shows the mean effective settling velocities of sand grains for the experiments in which 20 grams of fine sand was used. In the experimental data, $\overline{w^s_{s,eff}}$ seems to decrease with an increase in the local mud concentration, though the changes are small. A clear trend cannot be detected. Possible reasons will be given in the next chapter. Still, the settling velocity is much smaller than the Stokes' settling velocity for a single grain in clear water ($w^s_s = 10.9$ mm/s for sediment with $D_{50} = 110$ μm).
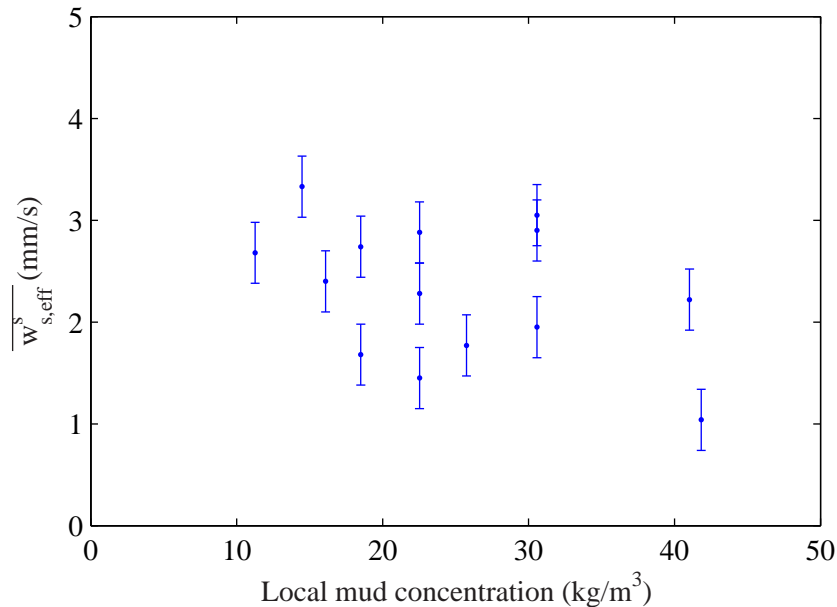

Figure 4.23. Measured mean effective sand settling velocities. The measured velocities are shown with their measuring error band.

The overall results suggest that settling takes place in three successive stages, depending on the local mud concentration:

1. Free settling stage: sand grains settle with their Stokes settling velocity.

2. Hindered settling stage: settling velocity of sand grains is reduced by the mud because volume effects start to play a role. Thereafter the settling velocity only decreases slowly with increasing suspension concentration.

3. Final stage: sand grains are arrested in the mud matrix and settle with the much lower suspension settling velocity ($\approx$ 0.1 mm/s). If dewatering channels are formed, sand grains can use these and their settling velocity increases again.

Although the mean effective settling velocities for many experiments were similar, the velocity distribution can be different. In figure 4.24, velocity distributions for four different experiments are given. The mean effective settling velocities in figures 4.24 a, b and c are comparable but the velocity distribution of figure 4.24 b is more skewed towards the left.

The histograms show that the velocity distribution is very wide, which is the result of segregation, decreased velocities by return flow and inaccuracies in the PIV method. The initial sand grain distribution can give an indication of the amount of segregation. Stokes' settling velocity calculated from the grain size distribution in figure 4.1 a, lies in the range of 7 - 15 mm/s for 70 % of the sand particles and 15 - 40 mm/s for 30 % of the sand particles, already indicating a particle size distribution that is skewed towards the left.

A good example of segregation or a decreased velocity due to return flow effect is presented in figure 4.25. The first histogram presents the velocity distribution in the first 20 seconds of sand input, while the second histogram presents the velocity distribution 30 seconds later. The mean velocity has decreased 20 % in this time span and the distribution in figure 4.25 b shows a higher percentage of low velocities and a peak velocity that has shifted towards the left. Either figure 4.25 a is dominated by the larger sand particles, while in figure 4.25 b the smaller particles pass by, or more sand grains are hindered by the mud and irregular flow in figure 4.25. This process of segregation and decreased velocities could not always be detected because of the short duration of every video (1 minute) compared to the long time span of sand passage.

From calculations we have estimated that the mean settling velocity of the sediment grains measured at the column's wall was decreased by about 0.3 mm/s because of wall effects. This would shift the velocity distributions in figure 4.24 and 4.25 slightly to the right. However, for the overall distribution this effect seems small. Furthermore, even though it was found that the sand was distributed evenly over the column's cross section, it is not known whether the sand grains along the wall represent the total grain size distribution or only the fastest or slowest settling particles.

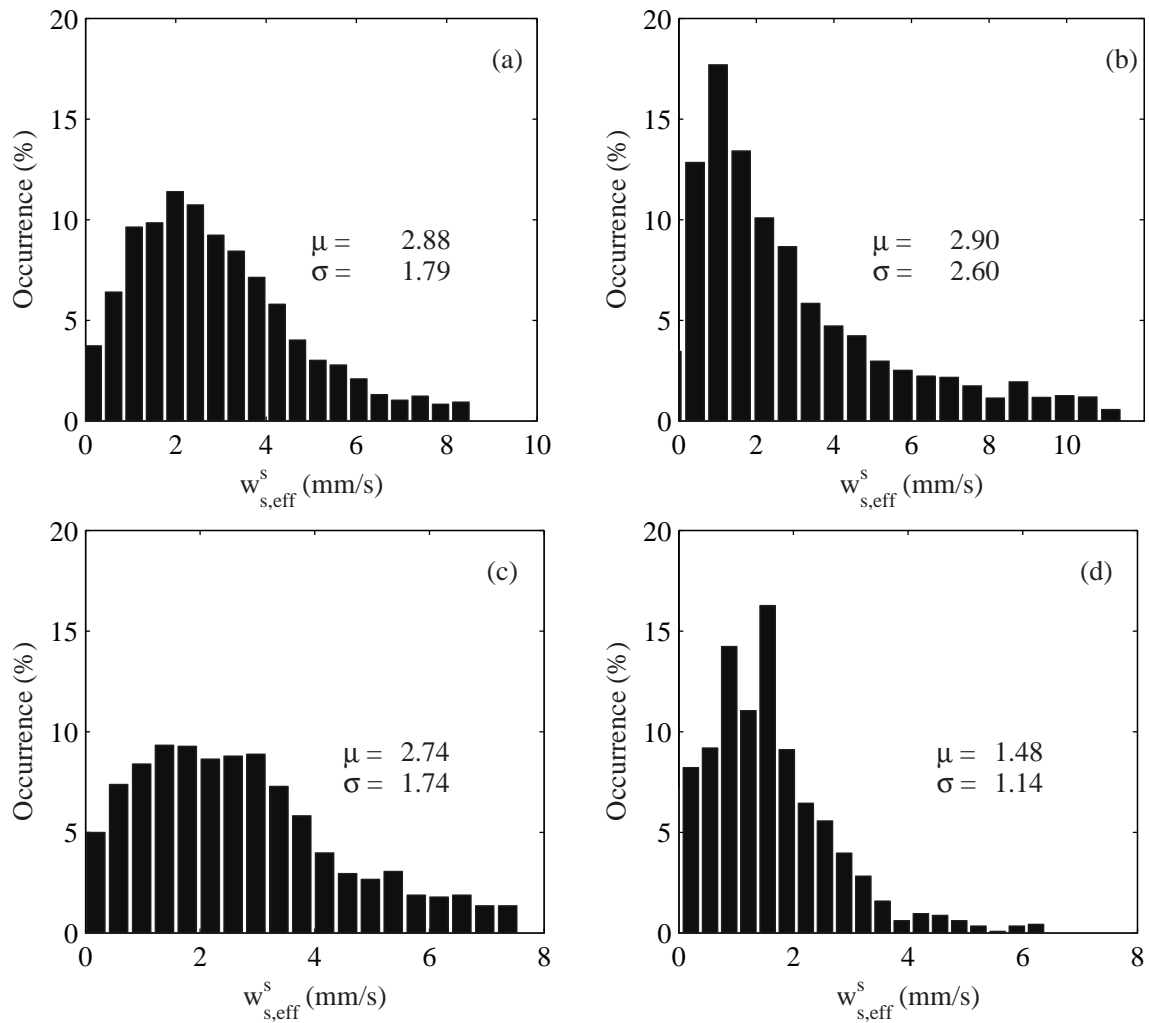**Figure 4.24.** Velocity distributions of sand grains settling through a mud suspension in experiment (a) Ox13 ($c_0 = 25$ kg/m^3), (b) Ox12 ($c_0 = 40$ kg/m^3), (c) Ox15 ($c_0 = 21$ kg/m^3) and (d) Ox17 ($c_0 = 40$ kg/m^3); μ = mean settling velocity (mm/s) and σ = standard deviation (mm/s).
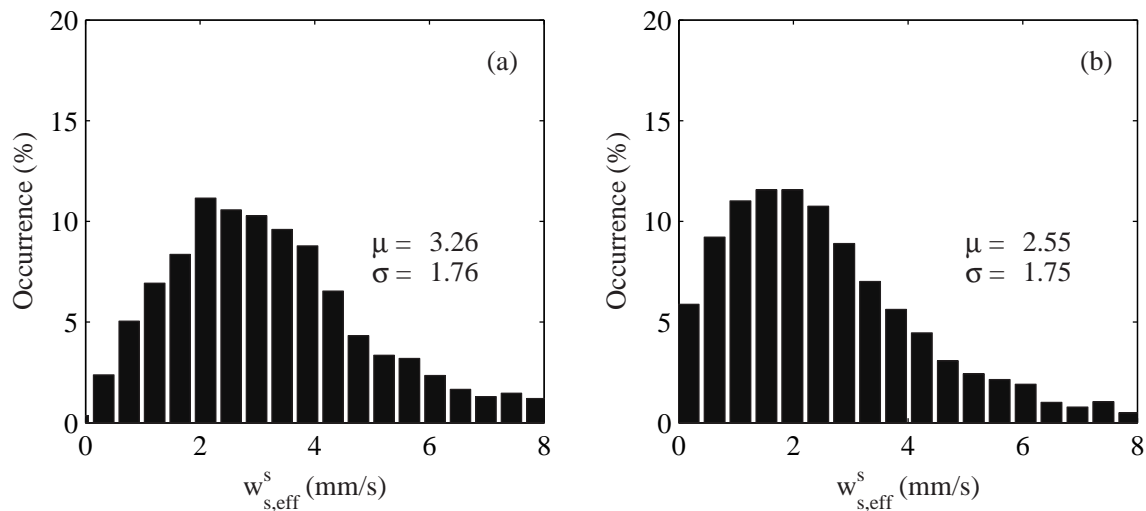
Figure 4.25.   Velocity distributions of sand grains settling through a mud suspension for PTV measurement in Ox13, μ = mean settling velocity (mm/s) and σ = standard deviation (mm^2/s^2). (a) For the time interval t = 0 - 20 s. (b) For the time interval t = 50 - 60 s. t = 0 is the start of the video measurement.

4.4   Discussion and concluding remarks

The goal of these experiments was to gain insight into the behaviour of both the mud and sand fraction in a highly concentrated mud suspension with a low sand concentration, and more specifically, to determine the settling velocity of both the mud and sand fraction. Various experiments were performed to reach this goal. An X-ray system was used to measure concentration profiles of settling suspensions. From these profiles, typical settling parameters such as the suspensions' settling velocity, the gelling concentration and the existence of interfaces within the suspension could be determined. The settling velocities of the sand grains were determined with PTV and PIV techniques. Next to an average settling velocity, these techniques also gave insight in the velocity distributions and the random occurrence of flow in the main mud suspension. This flow was induced by the settling of the sand grains and caused the suspension to flow upward locally. Much information on the processes in a settling suspension was gained by visual observations during the experiments.

This combination of various techniques has given more insight into the behaviour of settling suspensions. The suspensions were found to settle with velocities ranging from 0.02 to 0.3 mm/s, depending on the initial concentration. The sand grains were hindered by the suspension and their settling velocity was found to be in the order of a few mm/s, which is significantly lower than the calculated Stokes settling velocity of 1 cm/s. No clear relation was found between the settling velocity of sand in the mud hindered settling regime and the local suspension's concentration, although a slight decrease in sand settling velocity with an increase in mud concentration seems to occur.

The sand grains, that were introduced in the suspension, created considerable distur-

bance. Both strongly increased upward and downward flows were observed. A PTV - PIV comparison did not show a change in the mean sand settling velocity due to these disturbances. The PIV method was, however, not accurate, meaning that an influence of the mud flow on the sand settling velocity may have been present. Furthermore, even though the mean settling velocity of the sand grains was not influenced, the settling velocity distribution may have been altered.

Because settling columns were used in the experiments, wall effects may have influenced the measured velocities. Some grains got stuck on the walls, thereby decreasing the measured mean settling velocity. There were, however, no signs that the settling of sand grains occurred only at the wall or only in the middle of the column. Horizontal segments of the consolidated mud showed an equal distribution of sand grains and sand pockets throughout the horizontal cross-section.

Once the material started to consolidate the sand grains were expected to be arrested and settle together with the mud. Observations showed that this was not always the case. The sand grains travelled through dewatering channels deeper into the mud, thereby forming sand pockets at the end of the dewatering channels. This effect can both increase or decrease the consolidation rate. Either the sand grains keep the channels open for a longer time and the water is expelled faster from the soil, or the sand grains block the up flowing water, thereby decreasing the amount of water expelled from the soil. Which of the two processes is dominant is not investigated in this research. Furthermore, due to the presence of sand in the mud bed the permeability of the soil is increased, which should increase the consolidation rate. We anticipate that there exists a subtle interaction between the dewatering channels, the expelled pore water flow, the sand grains and the sand pockets formed in this way, affecting the overall settling and consolidation behaviour of the mixtures.

To the knowledge of the author a unique data set is obtained in this research. Further progress can be made through optimising the experimental methodology and measuring techniques, and the use of numerical models for data analysis. The latter is discussed in Chapter 5.

5

Modelling of hindered settling

5.1 Introduction

In this chapter, the experimental data sets, presented in Chapter 3 and 4, are used to test the hindered settling model in Winterwerp & Van Kesteren (2004). In the previous chapters the simple wave equation (equation 2.10) was used to describe the hindered settling regime. However, this equation cannot deal with the consolidation regime as the mass balance equation becomes parabolic when effective stresses become relevant (Winterwerp & Van Kesteren, 2004). Moreover, the simple wave equation describes hindered settling in still water only, while in flowing water also (turbulent) diffusion must be accounted for. To be able to deal with both hindered settling and early consolidation and with flowing water, hindered settling, turbulent diffusion and consolidation have been incorporated in one advection-diffusion equation, which has been implemented in a 1DV-Point model by Delft Hydraulics. The use of an advection-diffusion equation implies that this model is not optimal for solving the simple wave equation. However, if diffusion is small, as is the case with molecular diffusion, the model results should be accurate enough. This assumption is elaborated in the next section.

5.2 Model description

The model was developed on the basis of DELFT3D-FLOW by stripping all horizontal gradients, except the horizontal pressure gradient. It is described in Winterwerp (2002) and Uittenbogaard *et al.* (1996). The model equations are already partly described in Chapter 2 but are given again for convenience. The vertical transport of sediment is modelled with an advection-diffusion equation, using fractal theory, given by Winterwerp & Van Kesteren (2004):

$$\frac{\partial \phi_p}{\partial t} - \frac{\partial}{\partial z} \{\Xi_s \phi_p\} - \frac{\partial}{\partial z} \left\{ (D_{\mathrm{s}} + \Gamma_{\mathrm{T}} + \Gamma_{\mathrm{c}}) \frac{\partial \phi_p}{\partial z} \right\} = 0 \qquad (5.1)$$

with t is time, z is the vertical co-ordinate, ϕ_p is the volumetric concentration of the solids, D_{s} the molecular diffusion coefficient for sediment, Γ_T the eddy diffusivity, Γ_c the diffusion component in the consolidation formula (e.g. consolidation coefficient) and Ξ_s

is the settling function. Ξ_s consists of two parts, one for the hindered settling and one for the consolidation regime:

$$\Xi_s = w_\mathrm{s} + \frac{f_c}{1 + \eta f_c} \tag{5.2}$$

in which w_s is the effective settling velocity in the hindered settling regime, as given by equation 2.4 for mud and equation 2.6 for mud-sand mixtures, and the second term accounts for the effects of permeability. The parameter η is chosen such that a smooth curve is obtained. In this research we do not incorporate consolidation and there is no turbulence in our experimental set up. This means that the advection-diffusion equation can be reduced by taking out the turbulence and consolidation effects as described by the second and third term, leading to:

$$\frac{\partial \phi_p}{\partial t} - \frac{\partial}{\partial z} \{w_s \phi_p\} - \frac{\partial}{\partial z} \left\{ D_s \frac{\partial \phi_p}{\partial z} \right\} = 0 \tag{5.3}$$

The equations are solved on a staggered grid, existing of 100 layers in the vertical. A first order upwind scheme is used, together with a three-point scheme for the diffusion operator in vertical direction. A time step of 1 second or 1 minute is used. The numerical diffusivity (D_{num}) for the upwind scheme amounts to $D_{num} = w_\mathrm{s} \Delta z / 2 \approx (0.3 - 3)10^{-7}$ m^2/s (Winterwerp & Van Kesteren, 2004). In our case the particle diffusion is set to $D_\mathrm{s} = 5 \times 10^{-8}$ m^2/s. It follows from $w_s \approx 10^{-4}$ m/s and $D_\mathrm{s}/\Delta z \approx 10^{-6}$ m/s, that $w_s >> D_\mathrm{s}/\Delta z$ and diffusion is negligible. Only at the end of the hindered settling phase, where the settling velocity goes towards zero, numerical diffusion starts to play a role. The parameter settings were derived from the experiments and are explained in the next section.

5.3 Hindered settling of mud

First, the mud-only experiments, presented in Chapter 3, are simulated with the mud-only part of the model. Thereafter, in the section to follow, the model is extended to include the sand fraction in order to simulate the mud-sand experiments as presented in Chapter 4.

5.3.1 Calibration

The input parameters for the model are the initial concentration distribution, the gelling concentration (c_gel), the settling velocity of single flocs ($w_\mathrm{s,0}$) and the non-linearity parameter (m). Their values are derived from the mud experiments presented in Chapter 3. For the gelling concentration we use the mean gelling concentration from table 3.1, which is 81 kg/m^3. It is understood that the gelling concentration is not a constant, but lies within a certain range, depending largely on history effects, type of minerals, chemistry of pore water, organic components (EPS, TEP), etc. For modelling purposes these effects cannot be incorporated easily and a mean gelling concentration is justifiable. The factor m is set to 2 (Dankers *et al.*, 2006). This means that non-linearities in return flow are
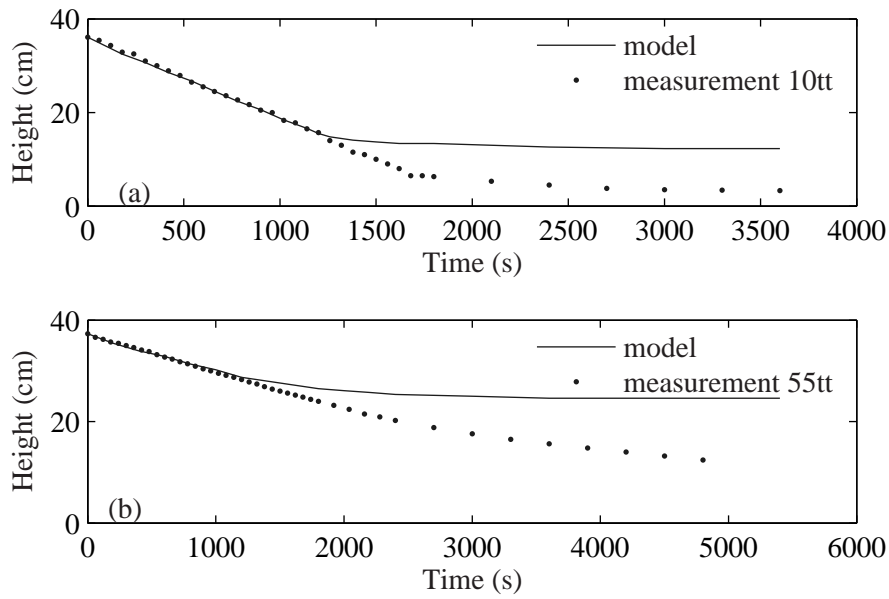
Figure 5.1. Fit of the model to experiment 10tt ($c_0 = 27$ kg/m^3) and 55tt ($c_0 = 54$ kg/m^3) to establish $w_{s,0}$.

taken into account, and the formation of a second interface is allowed. It is not possible to derive the parameter $w_{s,0}^m$ from measurement directly. With kaolinite suspensions it is impossible to distinguish single particles, as the entire suspension is milky, even at low kaolinite concentrations. Therefore, the value of $w_{s,0}^m$ is derived from fitting model results to the results of a few experiments. The $w_{s,0}^m$ values are expected to change with initial concentration, as larger flocs will be formed with increasing initial concentrations.

Figure 5.1 shows the fit of the model to the data. In figure 5.1a a settling velocity for single flocs of 0.7×10^{-3} m/s is obtained, while figure 5.1b gives a best fit with a settling velocity of 1.5×10^{-3} m/s. A good fit can be obtained in the hindered settling regime of the two data sets. However, when the consolidation phase is reached the model does not agree with the experiments any longer. This, of course, is due to the fact that consolidation is not incorporated in this model. In the hindered settling model the bed concentration cannot exceed c_{gel}, whereas in the experiments the concentration can become larger than c_{gel} because of consolidation. Hence the interface can settle further in the latter case.

5.3.2 Results

After the model is calibrated for experiment 10tt and 55tt, validation with the other experiments is performed. The value of $w_{s,0}^m$ for the other experiments is obtained through linear interpolation and extrapolation against concentration of the values obtained for experiment 10tt and 55tt (table 5.1). This means that $w_{s,0}^m$ is not a completely independent parameter. For both c_{gel} and m the mean value derived from the experiments is used, hence also these parameters are not completely independent.

Thus all parameters are now available to model the hindered settling behaviour of the suspensions. Three examples are presented in figure 5.2.

Figure 5.2 a, b and c show good results in the hindered settling regime but a deviation of the model in and just before the consolidation regime.

Table 5.1. Settling velocity of a single particle in still water for various initial concentrations.

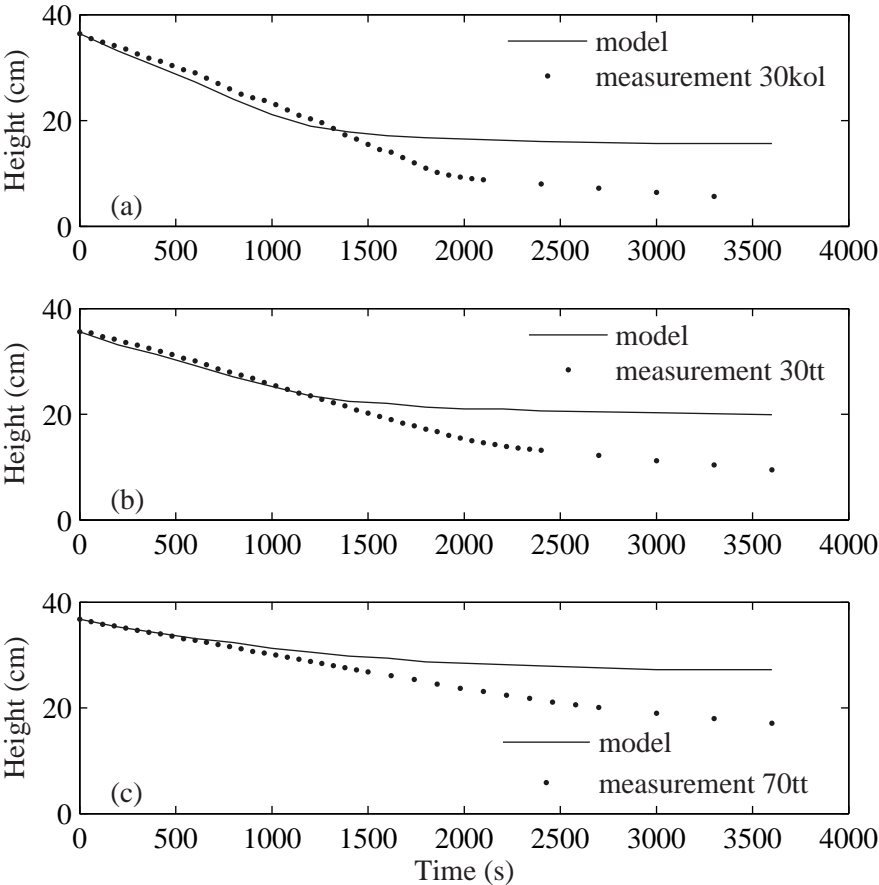| Id	c_0 (kg/m^3)	$w_{s,0}$ (mm/s)
30kol	35	0.95
40kol	46	1.28
50kol	61	1.73
60kol	71	2.03
70kol	84	2.42
80kol	100	2.90
10tt	27	0.71
20tt	39	1.07
30tt	46	1.28
40tt	48	1.34
50tt	68	1.94
55tt	54	1.52
60tt	77	2.21
70tt	60	1.70
80tt	96	2.78
90tt	108	3.14

Figure 5.2. Validation of the calibrated model with experiment 30kol ($c_0 = 35$ kg/m^3), 30tt ($c_0 = 46$ kg/m^3) and 70tt ($c_0 = 60$ kg/m^3).

In general, the higher the initial concentration, the sooner this deviation occurs. The reason for this deviation is that consolidation is ignored. As a result, the bed in the model stops to settle after some time.

All modelling results are summarised and compared to the experimental results in figure 5.3. Equation 2.4 gives good results for the lower initial volumetric concentrations ($\phi_0 < 0.7$ or $c_0 < 60$ kg/m^3). At higher concentrations the computed settling velocities are slightly lower than the measured settling velocities. The experimental results are also compared with the Richardson & Zaki (1954) formula (equation 2.3). First, n is set to 4 (RZ4), advocated by Mehta (1986). This results in an underestimation of the settling velocity. By fitting the model to the data, we find a value of $n = 3.3$ (RZ3.3) to be more appropriate, giving a representation of the data of comparable quality as equation 2.4. The measurements are presented together with their error bands. These error bands indicate the range of volumetric concentrations if not the mean $c_{gel} = 81$ kg/m^3 but its minimum $c_{gel} = 66$ kg/m^3 and maximum $c_{gel} = 90$ kg/m^3 are used to calculate the volumetric concentration from the mass concentration and gelling concentration.
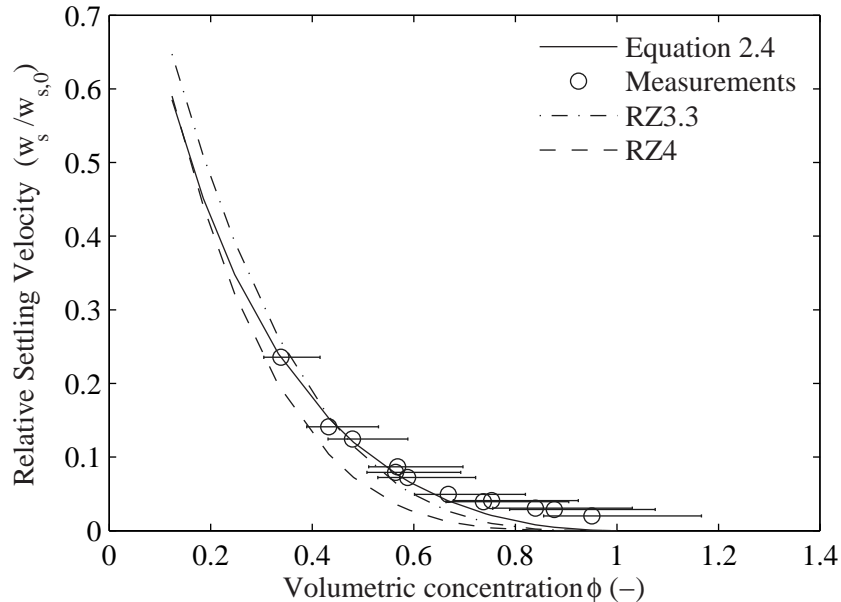

Figure 5.3. The relative settling velocity, obtained from experimental results (including measuring error) is compared with equation 2.4 with $m = 2$ and equation 2.3 (RZ3.3 and RZ4) with $n = 3.3$ and $n = 4$.

The sensitivity of the model to variations in gelling concentration is shown in figure 5.4, where the minimum and maximum values for c_{gel} are used, while all other parameters are kept constant.

The figure shows the bandwidth in between which the model results can vary when another gelling concentration is chosen. Only the experiments with $\phi_0 < 0.7$ are shown. Figure 5.4 shows that both mean and maximum values for c_{gel} describe the data properly,
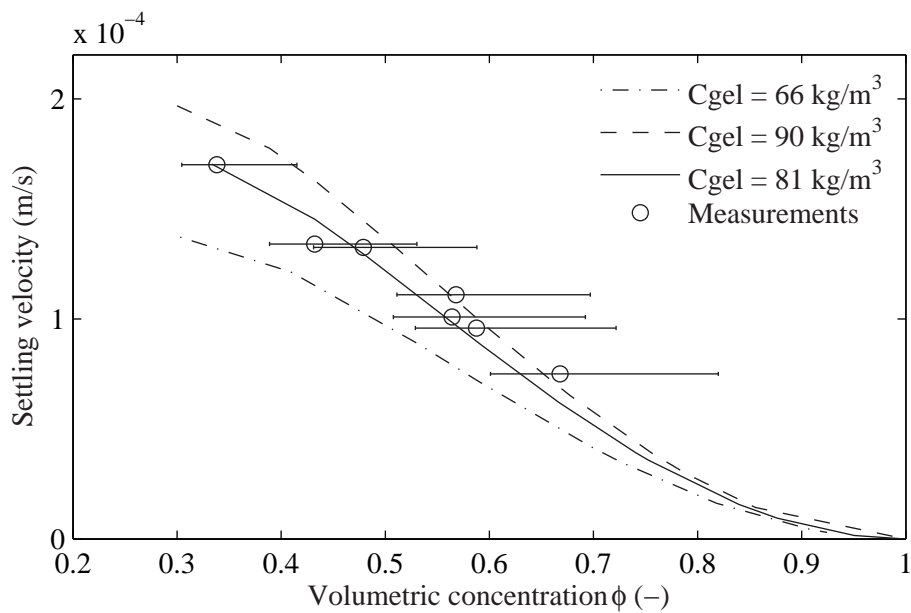
Figure 5.4. The sensitivity of the model to different gelling concentrations. The lines show the model fit at $c_{gel} = 66$ kg/m^3, $c_{gel} = 81$ kg/m^3 and $c_{gel} = 90$ kg/m^3.

the latter in particular at larger initial concentrations. For $c_{gel} = 66$ kg/m^3 there is a considerable deviation from the data.

A further evaluation is performed by analysing concentration time series of the measurements. In figure 5.5, concentration time series are shown for several experiments. This figure shows whether the model predicts the same settling velocity of the interface and whether the measured jump in concentration across the interface is properly modelled. The grey, regular lines represent the model results, showing a fair agreement with the data.

The concentration distribution computed at the lowest measuring point shows a small deviation. This is due to a small overshoot in the numerical solution of the vertical concentration distribution at the location of the interface. The gradual decrease in the measured concentration across the interfaces is due to the measuring volume of the instrument and its slow response and possibly also due to some segregation in the top layer.

The measurements in figure 5.5 are not plotted with an error band but the same error avails as for the concentration time series in figure 3.6, where the error was estimated to fall within a range of 5 kg/m^3 on either side.
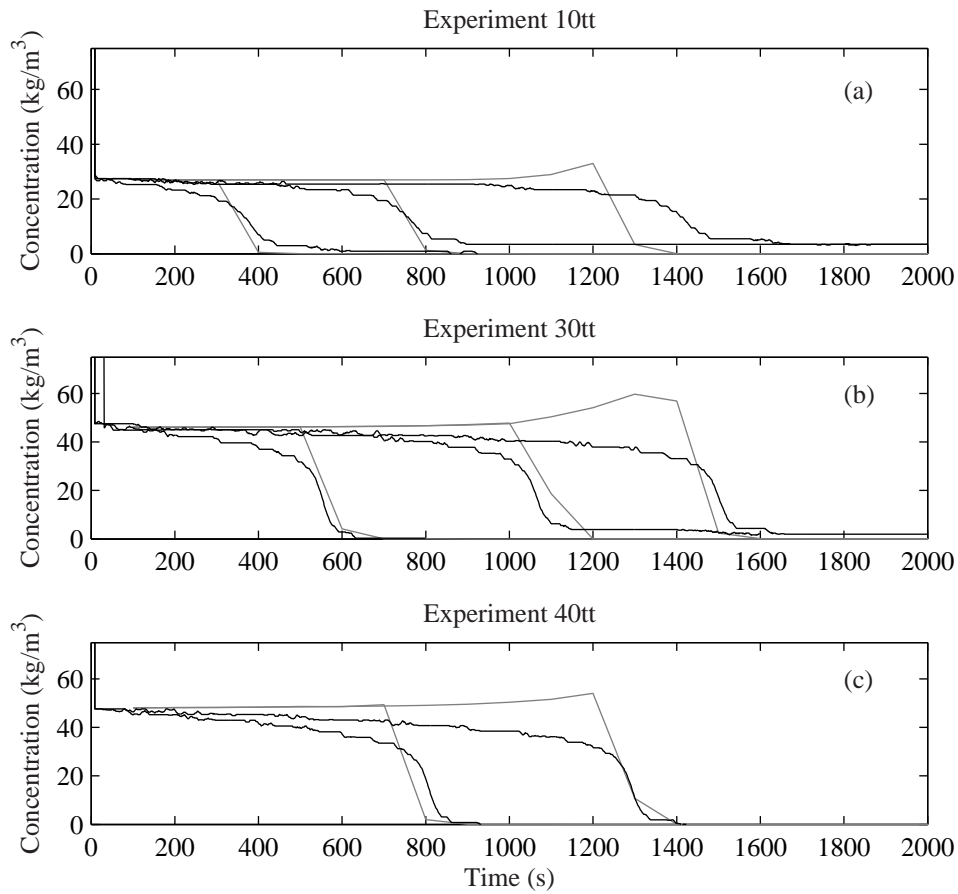
Figure 5.5. Comparison of model (grey lines) and experiments (black lines) for concentration time series. a) Experiment 10tt ($c_0 = 27$ kg/m^3) at 30, 23 and 15 cm above the column bottom. b) Experiment 30tt ($c_0 = 46$ kg/m^3) at 30, 25 and 23 cm above the column bottom. c) Experiment 40tt ($c_0 = 48$ kg/m^3) at 29 and 25 cm above the column bottom.

Finally, we investigate the sensitivity of the model to variations in m, as its actual value lies in the range of $1.4 < m < 2.6$. The lower value of m shows a better agreement at high ϕ, whereas at lower ϕ, $m = 2$ gives a better agreement with the data (figure 5.6). The sensitivity is not very large though, as long as $m > 1$, because then the behaviour of the settling curve changes in character and becomes non-monotonous.
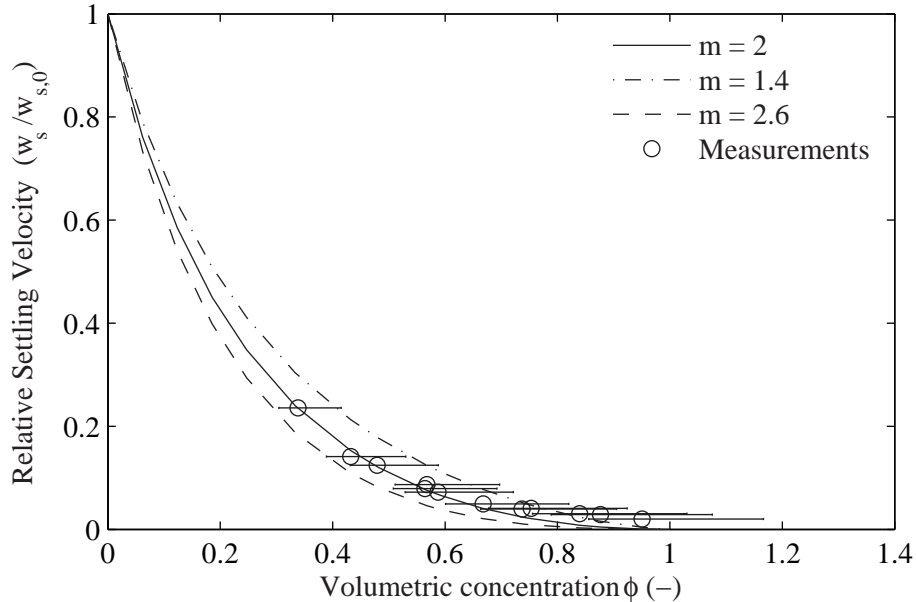

Figure 5.6. Comparison between model results for $m = 2$, $m = 2.6$ and $m = 1.4$.

5.4   Hindered settling of mud-sand mixtures

Next, the mud-sand experiments, presented in Chapter 4, are simulated. The effective settling velocity in the hindered settling regime, incorporated in the model by equation 5.2, is given, for both fractions in mud-sand mixtures separately, by equation 2.6. The gelling concentration input to the model was derived in Chapter 4. These concentrations did not show a trend with changing initial concentration. Therefore, the mean value of $c_{gel} = 91$ $\pm$ 12 kg/m^3 is used. $m = 2$ was already derived in Chapter 3. Both parameters are now independent as they were determined from different data than the mud-sand mixtures data that are used for the modelling. The settling velocity of a single sand grain can straight forwardly be determined from Stokes's law, giving $w_{s,0}^s = 11$ mm/s for sediment with $D_{50} = 110$ μm, while all other parameters and model settings were taken similar as in the mud-only simulations. The settling velocity of single mud flocs in still water, $w_{s,0}^m$, could not be derived from experiments and is therefore determined by calibration of the model against several mud-only experiments, making this an independent parameter as well. After the calibration, a validation of the complete model against the results of

the mud-sand mixture settling experiments can be performed, in which the prediction of the suspensions settling velocity, sand settling velocity and the behaviour within such a settling suspension can be tested.

5.4.1   Calibration

The SC-experiments and the mud-only Ox-experiments are used for a calibration of the model and determination of the $w_{s,0}^m$ values. A few examples are given in figure 5.7, while the corresponding $w_{s,0}^m$ values are given in table 5.2. The average $w_{s,0}^m$ value for natural mud is 0.5 mm/s, which is smaller than the derived values for kaolinite in table 4.2. Furthermore, there is no trend in $w_{s,0}^m$ values with changing initial mud concentrations and an average value shall therefore be used in the model validations.
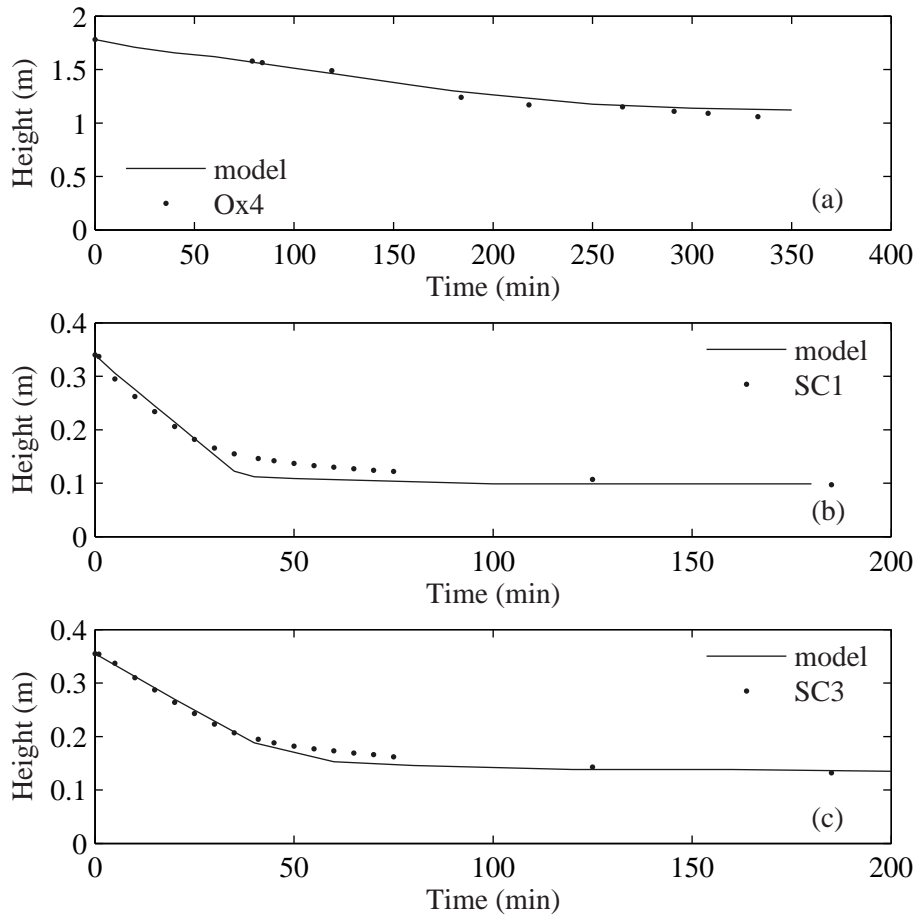

Figure 5.7.   Fitting of the model to experiment Ox4 ($c_0 = 53$ kg/m^3, $w_{s,0}^m = 0.6$ mm/s), SC1 ($c_0 = 26$ kg/m^3, $w_{s,0}^m = 0.35$ mm/s), and SC3 ($c_0 = 34$ kg/m^3, $w_{s,0}^m = 0.35$ mm/s).

Table 5.2. The settling velocity of primary particles in still water for various initial concentrations.

Id	c_0 (kg/m^3)	$w_{s,0}^m$ (mm/s)
SC1	26	0.35
SC2	47	0.6
SC3	34	0.35
SC4	41	0.5
SC5	21	0.5
SC6	19	0.7
Ox1	19	0.9
Ox2	23	0.6
Ox3	35	0.25
Ox4	53	0.6
Ox5	62	0.5

Table 5.3. Suspension settling velocities of mud-sand Ox-experiments and 1DV model.

Id	c_0 (kg/m^3)	Modelled with $w_{s,0}^m = 0.3$ mm/s w_s^m (mm/s)	Prediction error %	Modelled with $w_{s,0}^m = 0.5$ mm/s w_s^m (mm/s)	Prediction error %	Measured w_s^m (mm/s)
Ox6	19	0.125	2.5	0.206	68.9	0.122
Ox7	21	0.110	11.1	0.185	86.9	0.099
Ox8	55	0.018	-41.9	0.028	-9.7	0.031
Ox11	32	0.065	1.6	0.107	67.2	0.064
Ox12	40	0.045	2.3	0.073	65.9	0.044
Ox13	25	0.087	31.8	0.152	130.3	0.066
Ox14	11	0.186	-33.3	0.306	9.7	0.279
Ox15	21	0.111	85	0.188	213.3	0.060
Ox16	15	0.146	-2.0	0.253	69.8	0.149
Ox17	31	0.068	36	0.108	116	0.050
Ox18	41	0.034	-17.1	0.063	53.7	0.041
Ox19	18	0.126	-2.3	0.214	65.9	0.129

5.4.2 Validation

Suspension

A first step in model validation is the comparison between predicted and observed suspension settling velocities, or, in other words, the settling of the upper interface. It is assumed that the influence of sand is small and that the settling of the interface in the experiments will be the same as the settling of the mud fraction in the model. Validation is performed with $c_{gel} = 91$ kg/m^3, $m = 2$, a time step of 1 minute and $D_s = 5 \times 10^{-8}$ m^2/s. For $w_{s,0}^m$ both 0.5 mm/s and 0.3 mm/s are used. The first value was derived in Section 5.4.1, while the latter value is derived from figure 4.14. This figure shows that the suspension settling velocity of the sand-mud Ox-experiments is slightly lower than the mud Ox-experiments and SC-experiments, and is better represented by using $w_{s,0}^m = 0.2$ - 0.4 mm/s.

Some examples of the model-experiment comparison are presented in figure 5.8. The calculated suspension settling velocities are presented in table 5.3, showing that most experiments are represented best by $w_{s,0}^m = 0.3$ mm/s. Both figure 5.8 and table 5.3 show that the model predicts the settling of the total suspension in the hindered settling phase well. The prediction error (the difference between the predicted and measured settling velocity) is in most cases, i.e. for both $w_{s,0}^m = 0.3$ or 0.5 mm/s, smaller than 20%.

The measured velocities are actually the suspension settling velocities, while the model predicts the mud settling velocities. The fact that the model and measurement results agree well underpins therefore the assumption that, if $\phi^s << \phi^m$, the volumetric sand concentration does not influence the settling velocity of the suspension much.

Sand

The measured sand settling velocities are compared to the predicted sand settling velocities in figures 5.9 a and b. Equation 2.6b is used for the prediction. In figure 5.9 a, a D_{50} of 110 μm is used to calculate $w_{s,0}^s$ (= 11 mm/s). For $w_{s,0}^m$, a value of 0.3 mm/s is used. First, equation 2.6b is used with $m = 2$. Figure 5.9 a clearly indicates that in this case, the prediction and measurements do not agree. The value of $m = 2$ was derived in Chapter 3 for kaolinite suspensions. For the natural mud suspensions we were not able to derive a value. $m = 2$ might be an underestimation as the mud flow is affected largely in a chaotic way by the input of the sand, possibly increasing non-linear return flow effects. Therefore, the value of m is changed to 3 and 4, giving slightly better results in figure 5.9 a.

The largest differences between predicted and measured sand settling velocities occur at low mud concentrations. This can be an indication that our choice of $w_{s,0}^s$ is not right. Due to the nature of the measurements (in columns so wall effects can be important), and the nature of the sand input system (it is difficult to obtain a good homogeneous distribution of the sand grains over the horizontal) it is possible that the smaller grains travel mostly along the column wall and are detected with the PTV system. Furthermore, larger grains settle faster and might not have been detected with the PTV/PIV system.
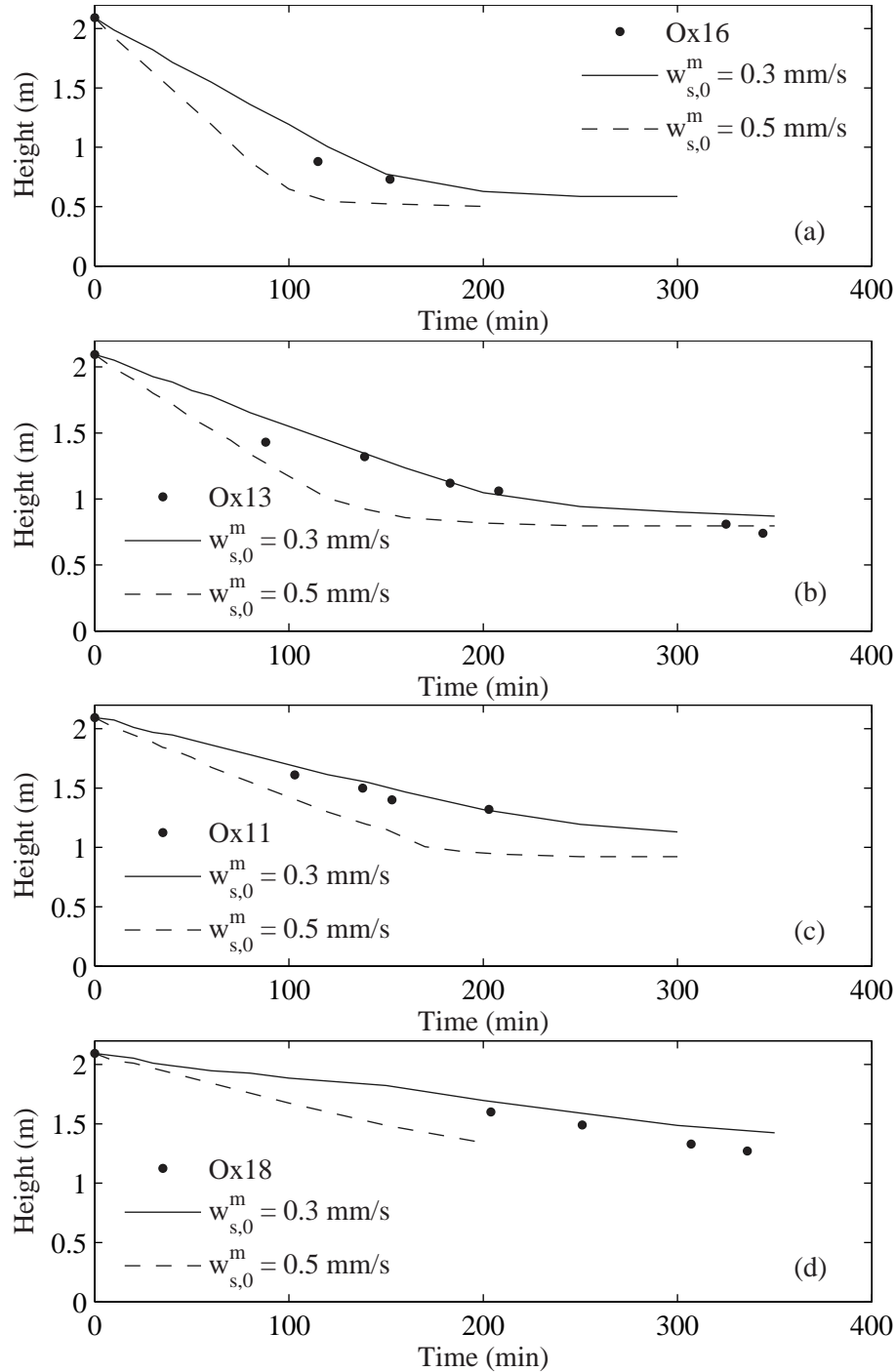
Figure 5.8. Simulation of the experiments. (a) Ox16 ($c_0 = 15$ kg/m^3), (b) Ox13 ($c_0 = 25$ kg/m^3), (c) Ox11 ($c_0 = 32$ kg/m^3) and (d) Ox18 ($c_0 = 41$ kg/m^3).
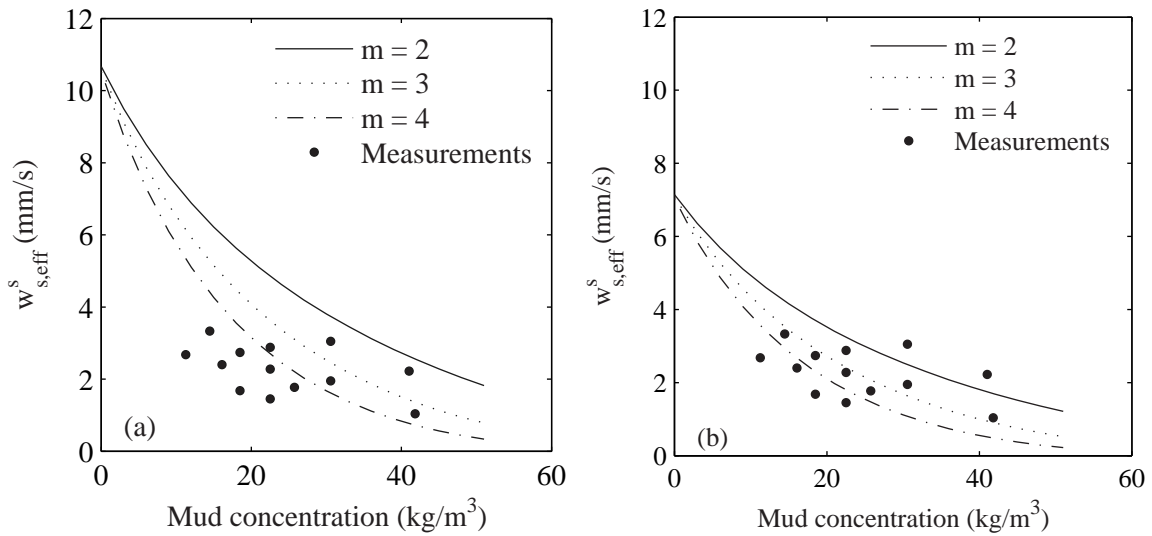
Figure 5.9. Comparison between measured effective sand settling velocities and predicted sand settling velocities (equation 2.6b). a) Model is used with $w_{s,0}^s = 11$ mm/s and $m = 2, 3$ and 4. b) Model is used with $w_{s,0}^s = 7.3$ mm/s and $m = 2, 3$ and 4.

Another possible cause for the observed deviation in figure 5.9 a, can be found in figure 4.1, where the grain size distribution of the used sand is given. The D_{50} can be found at 110 μm, and this value was used for the prediction of $w_{s,0}^s$. However, 50 % of the sand grains has a size between 75 and 110 μm. The sand grains settled past the video camera during a time span of a few minutes, while the video measurements had a duration of only 1 minute. It is possible that the larger grains already passed the measuring window before the camera was switched on. As a result, the grains detected by the camera may be biased towards the smaller size. Therefore, the value of $w_{s,0}^s$ in the model is changed to 7.3 mm/s (90 μm) in figure 5.9 b, yielding a better agreement. The prediction with $m = 3$ gives the best fit. Still, there are some large deviations between prediction and observation. These are mainly due to inaccuracies in the measuring method.

There are no data available at the low mud concentrations but it is expected that the sand settling velocity increases strongly with decreasing mud concentrations when $c < 10$ kg/m^3, as indicated by the model prediction. With respect to the model simulation, figure 5.9 b, with $w_{s,0}^s = 7.3$ mm/s, shows better results than figure 5.9 a. However, the choice of parameter values in figure 5.9 b is not based on hard data but on a few hypotheses. It is therefore clear that the hindered settling of mud-sand mixtures is not yet understood properly and that the model still qualifies for improvement, c.q. better validation.

As a next step, the experiments are simulated with the 1DV model instead of only the hindered settling equation for mud-sand mixtures. The mud-sand experiments started with a homogeneous mud suspension. After 35 - 40 minutes of settling, sand was released. Therefore, first, the mud suspension was modelled for 35 - 40 minutes, with the same parameter values as in the mud-only experiments. The resulting concentration distribution was used as input for the mud-sand modelling. The sand (5 grams) was placed in the top
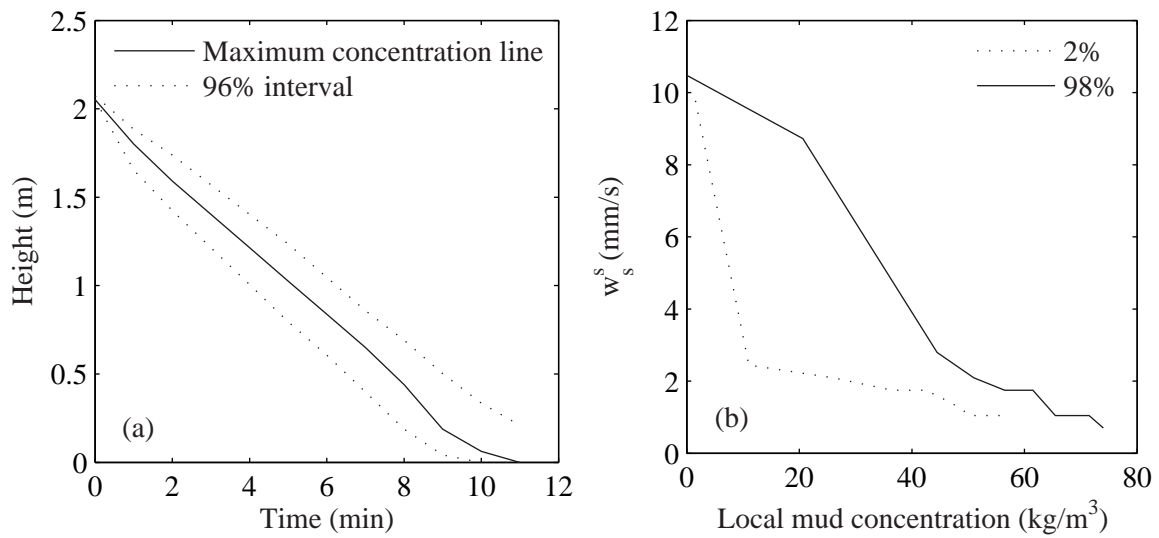
Figure 5.10. Model prediction for Ox11:(a) The amount of segregation within the inserted sand patch of 5 kg/m^3. t = 0 of sand input is equal to t = 35 from start of experiment. (b) Sand settling velocity of the fastest particles (98% is slower) and the slowest particles (2% is slower) that settle in a suspension with increasing concentration towards the bottom.

two layers of the model (in total there are 100 layers over the vertical in the model), after which the model was run for about 10 minutes with a time step of 1 second. In the model predictions the original values of $m = 2$ and $w_{s,0}^s = 11$ mm/s are used.

Figure 5.10 a shows the predicted settling of sand grains in time. Because of segregation and mixing, the initial patch of sand (inserted in the two top layers of the model) attains a more or less Gaussian distribution in space. Therefore we plotted the variation in height with time of the maximum of this distribution and its two tails. The latter two are characterised by the 0.1 kg/m^3 level. Thus figure 5.10 a represents the settling behaviour of about 96 % of the total amount of sand settling in the column. The deviation of the 96 % interval lines from the maximum concentration line gives an indication of the segregation within the sand patch. Most of the segregation is predicted to take place in the top part of the column, which contains water only. In the suspension, almost no segregation is predicted anymore, as indicated by the 96 % interval lines that remain parallel to the maximum concentration line.

Figure 5.10 b shows the predicted sand settling velocity through the Ox11 mud suspension for the fastest settling sand grains (98% of the sand particles is slower) and slowest settling sand grains (2% of the sand grains is slower). The sand grains that settle through this suspension experience an increasing concentration as they settle downwards. Both lines in figure 5.10 b start at the free settling velocity as the sand grains first settle through clear water. The settling velocity decreases when the sand grains reach the mud suspension. The slowest settling particles strongly decrease their settling velocity as soon as they reach the mud suspension. The fastest settling particles decrease more gradually in settling velocity. The segregation of the sand grains themselves indicates the importance

of a long enough measuring record. In the PTV-PIV experiments the measuring time per video was restricted to 1 minute because of memory capacity. As said, it is therefore likely that only the slowest settling particles were tracked with the PTV-PIV system.

Predicted behaviour

Next to settling velocities of the mud suspension and the sand fraction, the model should predict the right behaviour within such a settling suspension. The occurrence of a lower interface is an important aspect in the resulting vertical concentration distribution and should therefore be modelled well.

In figure 5.11, mud-only experiment Ox3 is compared to the model prediction at various times (time in minutes). The upper interface in figure 5.11 a, b and c is predicted well. Only in figure 5.11 d, a higher level is predicted due to the absence of consolidation in the model. In the model the concentration cannot become larger than the prescribed gelling concentration of 91 kg/m^3.

In figure 5.11 there is no clear prediction of a lower interface. The increase in concentration looks more like a rarefaction wave (a gradual increase in concentration). The measured profile in figure 5.11 b does indicate a lower interface at a height of about 0.45 m, but it is not very distinct. In figure 5.11 c, the measured profile looks more like a rarefaction wave. Figure 5.11 a has an irregular measured vertical concentration profile. This is probably due to measuring inaccuracies. Overall, it can be seen that the model predicts the settling of mud suspensions and their vertical concentration profiles rather well for suspensions in the hindered settling and fluid mud phase.
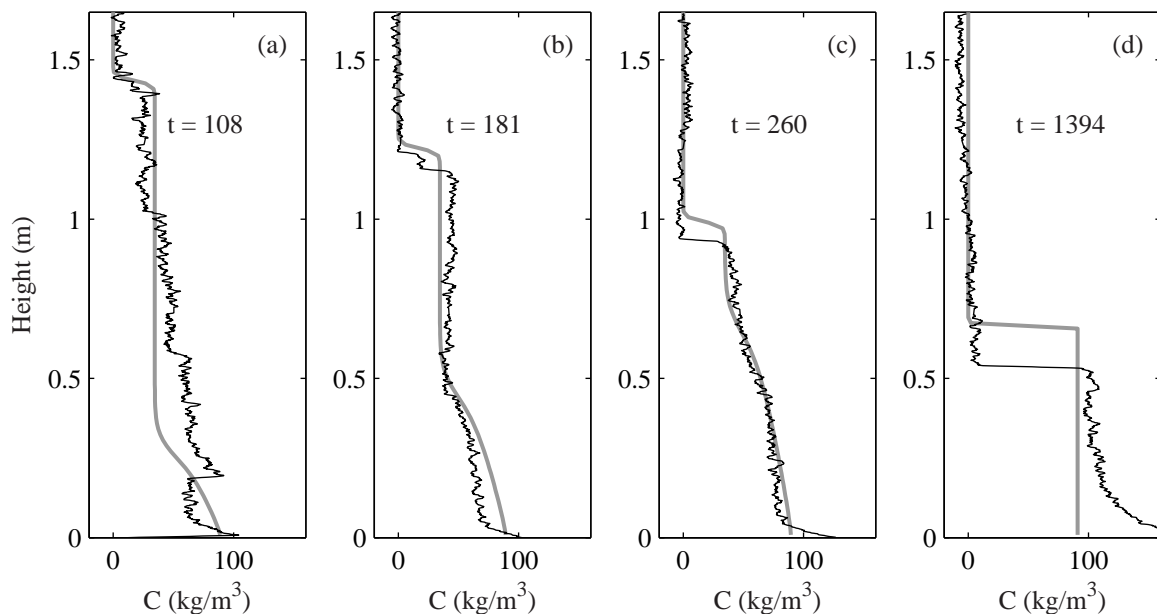

Figure 5.11. Comparison between predicted and measured concentration profiles for Ox3 at several moments in time, time in minutes.

As a next step, a model simulation of mud-sand experiment Ox11 is performed. The model was first run for 35 minutes with mud only. Hereafter, 5 gram sand was placed in the two upper model layers (top of the column). After 20 minutes a second sand input was performed, again with 5 gram sand in the two upper layers, followed, after 10 minutes by a third sand input of 5 gram sand, again in the two upper layers. A time step of 1 second was used.

In figure 5.12, model simulations of mud-sand experiment Ox11 are compared to measured profiles. The upper interfaces are predicted well. In figure 5.12 a, this interface is not visible yet, as its height is larger than the maximum measuring height of the X-ray. The vertical concentration profiles are predicted reasonably well. In figure 5.12 b, the model prediction is fair, but in the other figures there is a small deviation. This is mainly due to measuring inaccuracies, which are especially present in figure 5.12 d over the whole height and in figure 5.12 c at a height of about 0.1 - 0.3 m.

A lower interface is not predicted and these are also not present in the measured profiles. The increase in concentration from the hindered settling phase to the consolidation phase is gradual and depicts the presence of a rarefaction wave.

Figure 5.13 shows the model prediction for Ox18 at $t = 204$ minutes, for Ox13 at $t = 183$ minutes and for Ox16 at $t = 104$ minutes. In all three figures the upper interface is predicted well. Figure 5.13 a, shows similarities between the predicted and observed vertical concentration profile. The increase in concentration starts at more or less the same height, but the shape of the profile is not similar. Figures 5.13 b and c show a deviation between predicted and observed profile at a height of about 0.5 meter. The increase in concentration is predicted to occur much faster, at a higher level and looks
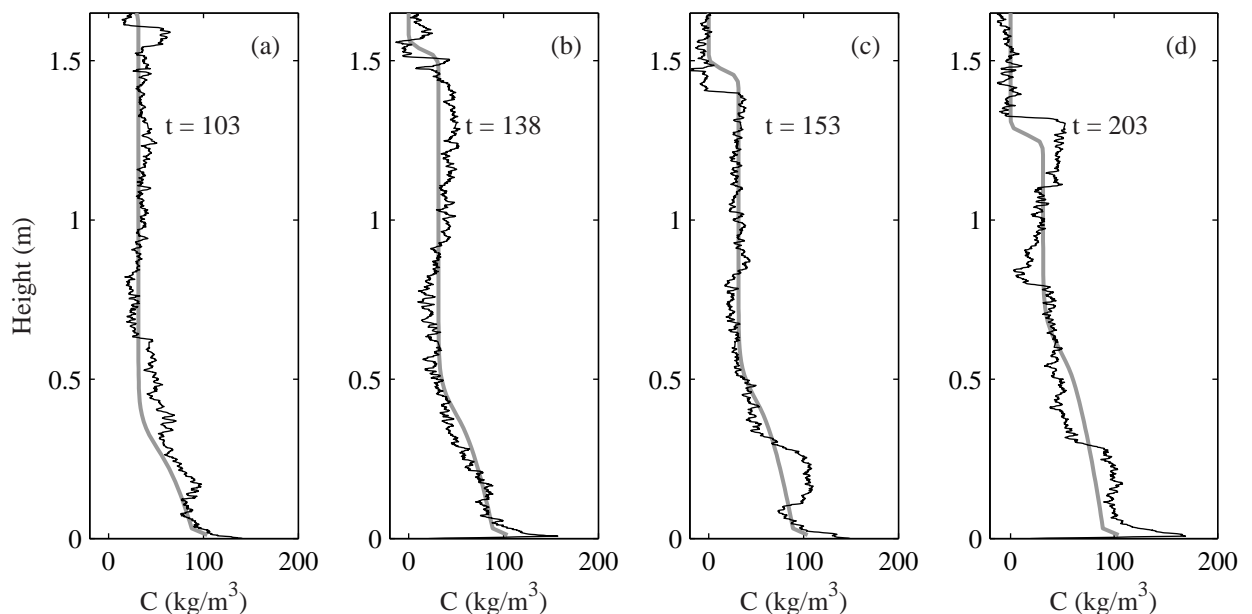

Figure 5.12. Comparison between predicted and measured concentration profiles for mud-sand experiments Ox11 at several moments in time, time in minutes.
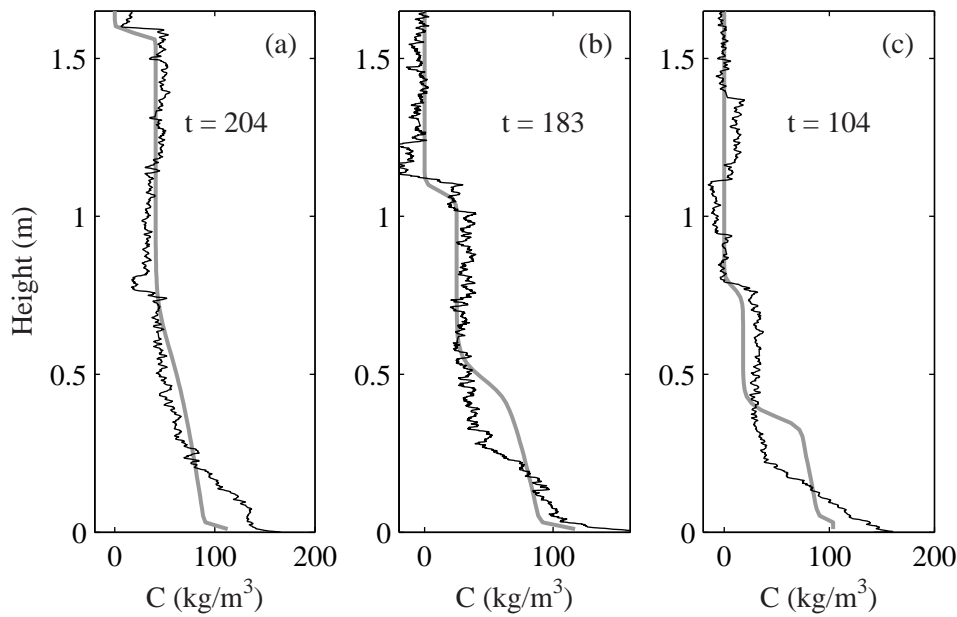
Figure 5.13. Comparison between predicted and measured concentration profiles for mud-sand experiments. (a) Ox18, (b) Ox13, (c) Ox16, with t is time in minutes.

more like a lower interface than a rarefaction wave. Both experiment Ox13 and Ox16 have lower initial concentrations, $c_0 = 25$ kg/m^3 and 15 kg/m^3 respectively, than Ox11 and Ox18 with $c_0 = 32$ kg/m^3 and 41 kg/m^3 respectively. It is not understood why this deviation occurs for the experiments with lower initial concentrations.

5.5   Conclusions

In this chapter experiments with mud and mud-sand mixtures were simulated with a 1-DV model. This model uses an advection-diffusion equation to enable a complete description of hindered settling and consolidation from the water level into the bed. The use of the advection-diffusion equation implies that the model is not optimally suited to solve the simple wave equation. However, if diffusion is small, the model should give accurate enough results.

As a first step, the settling velocity of mud suspensions was simulated. The model parameters c_{gel} and m were derived from the experiments. The value of $w_{s,0}$ had to be determined by calibration of the model. The gelling concentration was chosen to be constant. From the experiments a mean gelling concentration of 81 kg/m^3 was derived. This concentration and the maximum and minimum concentration of 61 and 94 kg/m^3 were used in the model. The 1DV-model was tested against data, which were also used to determine a number of model parameters. However, because mean values were used, the parameters were only partly dependent. The model predicts the suspension settling velocity well in the hindered settling phase for $c_{gel} = 81$ kg/m^3. In the early consolidation

phase the model shows a deviation from the measurements. A change to $c_{gel} = 94$ kg/m^3 showed that the data are still represented well, while a change to $c_{gel} = 61$ kg/m^3 causes an underprediction of the suspension settling velocity.

A change in the return flow parameter from the average value of $m = 2$ to $m = 1.4$ and $m = 2.6$, showed that the influence of this parameter is not large. For the given values of m, the settling behaviour is similar. Only when $m \leq 1$ the settling behaviour changes to settling with one interface.

A next step was to model the settling of mud-sand suspensions by determining the settling velocity of both fractions separately and the behaviour of these suspensions. Three types of experiments were performed. Experiments with natural mud in small columns (SC-experiments), experiments with natural mud in large columns (mud-only OX-experiments), and experiments with mud-sand mixtures in large columns (mud-sand Ox-experiments). The first two types of experiments were mainly performed to obtain model parameters for the third type of experiments. The value of c_{gel} was determined from the SC-experiments, while the value of m was taken similar to the value that was derived from the kaolinite experiments. The value of $w^m_{s,0}$ was determined from a calibration of the mud-only OX-experiments. The modelling of the mud only Ox-experiments was thus performed with one dependent parameter ($w^m_{s,0}$), while the mud-sand Ox-experiments were performed with all independent parameters.

In both the mud-only experiments and the mud-sand experiments the mud suspension settling velocity is predicted well. In contrast, the predicted sand settling velocity shows strong deviations from the observed velocities. A closer look at the grain size distribution shows that the used value of $w^s_{s,0}$ is possibly too large and maybe closer to 7.3 mm/s than to 11 mm/s. For the kaolinite experiments in Chapter 3 the value of $m = 2$ was determined. A change to $m = 3$ for the mud-sand experiments, in combination with $w^s_{s,0}$ = 7.3 mm/s, gives a better prediction of sand settling velocities. This may be the result of the irregular motions initiated by the input of sand.

The behaviour within suspensions and especially the occurrence of interfaces is also computed. In the mud-only experiments two interfaces are formed at some occasions, while the model does not predict two interfaces. An upper interface is found in both the experiment and the model simulation at the same height. A lower interface is not present in the predicted profile, instead a rarefaction wave is found. This rarefaction wave occurs at the same height as the observed interface, resulting in a vertical concentration profile that is quite similar to the measured concentration profile. A possible reason for the prediction of a rarefaction wave instead of an interface is the introduction of diffusion in the model, smearing out the lower interface.

In the mud-sand experiments the model predicts the development of one interface and this is confirmed by the measurements. The predicted and observed upper interfaces are found at more or less the same height. The vertical concentration profiles are predicted reasonably well in many cases, although the predicted profiles have a more convex shape, while the measured profiles have a more concave shape. For the lower initial concentrations there is a stronger deviation, especially in the lower part of the profile.

Overall, it can be concluded that the model predicts the settling of mud suspensions

fairly well and also the predicted vertical concentration profiles are reasonable. The predicted sand settling velocities are, however, not good. The deviation between predicted and measured settling velocities can have various causes. Measuring inaccuracies are an important factor. However, this was the first attempt to measure sand settling velocities in highly concentrated mud suspensions and many improvements, such as measuring time and detection method, can be made. Furthermore, wall effects might have played a role and the distribution of the sand grain sizes over the horizontal in the column is not known. It is clear that the settling of sand in highly concentrated mud suspensions is not yet fully understood. Further research might improve this understanding and can result in an improved model.

6

Conclusions and recommendations

In this thesis the hindered settling of highly concentrated suspensions of mud and mud-sand mixtures is described. These suspensions occur in the natural environment but have not received much attention. In recent years, awareness of decision makers on the importance of the ecosystem and factors that influence it, such as cohesive sediment, has arisen. Furthermore, it is realised that cohesive sediment suspensions can affect harbour operations and that large concentrations of cohesive sediment can result in increased or decreased erodibility, the generation of fluid mud layers and increased turbidity, amongst others. As a result, knowledge on the behaviour of cohesive sediment has become more important. Questions related to the impact of large infrastructural projects on transport and behaviour of cohesive sediment suspensions and consequences for the environment have to be addressed. Before this can be realised, the processes within settling cohesive suspensions, such as mud suspensions and mud-sand mixtures, have to be understood better.

This thesis focusses on highly concentrated suspensions of mud and mud-sand mixtures (mud concentration $> 10 \, \text{kg/m}^3$). The main goal was to get a better understanding of the behaviour of highly concentrated suspensions of mud and mud-sand mixtures by, firstly, obtaining data, secondly, testing theories that predict the behaviour of these suspensions, and thirdly, to test a model that predicts the behaviour and the settling velocity of these suspensions, and the separate fractions, in case of mixtures. The main characteristics, which are analysed, are the settling velocities of highly concentrated mud suspensions and mud-sand mixtures, the settling velocities of both fractions separately, and the settling behaviour. The latter includes the vertical concentration distribution during settling, an important factor in predicting sediment transport rates.

Chapter 2 starts with an introduction to the characteristics and behaviour of cohesive sediment. It introduces theories and models that can be used to predict the behaviour within settling suspensions and the settling velocities of the mud and sand fraction within these suspensions. It was concluded that a lack of knowledge exists on the settling of highly concentrated suspensions of mud and mud-sand mixtures, which is the focus of this research.

During the process of settling, five stages can be identified.

1. A hindered settling stage.

2. A stage where hindered settling and early consolidation overlap.

3. A stage of early consolidation, where permeability is important.

4. A consolidation stage, where permeability and effective stress are important.

5. A consolidation stage, where effective stress is important.

At stage 1, the suspension is in the hindered settling phase. At stage 2, the suspension is in the "fluid mud" phase and at stage 3, 4 and 5, the suspension is in the consolidation phase. If the process of hindered settling and consolidation is described with an advection-diffusion equation then the consolidation phase, in which effective stress is important, is described by the diffusion term in the advection-diffusion equation. For very small effective stresses, the advection-diffusion equation degenerates into the simple wave equation, which describes hindered settling and early consolidation properly. This equation forms the basis for Kynch's approach.

Kynch's theory of a settling suspension is elaborated and explained in Chapter 2. The simple wave equation can be solved with the method of characteristics and its solution yields the formation of shocks or interfaces within the settling suspension. If the characteristics cross, an interface or shock, called a regular shock, is formed. When the characteristics cross from one side and move away on the other side, the interface or shock is called a compound shock. When the characteristics diverge there is no interface or shock. This is called a rarefaction wave.

Within Kynch's theory, two types of settling can occur, depending on the initial concentration. When the initial concentration is lower than a critical value, the suspension settles with an upper interface (regular shock) and a lower interface (compound shock). The upper interface is the interface between the water and the settling suspension, while the lower interface is the interface between the suspension and the developing bed. Hindered settling takes place in between the upper and lower interface and the concentration in this region remains equal to the initial concentration. Below the lower interface the concentration gradually increases. In this lower area, hindered settling takes place if the concentration is lower than the gelling concentration, while consolidation takes place at concentrations larger than the gelling concentration.

If the initial concentration is larger than the critical value, settling with one interface only, the upper interface, takes place. The upper interface is a regular shock, while in the suspension a rarefaction wave is present.

The type of settling is thus especially important for the developing vertical concentration distribution, which can be analysed with Kynch's theory. This is elaborated in Chapter 3 and 4, where experiments on highly concentrated mud suspensions and highly concentrated mud-sand mixtures are presented. The former experiments were performed with the clay mineral kaolinite in small settling columns. The settling of the interface

was visually recorded and the development of the concentration with time was measured with a conductivity probe. The measured suspension settling velocities were in the order of 0.01 - 0.1 mm/s. Application of Kynch's theory to the data showed that indeed one or two interfaces developed. Furthermore, important parameters for modelling of hindered settling in Chapter 5, such as the gelling concentration and the return flow factor, could be determined from the experiments.

Next, experiments with natural mud suspensions and natural mud-sand mixtures were performed. These experiments are presented in Chapter 4. They were performed in large settling columns filled with high concentrations of natural mud and low concentrations of sand. Various techniques were used during the experiments, in order to determine as many parameters as possible. An X-ray system was used to determine vertical concentration profiles, the occurrence of interfaces and the settling velocity of the mud fraction. PTV/PIV, an optical technique, was used to determine the settling velocity of the sand grains.

Visual observations showed that the sand grains caused irregular flow of the mud suspension. Furthermore, the sand grains were seen to settle through the dewatering channels that developed in the consolidating mud. In this way, the sand grains were not arrested in the mud suspension, but were able to settle further and faster than expected. Finally, the sand grains were arrested at the end of the dewatering channels, leading to patches of sand at various heights in the mud bed.

X-ray measurements of the mud-only experiments showed that two interfaces developed. In contrast, the experiments with mud and sand never showed a lower interface. This is likely a result of the irregular flow that was produced by the sand grains that were released in the mud suspension from the top.

Sand grains close to the column wall were followed with the PTV/PIV technique. This resulted in a data set of sand settling velocities. The measured sand settling velocities were in the order of 1 - 3 mm/s. A disadvantage of the PTV/PIV technique is that only particles close to the wall can be followed, resulting in measured velocities that are possibly influenced by wall effects. Sand particles in the centre of the column could not be detected with the PTV/PIV technique. However, inspection of a horizontal slice of consolidated material showed that the sand was distributed evenly over the area, and no preference in settling location was observed.

In Chapter 5, the data sets from Chapter 3 and Chapter 4 are compared to model results. In Chapter 3 and 4 the behaviour of suspensions was analysed with Kynch's theory. A disadvantage of this theory is that it cannot be applied in flowing water, nor can it be applied in the consolidation phase. As the ultimate goal is to derive a complete 3-D description of settling and consolidation in flowing water it was chosen to use an advection-diffusion equation instead. This equation, based on Winterwerp & Van Kesteren (2004), was incorporated in a 1-DV model by Delft Hydraulics.

The parameters c_{gel}, $w_{s,0}^m$ and m are model input parameters and their values were derived from the experiments. For the kaolinite experiments, the same data set was used for both the derivation of the parameters as the model validation. However, because mean values were used for c_{gel} and m, and interpolated values for $w_{s,0}^m$, these parameters are

only partly dependent. For the mud-sand experiments, the parameter values were derived from a different data set than the validation data set. Therefore, in this case, all model parameters and results are independent.

The model parameter m, which determines whether non-linear return flow effects, such as curvature of streamlines are incorporated, proved to be an important model parameter. This parameter determines the type of settling that can occur. If $m > 1$, both settling with two interfaces and settling with one interface may occur, depending on the initial mud concentration. If $m = 1$, only settling with two interfaces occurs.

For the mud-only experiments, the model proved to predict the settling velocity of both the kaolinite and the natural mud suspensions well. However, the type of settling was not always predicted well. Two interfaces were observed in most experiments but only one interface was predicted by the model. The lower interface in the experiments yielded a rarefaction wave in the model results. This, however, did not have significant effects on the predicted vertical concentration profiles, which showed fair agreement with the experimental results.

A comparison between model results and the mud-sand experiments gave different results. The settling velocity of the mud fraction was predicted well, while the settling velocity of the sand fraction was not predicted well. The settling velocity of the sand grains in the experiments did not seem to be influenced much by the initial mud concentration. This in contrast to the expectations and the model prediction, which showed a strong decrease in sand settling velocity with increasing initial mud concentration. A change in some model parameter values improved the fit, but it can be concluded that the settling of sand grains in highly concentrated mud suspensions is not understood well enough yet.

The occurrence of interfaces in the mud-sand experiments was predicted well by the model. Only one interface was observed in the experiments and also predicted by the model. The vertical concentration profiles were predicted well in some cases, while in other cases the predicted profiles had a more convex shape, instead of the measured concave shape. Also, for the lower initial concentrations a more apparent rarefaction wave was predicted than observed.

Two unique data sets were produced. Where earlier data sets mainly focussed on lower initial concentrations (free settling phase) or larger initial concentrations (consolidation phase), this research deals with concentrations in the hindered settling phase. Furthermore, to the author's knowledge, sand settling through highly concentrated mud suspensions was never studied before. Research questions on how highly concentrated suspensions of mud settle and what the settling velocities are, have been answered reasonably well. In contrast, sand settling velocities were difficult to determine. The model results for the mud suspensions are fair, while the results for the mud-sand mixtures show that the settling of sand through a highly concentrated suspension of mud is not understood well yet. Still, the data sets have given us a better understanding of the behaviour of highly concentrated settling suspensions and on the settling velocity of these suspensions and the separate fractions in the suspension. Furthermore, knowledge is gained on how the separate fractions in mud-sand mixtures interact, but the detailed processes are not understood yet.

It is anticipated that this is only a first step in the modelling of highly concentrated mixtures. Improvements can be made by more detailed experiments, for instance by improving the use of PTV/PIV techniques.

The results of this study can help to improve the prediction of effects of a large disturbance in the form of an increased concentration, for example due to dredge slurry dumping or from the resuspension during storms. A better prediction of concentration distributions gives information on the amount of sediment transport that can take place and on the turbidity in the water column. Furthermore, a realistic prediction of the settling velocity gives an indication on how long disturbances due to increased turbidity are present and at which distance from the initial disturbance the effects can be found. As a result, decision makers are helped to base their decisions on scientific knowledge, rather than on best guess.

References

BALDOCK, T.E., TOMKINS, M.R., NIELSEN, P., & HUGHES, M.G. 2004. Settling velocity of sediments at high concentrations. *Coastal Engineering*, **51**(1), 91–100.

BARTHOLOMEEUSEN, G., DE STERCK, H., & SILLS, G.C. 2003. Non-convex flux functions and compound shock waves in sediment beds. *Hyperbolic Problems: Theory, Numerics, Applications: Proceedings of the Ninth International Conference on Hyperbolic Problems*, 347–356.

BEEN, K. 1980. *Stress-strain behaviour of a cohesive soil deposited under water.* Ph.D. thesis, Oxford University.

BÜRGER, R., & TORY, E.M. 2000. On upper rarefaction waves in batch settling. *Powder Technology*, **108**, 74–87.

BUSCALL, R. 1990. The sedimentation of concentrated colloidal suspensions. *Colloids and surfaces*, **43**, 33–53.

BUSCALL, R., MILLS, P.D.A., GOODWIN, J.W., & LAWSON, D.W. 1988. Scaling behaviour of the rheology of aggregate networks formed from colloidal particles. *Journal of the Chemical Society, Faraday Transactions I*, **84**(12), 4249–4260.

BUSTOS, M.C., CONCHA, F., BÜRGER, R., & TORY, E.M. 1999. *Sedimentation and Thickening. Phenomenological Foundation and Mathematical Theory.* Mathematical Modelling: Theory and Applications, vol. 8. Kluwer Academic Publishers.

DANKERS, P.J.T., WINTERWERP, J.C., & VAN KESTEREN, W.G.M. 2006. A preliminary study on the hindered settling of kaolinite flocs. *In:* MAA, J., SANFORD, L., & SCHOELHAMER, D. (eds), *Estuarine and coastal fine sediment dynamics. Proceedings of Intercoh 2003.*

DARCOVICH, K., GIERER, C., & CAPES, C.E. 1996. The application of dynamic clustering data to the sedimentation rates of concentrated suspensions. *Advanced Powder Technology*, **7**(1), 1–19.

DAVIS, R.H. 1996. *Velocities of sedimenting particles in suspensions.* Advances in fluid mechanics. Southampton: Computational mechanics publications. Chap. 6, pages 161–198.

DE WIT, P.J. 1992. *Liquefaction and erosion of mud due to waves and current.* Tech. rept. 10-92. Delft University of Technology.

DOUBEN, K. 1989 (Januari). *De invloeden van baggerwerkzaamheden op het aquatisch milieu. Literatuurstudie omtrent het baggerprobleem in het Eems-Dollard estuarium en de Waddenzee.* Tech. rept. Waddenvereniging, Groningen.

DYER, K.R. 1989. Sediment processes in estuaries: Future research requirements. *Journal of geophysical research,* **94**(C10), 14,327–14,339.

ESSINK, K. 1999. Ecological effects of dumping of dredged sediments; options for management. *Journal of Coastal Conservation,* **5**, 69–80.

GREGORY, J. 1997. The density of particle aggregates. *Water Science Technology,* **36**(4), 1 – 13.

GROENEWOLD, S., & DANKERS, N.M.J.A. 2002. *Ecoslib, de ecologische rol van slib.* Tech. rept. 519. Alterra, Wageningen.

HERBICH, J.B. 2000. *Handbook of dredging engineering.* Vol. 1. McGraw-Hill.

HULSEY, J.D. 1961. Relations of settling velocity of sand sized spheres. *Journal of sedimentary Petrology,* **31**(1), 101–112.

IADC/CEDA. 2000. *Effects, ecology and economy.* Environmental aspects of dredging.

JANKOWSKI, J.A., & ZIELKE, W. 1996 (March). *Data support for the deep-sea mining impact modelling.* http://www.hydromech.uni-hannover.de/Mitarbeiter/JANKOWSKI/exper/e.html.

JOHNSON, C.P., LI, X., & LOGAN, B.E. 1996. Settling Velocities of Fractal Aggregates. *Environmental Science Technology,* **30**, 1911–1918.

KRANENBURG, C. 1992. *Hindered settling and consolidation of mud–analytical results.* Tech. rept. 11-92. Delft University of Technology.

KYNCH, G.J. 1951. A theory of sedimentation. *Trans. Faraday Soc.,* **48**, 166–176.

LANDMAN, K.S., & WHITE, L.R. 1992. Determination of the Hindered Settling Factor for Flocculated Suspensions. *AIChE Journal,* **38**(2), 184–192.

LESTER, D.R., USHER, S.P., & SCALES, P.J. 2005. Estimation of the Hindered Settling Function $R(\phi)$ from Batch-Settling Tests. *AIChE Journal,* **51**(4), 1158 – 1168.

MANDERSLOOT, W.G.B., SCOTT, K.J., & GEYER, C.P. 1986. Sedimentation in the hindered settling regime. *Chap. 3, pages 63–77 of:* MURALIDHARE, H.S. (ed), *Advances in Solid-Liquid Separation.* Battle press.

MAUDE, A.D., & WHITMORE, R.L. 1958. A generalized theory of sedimentation. *British Journal of Applied Physics*, **9**, 477–482.

MEHTA, A.J. 1986. Characterisation of cohesive sediment properties and transport processes in estuaries. *Pages 290–325 of:* MEHTA, A.J. (ed), *Estuarine Cohesive Sediment Dynamics, Lecture Notes in Coastal and Estuarine Studies.* Springer, Berlin.

MERCKELBACH, L. 2000. *Consolidation and strength evolution of soft mud layers.* Ph.D. thesis, Delft University of Technology.

MOUDGIL, B.M., & VASUDEVAN, T.V. 1988. Characterisation of flocs. *Pages 167 – 178 of:* MOUDGIL, B.M., & SCHEINER, B.J. (eds), *Flocculation & Dewatering.*

ODD, N.V.M., & COOPER, A.J. 1989. A two-dimensional model of the movement of fluid mud in a high energy turbid estuary. *Journal of Coastal Research*, 175–184.

PARTHENIADES, E. 1980. *Cohesive sediment transport mechanics and estuarine sedimentation.* Lecture notes.

RAFFEL, M., WILLERT, E., & KOMPENHANS, J. 1998. *Particle Image Velocimetry. A practical guide.* Experimental Fluid Mechanics. Springer.

RICHARDSON, J.F., & ZAKI, W.N. 1954. The sedimentation of a suspension of uniform spheres under conditions of viscous flow. *Chem. Eng. Science*, **3**, 65–73.

SCOTT, K.J. 1984. *Hindered settling of a suspension of spheres; Critical evaluation of equations relating settling rate to mean particle diameter and suspension concentration.* Tech. rept. 497. Chemical engineering research group, Pretoria, South Africa.

SILLS, G.C. 1997. Hindered settling and consolidation in cohesive sediments. *Pages 107–120 of:* BURT, N., PARKER, R., & WATTS, J. (eds), *Cohesive Sediments (Intercoh 1994).* John Wiley & Sons, Chichester.

SILLS, G.C. 1998. Development of structure in sedimenting soils. *Philosophical Transaction of the Royal Society of London*, 2515–2534.

STOLZENBACH, K.D., & ELIMELICH, M. 1994. The effect of density on collisions between sinking particles: implications for particle aggregation in the ocean. *Journal of Deep Sea Research I*, **41**(3), 469 – 483.

TERZAGHI, K. 1943. *Theoretical Soil Mechanics.* John Wiley and Sons.

THACKER, W.C., & LAVELLE, J.W. 1977. Two-phase flow analysis of hindered settling. *The Physics of Fluids*, **20**(9), 1577–1579.

TOORMAN, E.A. 1992. *Modelling of fluid mud flow and consolidation.* Ph.D. thesis, Katholieke Universiteit Leuven, Faculteit Toegepaste Wetenschappen.

TOORMAN, E.A., & BERLAMONT, J.E. 1991. A Hindered Settling Model for the Prediction of Settling and Consolidation of Cohesive Sediment. *Geo-Marine Letters*, **11**, 179–183.

TORFS, H., MITCHENER, H., HUYSENTRUYT, H., & TOORMAN, E. 1996. Settling and consolidation of mud/sand mixtures. *Coastal Engineering*, **29**, 27–45.

UITTENBOGAARD, R.E., WINTERWERP, J.C., VAN KESTER, J.A.Th.M., & LEEPEL, H.H. 1996 (March). *3D Cohesive Sediment Transport - A preparatory study about implementation in DELFT3D*. Tech. rept. Z1022. Delft Hydraulics.

VAN LEUSSEN, W. 1994. *Estuarine macroflocs and their role in fine-grained sediment transport*. Ph.D. thesis, Utrecht University.

VAN OLPHEN, H. 1977. *An introduction to Clay Colloid Chemistry*. 2nd edn. New York, London: John Wiley & Sons.

WANG, Z., NESTMANN, F., & DITTRICH, A. 1995. Fall velocity of sediment in clay suspensions. *Sixth International Symposium on River Sedimentation, New Delhi, India*, 314–322.

WILLIAMS, P.R., & WILLIAMS, D.J.A. 1989. Theometry for concentrated cohesive suspensions. *Journal of Coastal Research*, 151–164.

WINTERWERP, J.C. 1998. A simple model for turbulence induced flocculation of cohesive sediment. *Journal of Hydraulic Research*, **36**(3), 309 – 326.

WINTERWERP, J.C. 1999. *On the dynamics of high-concentrated mud suspension*. Ph.D. thesis, Delft University of Technology.

WINTERWERP, J.C. 2002. On the flocculation and settling velocity of estuarine mud. *Continental Shelf Research*, **22**, 1339–1360.

WINTERWERP, J.C., & VAN KESTEREN, W.G.M. 2004. *Introduction to the Physics of Cohesive Sediment in the Marine Environment*. Developments in Sedimentology, vol. 56. Elsevier.

List of symbols

Roman symbols

C_c	Wave celerity
c	Concentration by mass
c_{gel}	Gelling concentration
c_0	Initial mass concentration
D	Particle diameter
D_{num}	Numerical diffusivity
D_p	Diameter primary mud particles
D_s	Molecular diffusion coefficient
D_{50}	Median of the grain size distribution
$F(\phi)$	Derivative of $f(\phi)$
$f(\phi)$	Hindered settling function
g	Acceleration of gravity
h	Height
k	Permeability
m	Parameter that accounts for non-linearity in return flow effect
N	Count rate
N_0	Reference value for count rate
n	Exponent in hindered settling formula by Richardson and Zaki
n_f	Fractal dimension of mud flocs
Re_p	Particle Reynolds number
S	Vertical particle transport flux
s	Speed of shock wave
t	Time
w_s	Effective settling velocity
$w_{s,0}$	Settling velocity in still water
$w_{s,eff}^s$	Sand settling velocity relative to mud flow
w_z	Flow velocity of mud
z	Vertical coordinate
z_0	Initial height

Superscripts

^{s} Sand
^{m} Mud

Greek symbols

α	Shape factor sediment
β	Shape factor sediment
Γ_c	Diffusion component
Γ_T	Eddy diffusivity
δ	Height of sediment or suspension layer
η	Heuristic parameter
μ	Dynamic viscosity
ν	Kinematic viscosity
Ξ_s	Settling function
ρ_{gel}	Gelling density
ρ_s	Density of primary sediment particles
ρ_w	Density of water
$\Delta\rho_f$	Differential density
ϕ	Volumetric concentration
ϕ_{cr}	Critical volumetric concentration
ϕ_d	Volumetric concentration below shock
ϕ_{gel}	Volumetric gelling concentration
ϕ_{max}	Volumetric concentration of consolidated soil
ϕ_p	Volumetric concentration of primary particles
ϕ_u	Volumetric concentration above shock

Acknowledgements

For 4 years I've been working at the TU Delft on my thesis. And now it's finished. Many people have helped and supported me during these mostly wonderful, but sometimes difficult, years. I would like to thank my supervisor Han Winterwerp for his support and very good guidance, for always being critical but also being able to give compliments. I enjoyed working with him but also enjoyed guiding him through Kyoto and wandering through hurricane smashed Virginia. Further I wish to thank my promoter Marcel Stive. He was not only there to keep an eye on the structure and direction of my work, but also for any other question I might have.

This work is funded by the DIOC-Water Project (Transient processes in Hydraulic Engineering and Geohydrology) of Delft University of Technology. The laboratory experiments in Oxford were made possible by a scholarship granted by the Netherlands Organization for Scientific Research (NWO).

Although officially a member of the Hydraulic engineering section, my actual place was in the Laboratory of Fluid mechanics with all the people from the Environmental Fluid Mechanics section. I enjoyed working together with all my colleagues, but I especially want to thank my colleagues and friends in the fluid lab + 2nd floor. Ankie, Bram, Bas, Elmar, Federico, Gerben, Alexander, Francesca, David, Walter, Michel, Stefan, Andre, Harmen, Wim and Rob were the best colleagues I could have wished for. I also would like to thank Karel de Bruin, Fred van der Brugge, Jaap van Duin, Hans Tas and Arie den Toom, Michiel van der Meer and Frank Kalkman for always helping me when I needed something done, ranging from carrying buckets of mud to fixing my bike. For questions or just a chat I could always walk into the secretary offices of Otty and Chantal.

During my research I spent almost 4 months in Oxford. During these months the working days were very long, but I have to say that they are amongst the best months of my research. I would like to thank Gilliane Sills for giving me the opportunity to work in the laboratory in Oxford. During my stay in Oxford I learned many things from her and I'm happy that, after I returned, our collaboration continued. The work in the laboratory in Oxford could never have been performed so well without the help of Chris Waddup, who could fix almost everything, and Niels Eernink, who was crazy enough to spend his training period with me. Furthermore, I would like to thank my Oxford colleagues and especially Jens, Anthony, Phil and Miguel, as they were one of the reasons that I liked Oxford so much.

I gratefully acknowledge the help of Walther van Kesteren and all the members of my user panel for their interest in my work and the time they made available. I want to thank Lucas Merckelbach for helping me starting up the experiments and for always being there

Publications

Dankers, P.J.T., Sills, G.C. and Winterwerp, J.C.: The hindered settling of mud-sand mixtures. Accepted for: Proceedings Intercoh 2005, Saga, Japan.

Dankers, P.J.T. and Winterwerp, J.C.: Hindered settling of mud flocs: theory and validation. Submitted to Continental Shelf Research.

Dankers, P.J.T. (2005). The intrusion of fine suspended sediment into a sandy sediment bed: A literature review. Internal report. Delft University of Technology.

Dankers, P.J.T., Winterwerp, J.C. and Van Kesteren, W.G.M. (2005). A preliminary study on the hindered settling of kaolinite flocs. Estuarine and Coastal fine sediment dynamics - Intercoh 2003. J. Maa, L. Sanford and D. Schoelhamer (eds.), Elsevier, Amsterdam.

Kleinhans, M.G., Montfort, O., Dankers, P.J.T. and Van Rijn, L.C. (2005). Mud dynamics on the shoreface and upper shelf. Noordwijk, The Netherlands. EU Sandpit Project: Sand transport and morphology of offshore sand mining pits. L. van Rijn (ed.), Aqua publications.

Dankers, P.J.T. and Winterwerp, J.C. (2004). Measuring techniques for highly concentrated mud-sand mixtures. Proceedings of the 9th International conference on River Sedimentation, Yichang, China.

Dankers, P.J.T. (2002). The behaviour of fines released due to dredging: A literature review. Internal report, Delft University of Technology.

Curriculum Vitae

Petra Dankers was born on the 4th of April 1978 on the island of Texel. Here she graduated in 1996 for her VWO at "De Hoge Berg". In the same year she started her academic career at the University of Utrecht, where she studied Physical Geography. During her studies she did a training period in the Red River Delta of Vietnam ("Temporal and lateral variability of the Ba Lat river plume") and a graduation project in Teignmouth, UK ("Sediment transport in the swash zone of a steep, coarse sandy beach"). This resulted in 2001 in an MSc in Coastal and River morphodynamics. In October 2001 she started her PhD research on the hindered settling of suspensions of mud and mud-sand mixtures at the Hydraulic Engineering section and the section of Environmental Fluid Mechanics of Delft University of Technology. The result of this research project lies before you. As from June 2006 Petra works for Royal Haskoning, Division Coastal and Rivers, in Nijmegen.